Results

3.0 Results

PART- I

3.1 FADD REGULATES EXPRESSION OF ANTI-APOPTOTIC PROTEIN CFLIP$_L$ AND AUGMENTS EXTRINSIC SIGNALING OF APOPTOSIS

3.1.1 Determination of endogenous expression of FADD and cFLIP$_L$ in different origin of cancer cells

Earlier reports suggest that, FADD is an important component for regulation of cell death and survival (Tourneur and Chiocchia 2010; Tourneur et al. 2003). Previous reports suggest that the low expression of FADD and elevated expression of cFLIP blocks death receptor signaling of apoptosis and promote malignancy (Tourneur and Chiocchia 2010; Golks et al, 2005; Safa, 2012). First the basal expression of FADD and cFLIP$_L$ were examined in different origin of cancer, transformed and non transformed cells were monitored. The mRNA and protein analysis suggest an inadequate expression of FADD and elevated expression of cFLIP$_L$ was found in cancer and transformed cells as compared to non-cancerous NIH 3T3 cells (Fig 19a-c). Next, the subcellular localization of FADD was examined in HEK 293T cells by immunostaining. Notably, expression of endogenous FADD was only detected in the nuclear region, whereas transient expression of the FADD (post 48 h) was observed at the periphery of the nucleus and throughout the cytoplasmic space of cells (Figure 19d) (Ranjan and Pathak, Sci. Rep., 2016).

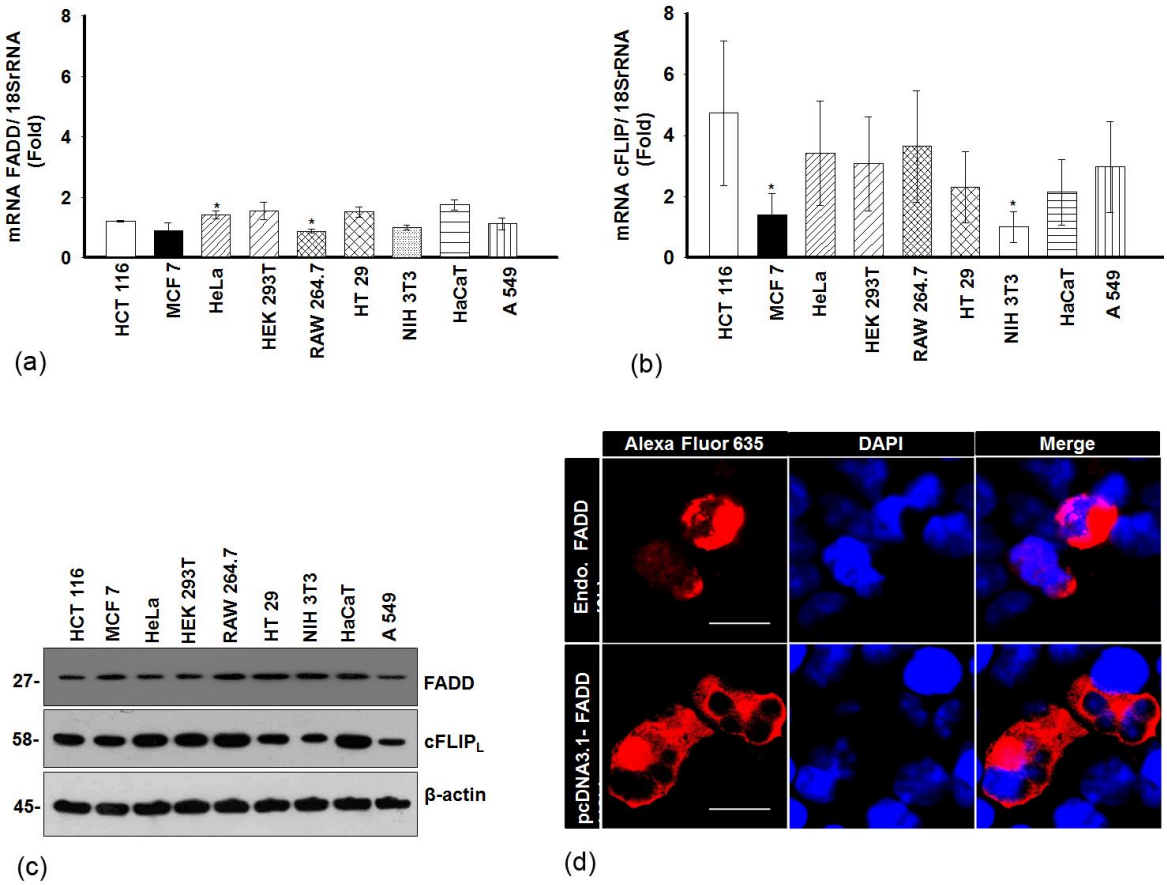

Figure 19. Expression of FADD and cFLIP$_L$. The RT-qPCR analysis to monitor the mRNA expressions of (a) endogenous FADD, (b) endogenous cFLIP$_L$ in mentioned cell lines, the results were compared with mRNA expression of the non-cancerous NIH 3T3 cells (c) The total cell lysate was extracted from the mentioned cell lines and the expression of endogenous FADD and cFLIP$_L$ were monitored by Western blotting, (d) Immunostaining of endogenous FADD and pcDNA3.1-FADD transfected HEK 293T cells (post 48 h), scale bar- 5 µm. Error bars represent mean±SD; The P value indicates *P ≤0.05, Cancerous/ transformed vs. NIH 3T3 transfected cells (n ≥ 3, where n is the number of independent experiments)

3.1.2 Over expression of FADD induces cell death

Next, the pEYFP-FADD construct was transfected into HEK 293T cells and incubated for 24, 48, 72 and 96 h and then functional localization and the expression of FADD were examined. After completion of incubations, the HEK 293T cells were counterstained with nuclear staining dye 4′ 6′-diamidino-2-phenylindole (DAPI) and observed under fluorescent microscope. It was noticed that pEYFP-FADD is constitutively expressed in the cytoplasm and post 48 h, it tends to get localized in the periphery of the cell membrane (Figure 20a). Moreover, the appearance of apoptotic features like formation of apoptotic bodies, cell shrinkage, and surface detachment was also noticed around the similar time points (Figure 20b). Next, the expression of FADD was confirmed by Western blot analysis and found a prominent expression of YFP-FADD (~53 kDa) in HEK 293T cells after 24 h of

transfection as compared to control (vector (pEYFP) transfected cells) (Figure 20c). The adaptor protein FADD is known to induce apoptotic cell death signaling (Chinnaiyan et al., 1995; Siegel et al., 1998). The cell viability was carried out during overexpression of FADD by trypan blue exclusion assay. The obtained results show a reduction in percent cell survival from 24 h onwards (Figure 20d). Thus, these above results indicate that over expression of FADD has an immense potential for induction of cell death in HEK 293T cells (Ranjan et al., JCCS, 2012).

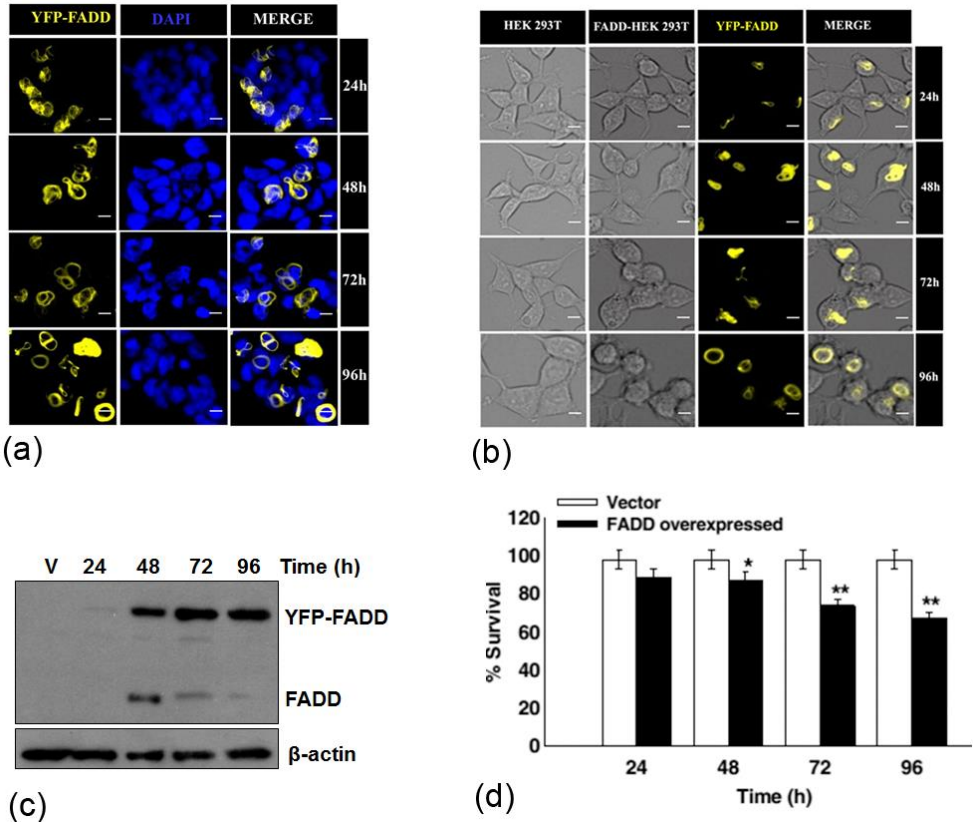

Figure 20. Overexpression of pEYFP-FADD. The HEK 293T cells were transfected with pEYFP-FADD and expressed for 24-96 h, control represents vector (V) pEYFP transfected cells; (a) Cellular localization of pEYFP-FADD, cells counterstained with DAPI (1 µg/ml), Scale bar- 2 µm, (b) Morphology of cells were observed under light microscope in DIC mode, (c) The expression of YFP-FADD (~ 53 kDa) and endogenous FADD (~27 kDa) in cytosolic fractions and (d) percent cell survival, Error bars represent mean±SD; The P value indicates *P ≤0.05, **P ≤0.01, vector (pEYFP) vs. FADD transfected cells (n ≥ 3, where n is the number of independent experiments)

3.1.3 Overexpression of FADD attenuates the expression of cFLIP$_L$ and activates extrinsic cell death signaling

The potential of FADD to execute apoptotic cell death in HEK 293T cells was confirmed by Annexin V-FITC/ PI staining assay. The results showed a gradual increase in propidium iodide (PI) positive cells in apoptotic death as the expression of FADD progress from 24 h onwards (Figure 21a & b). Earlier reports suggest that elevated expression of cFLIP

hinders apoptosis signaling (Golks et al. 2006; Shirley and Micheau 2010). Therefore, expression of $cFLIP_L$, procaspase-8 and caspase-3 was examined during FADD over expressed conditions in HEK 293T cells. The result shows that overexpression of FADD attenuates the expression of $cFLIP_L$ from 48–96 h as compared to the control (vector pEYFP trancfected) cells (Figure 21c). Next, the strength of caspase activation in apoptosis was validated. The result shows a reduction in the level of the pro form of procaspase-8 with the progression of time, which indicates processing and activation of procaspase-8 upon sufficient availability of FADD. In addition, the subsequent processing and activation of procaspase-3 into cleaved subunit was observed from 24 h onwards (Figure 21c). The activity of major initiator caspase-8 was found significantly increased in FADD over expressed conditions for 24–96 h as compared to the controls (Figure 21d). The obtained results clearly indicate that overexpression of FADD attenuates the expression of anti-apoptotic protein $cFLIP_L$ which resulted subsequent activation of cascade of extrinsic caspases to execution of apoptosis in HEK 293T cells (Ranjan et al., JCCS, 2012).

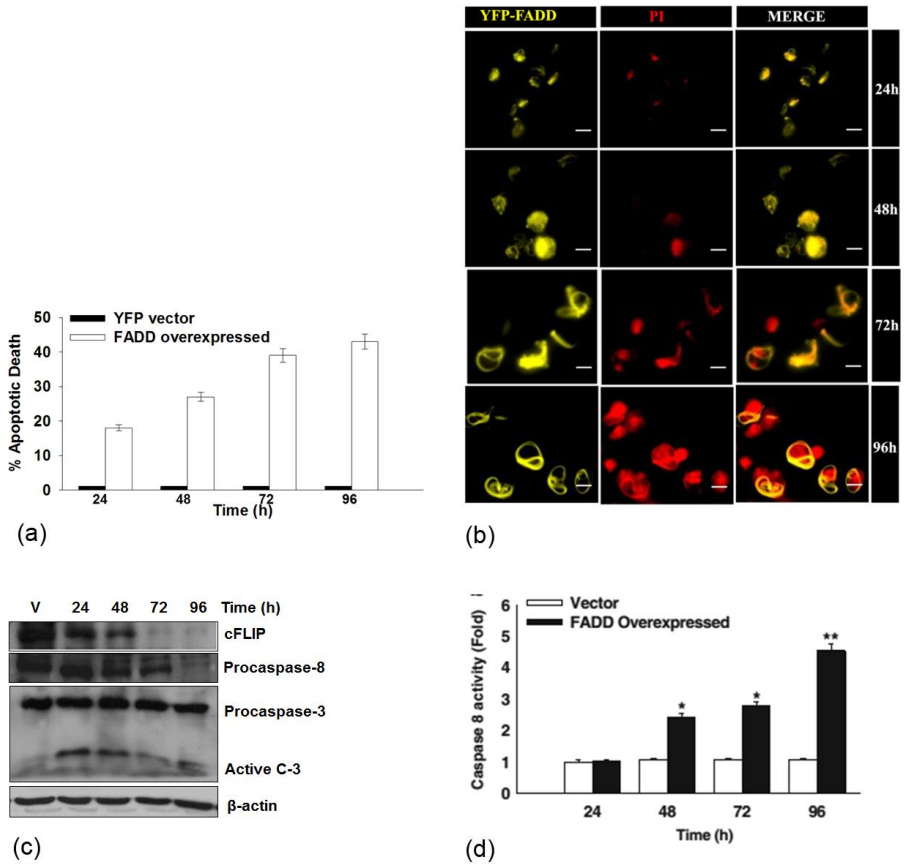

Figure 21. Induced expression of FADD attenuates expression of $cFLIP_L$ and activates cascades of extrinsic caspases. HEK 293T cells were treated as mentioned in figure legend 20, post incubation; (a) Annexin-V FITC/ Propidium iodide (PI) assay and (b) Propidium iodide (PI) staining, the figure shown is representative of more than 100 cells analyzed from three random fields. Scale bar- 2 µm. (c) Expression of $cFLIP_L$ procaspase-8, procaspase-3 and cleaved caspase-3 (active C-3) were examined by Western blot analysis (d) Activity of caspase-8. Error bars represent mean±SD; The P value indicates *P ≤0.05, **P ≤0.01, vector (pEYFP) vs. FADD transfected cells (n ≥ 3, where n is the number of independent experiments).

3.1.4 FADD potentiates CD95L mediated apoptosis

It has been well evident that stimulation of death ligand CD95L quickly stimulates the DISC formation by aggregating adaptor protein FADD and procaspase-8 to activate the death receptor (DR) signaling (Ashkenazi and Dixit, 1998). However, insufficient availability of FADD and hyper expression of $cFLIP_L$ restricts DR signaling (Golks et al, 2005; Safa, 2012). As shown above the expression and localization of pEYFP-FADD in HEK 293T cells were prominent at 48 h of post transfection, therefore the following experiments were performed with 48 h of FADD expressed cells. Here, results show that the CD95L stimulation to 48 h of pEYFP-FADD transfected HEK 293T cells precede cytoslic localization of FADD with progressive induction of cell death from 1-4 h as compared to control and alone CD95L treated cells (Figure 22a-c). In addition, CD95L treatment on FADD overexpressed cells diminishes expression of $cFLIP_L$ within 2 h of treatment as compared to untreated control and alone CD95L treated cells (Figure 22d & e). Moreover, CD95L exposure to FADD expressed cells facilitates processing and activation of procaspases-8 and procaspases-3 to execute apoptotic cell death (Figure 22d-f) (Ranjan et al., JCCS, 2012).

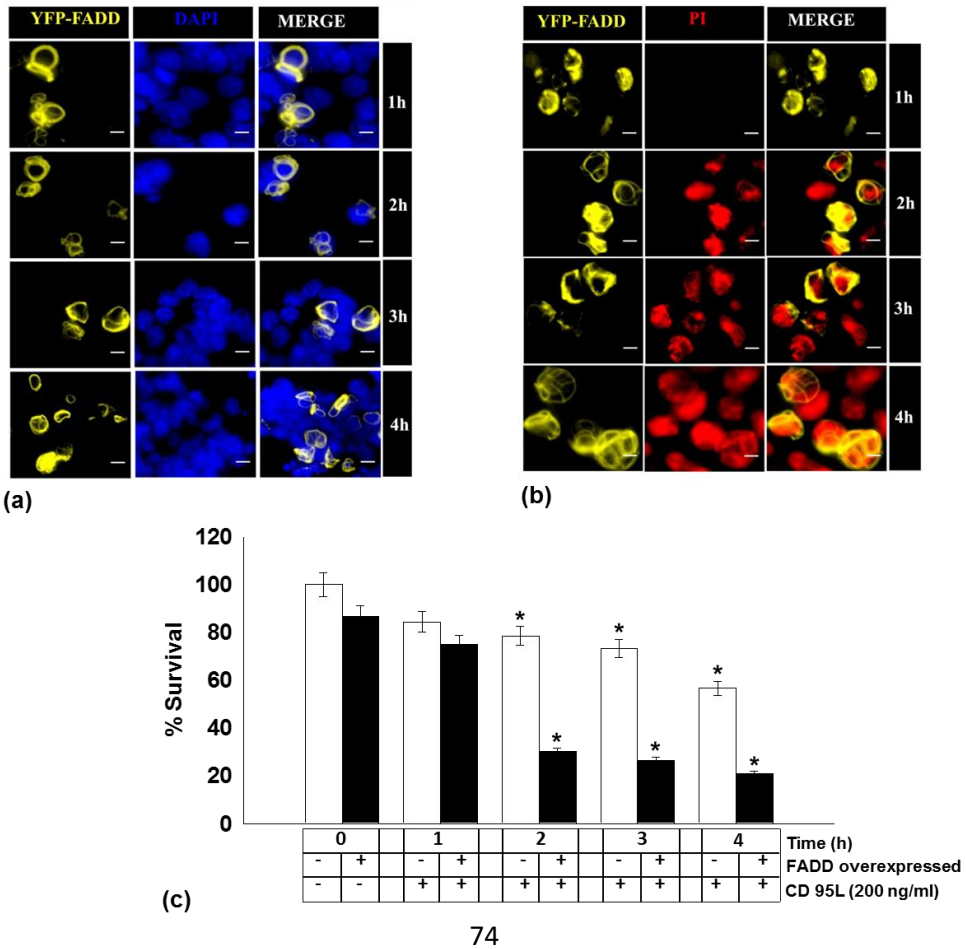

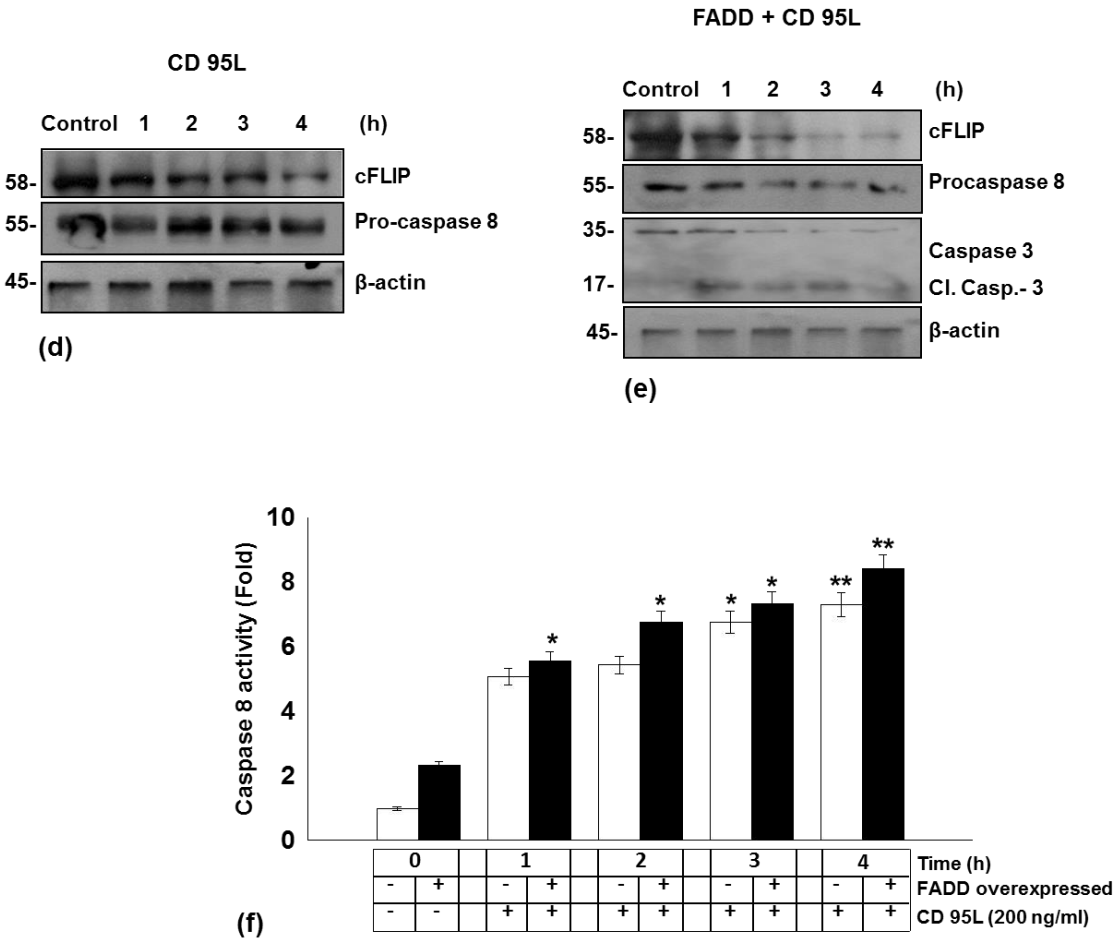

Figure 22. FADD potentiates CD95L induced apoptosis. HEK 293T and pEYFP-FADD expressed (48 h) HEK 293 cells were treated with CD95L (200 ng/ml) for 1-4 h, without CD95L treated (white bar) and 48 h post FADD transfected cells (black bar) (shown as 0 h time) were taken as controls; (a) Cellular localization of pEYFP-FADD, cells counterstained with DAPI (1 µg/ml), (b) PI staining, (c) percent cell survival, (d) Expression of $cFLIP_L$ and procapsase-8 in CD95L treated cells, control represents untreated cells (e) Expression of $cFLIP_L$, procapsase-8, procaspase-3 and cleaved caspase-3 (Cl. Casp.-3), control represents FADD expressed (48 h) untreated cells and (f) Activity of caspase-8. Figures shown are representative of more than 150 cells analyzed of random fields. Scale bar-2 µm. Error bars represent mean±SD; The P value indicates *P ≤0.05, **P ≤0.01, control vs. FADD transfected cells (n ≥ 3, where n is the number of independent experiments)

3.1.5 Sufficient availability of FADD ablates $cFLIP_L$ binding at the DISC

Indeed, the formation of a deathh inducing signalling complex (DISC) is obligatory for the processing and activation of procaspase-8 followed by downstreamm signalling of extrinsic apoptosis (Peter and Krammer, 2003). However, cFLIP inhibits the binding of procaspase-8 to FADD at DISC and abrogates apoptosis (Golks et al., 2006). As shown above, the overexpression of FADD regulates the expression of $cFLIP_L$ in HEK 293T cells. Now, it was important to investigate the FADD mediated regulation of $cFLIP_L$ at the DISC. The HEK 293T cells were transfected with pEYFP-FADD and expressed for 24-96 h followed by immunostaining analysis of $cFLIP_L$. The results show that integrity of $cFLIP_L$ proportionally challenged, as the expression of pEYFP-FADD progressed from 48 h

onwards (Figure 23a). Moreover, the binding of procaspase-8 and cFLIP$_L$ with FADD were examined by co-immunopreciptation assay. The results showed that sufficient availability of wild type (wt) FADD allows progressive binding of procaspase-8 at the DISC rather than cFLIP$_L$, however, expressing mutant (mut.) of the FADD (FADD-SLT4; carrying a mutation in the death effector domain (DED) of FADD (Tungteakkhun et al., 2008)) in HEK 293T cells restrict the binding of cFLIP$_L$ without impairing procaspase-8 interaction at the DISC (Fig 23b & c). Thus, these results show that sufficient availibility of FADD in cytosol profoundly interacts with procaspase-8 and exclude cFLIP$_L$ from the DISC to execute apoptotic cell death (Ranjan and Pathak, Sci. Rep., 2016).

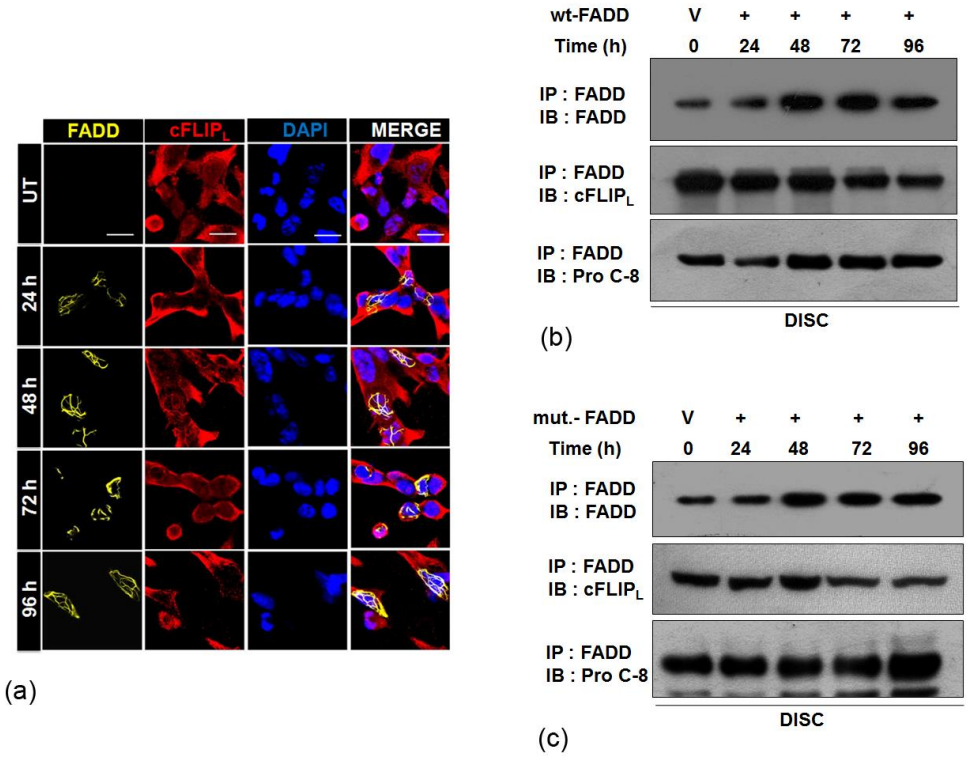

Figure 23. Analysis of FADD, cFLIP$_L$ and pro-caspases-8 binding at DISC. (a) The HEK 293T cells were transfected with pEYFP-FADD and expressed for 24-96 h. Post incubations the cells were immunostained by using anti-cFLIP$_L$ antibody and the expression was detected by Alexa fluor 635 conjugated secondary antibody, cells were counterstained with DAPI (1 µg/ml) and untransfected (UT) cells were taken as control. More than 100 cells from three random fields were selected, scale bar- 5 µm. DISC immunoprecipitation analysis in, (b) The pcDNA3.1-FADD plasmid and (c) The pcDNA-FADD-SLT4 (mut. FADD) plasmids, transfected to HEK 293T cells and expressed for 24-96 h, post incubation total cell lysate was extracted and subjected to co-immunoprecipition assay using anti-FADD antibody followed by Western blotting with the mentioned antibodies. The vector (V) pcDNA 3.1vector transfected HEK 293T cells for 48 h (shown as 0 h time point) was taken as a control, IP = immunoprecipitation; IB = immunoblotting.

PART II

3.2 EXPRESSION OF FADD AND CFLIP$_L$ BALANCES MITOCHONDRIAL INTEGRITY AND CELL DEATH

3.2.1 Expression of FADD and cFLIP$_L$ modulates mitochondrial integrity

Previously, it has been shown that, low expression of FADD and elevated expression of the cFLIP is common in human cancer and develops resistance to extrinsic signaling of apoptosis (Safa, 2012; Tourneur and Chiocchia, 2010). However, the direct involvement of FADD and cFLIP$_L$ in regulation of mitochondrial mediated apoptosis (intrinsic) remains to be elucidated. Although, some recent reports highlighted the role of cFLIP in maintaining the morphology of mitochondria, however the downstream signaling of apoptosis has not been explored (Marini et al., 2015). Here, first the potential of FADD and cFLIP$_L$ in regulation of mitochondrial integrity was examined. To achieve this aim, the expression of cFLIP$_L$ was selectively knockdown (cFLIP$_L^{KD}$) in HEK 293T and FADD expressed HEK 293T cells with subsequent examination of mitochondrial integrity. The results showed that, cFLIP$_L^{KD}$ in FADD expressed cells vanquishes the mitochondrial integrity accompanied with diminished expression of Bcl-2 and cytochrome c as compared to the control cells (Figure 24a & b). In addition, the successive demise of Bcl-2 pulverizes the integrity of mitochondrial outer membrane (MOM) with rapid loss of mitochondrial membrane potential (MMP) (Figure 24c & d). Next, the DD of FADD (FADD-DD) and a mutant FADD-SLT2 (FADD carries mutated DED (Tungteakkhun et al., 2008)) were expressed in HEK 293T cells. The results show reduced mitochondrial integrity and altered expression of mitochondrial cytochrome c and Bcl-2 in pEYFP-FADD expressed cells, as compared to control, FADD-DD and FADD-SLT2 transfected cells (Figure 24e-g). These outcomes demonstrate that, keeping the elevated expression of cFLIP$_L$ provides strength to cancer cells an additional line of defense to protect the integrity of mitochondrial by sequestering the expression of Bcl-2. Interestingly, pro-apoptotic protein FADD was found in the cohesive regulation of Bcl-2 expression and mitochondrial membrane potential.

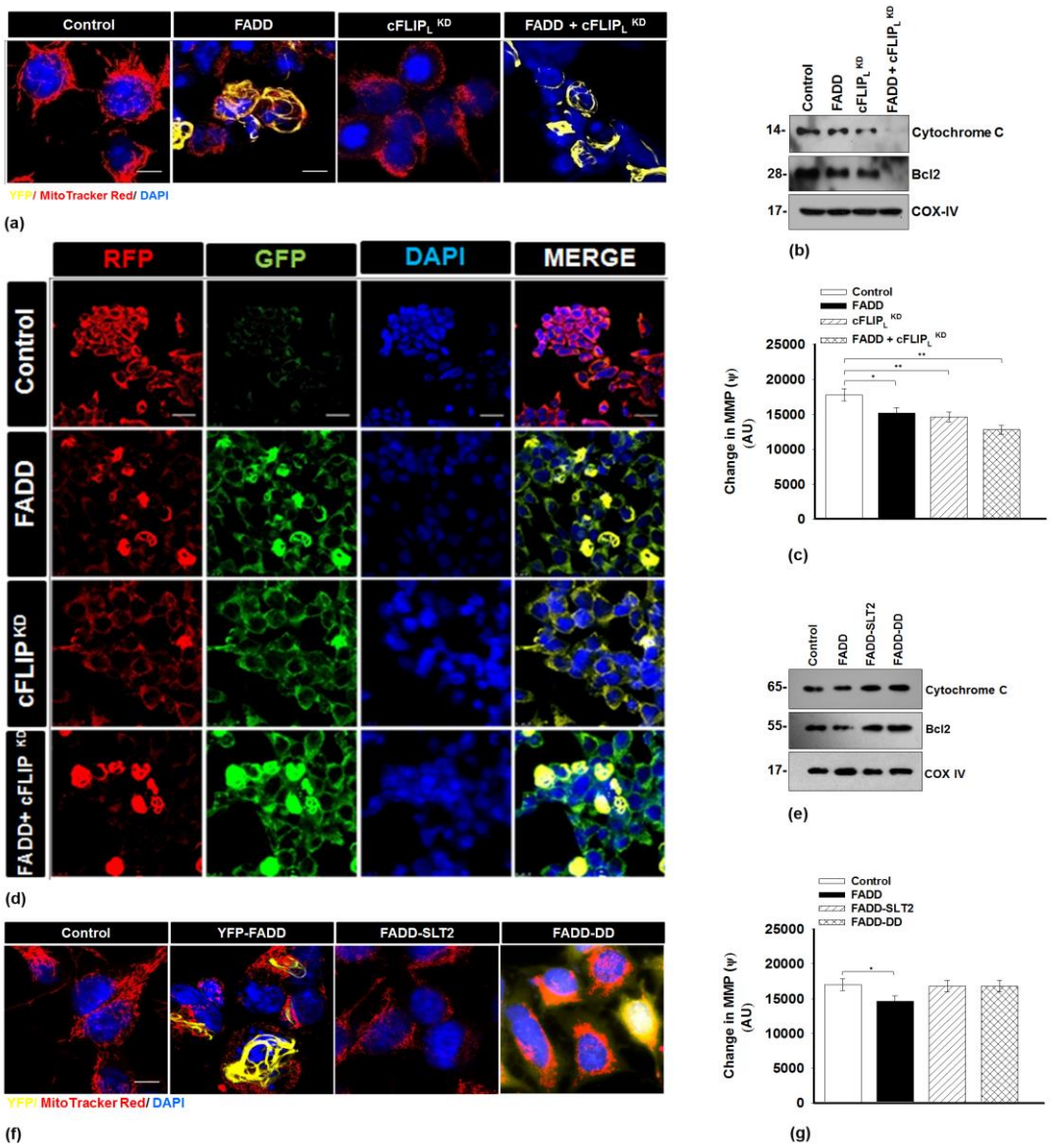

Figure 24. FADD and cFLIP$_L$ balances mitochondrial integrity. HEK 293T cells transfected with pEYFP-FADD (lane 2), siRNA directed against cFLIP$_L$ (cFLIP$_L^{KD}$; lane 3) and pEYFP-FADD with cFLIP$_L^{KD}$ (FADD + cFLIP$_L^{KD}$; lane 4), control represents vector and nontargeting siRNA transfected cells (lane1), the total incubation was for 48 h, post incubation; (a) Mitotracker red stained cells, observed under confocal microscope, (b) Western blot of cytochrome c, Bcl-2 and COX-IV (c) MMP assay by JC-1 dye and (d) JC-1 stained cells observed under confocal microscope. HEK 293T cells transfected with pEYFP-FADD (lane 2), pcDNA-FADD-SLT2 (lane 3), pEYFP-FADD (lane 4), and control represents un-transfected cells (lane 1) from (e-g) as mentioned in figure legend 24 a-c. More than 100 cells from three random fields were observed, for (a) & (f) scale bar- 10 µm; for (d) scale bar- 5 µm. Error bars represent mean±SEM from three independent experiments. The P value indicates *P≤0.05, **P≤0.01, control vs. experimental cells (n ≥ 3, where n is the number of independent experiments).

3.2.2 Expression of FADD and cFLIPL regulates mitochondrial signaling of apoptosis

Next, the mitochondrial signaling of apoptosis was validated in FADD and $cFLIP_L$ modulated HEK 293T cells. The apoptotic death analysis by FACS analysis and Tali™ image based cytometer revealed maximum percent of apoptotic cell death in FADD expressed and $cFLIP_L^{KD}$ cells as compared to the control. In addition, percent of cell death was more progressive in FADD co-expressed with $cFLIP_L$-siRNA transfected HEK 293T cells (Figure 25a-d). Mechanistically, caspae-8 mediated processing of cytosolic protein Bid to truncated Bid (tBid) is instrumental to connect the extrinsic pathway of apoptosis with intrinsic pathway (Li et al., 1998). It was found that, the induced expression of FADD and $cFLIP_L^{KD}$ expedites the processing and activation of procaspase-8 to facilitate truncation of Bid into tBid (Figure 26d). Next, the cascade of mitochondrial apoptosis in FADD overexpressed cells, $cFLIP_L^{KD}$ and FADD expressed cell co-transfected with $cFLIP_L$-siRNA were analyzed. The results show that, $cFLIP_L^{KD}$ in FADD expressed cells channelize the activation of initiator and effector caspases such as procaspase-8, -9 and -3 accompanied by cleavage of PARP with elevated caspase-3 activity (Figure 26a-d). Altogether, these results suggest that FADD and $cFLIP_L$ has enormous potential to maintain mitochondrial integrity and cell death signaling.

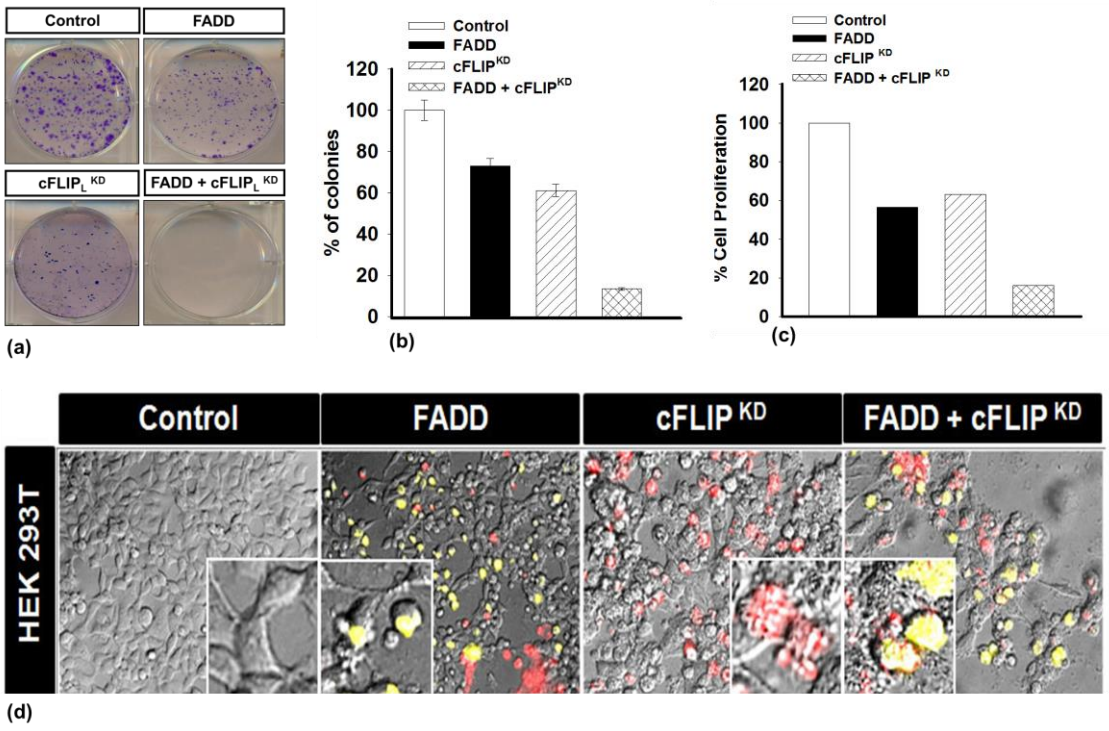

Figure 25. FADD and cFLIP in regulation of cell viability. HEK 293T cells transfected with pEYFP-FADD (lane 2), siRNA directed against $cFLIP_L$ ($cFLIP_L^{KD}$; lane 3) and pEYFP-FADD with $cFLIP_L^{KD}$ (FADD + $cFLIP_L^{KD}$; lane 4), control represents vector and nontargeting siRNA transfected cells (lane1), all incubation were of 48 h, post incubation; (a-b) Colony formation assay, (c) percent cell proliferation, (d) PI staining, more than 150 cells from three random fields were analysed, scale bar- 2µm. Error bars represent mean±SEM from three independent experiments. The P value indicates *P≤0.05, control vs. experimental cells (n ≥ 3, where n is the number of independent experiments).

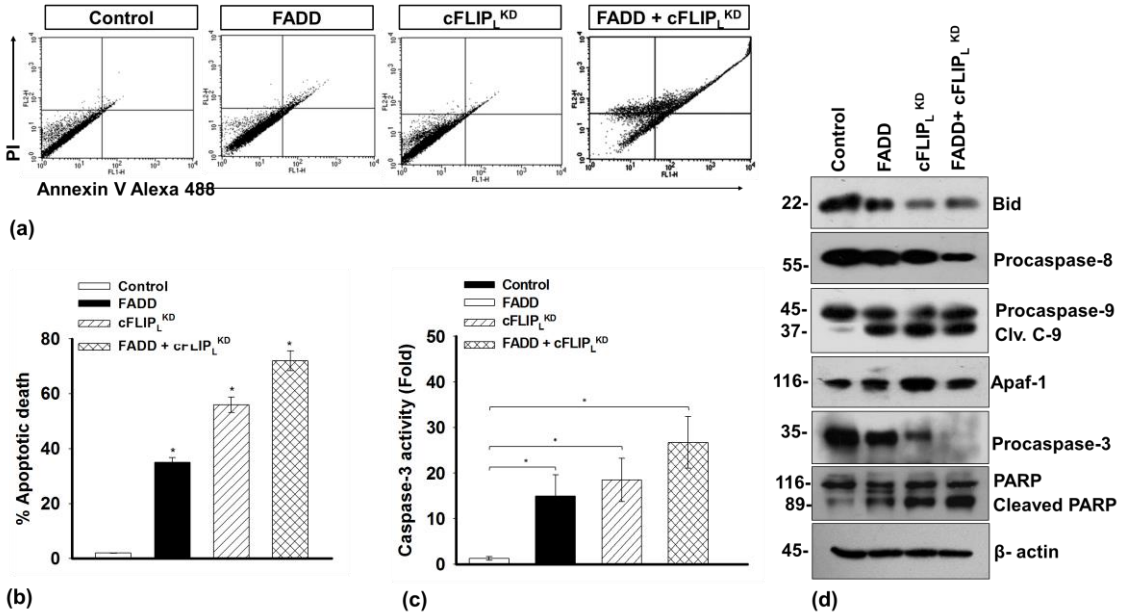

Figure 26. FADD and cFLIP$_L$ expression commences apoptotic cell death. HEK 293T cells treated as mentioned in figure legend 27, post incubation, (a) FACS analysis, (b) percent apoptotic death by Tali cytometer, (c) caspases-3 activity, (d) Western blot images of mentioned proteins, vector and non-targeting siRNA transfected cells were taken as control. Error bars represent mean±SEM from three independent experiments. The P value indicates *P≤0.05, control vs. experimental cells (n ≥ 3, where n is the number of independent experiments).

3.2.3 Knockdown of cFLIP$_L$ induces cell death

Previous reports suggest that death receptor (DR) mediated activation of caspase-8 sequentially channelize the permeabilization of mitochondrial outer membrane (MOM) followed by activation of intrinsic apoptosis signaling (Li et al., 1998; Werner et al., 2002). However, cFLIP$_L$ which is an endogenous inhibitor of procaspases-8 blocks the activation of DR mediated apoptosis (Golks et al., 2005; Safa, 2012). In contrast, the integrity of MOM is protected by pro and anti-apoptotic Bcl-2 family of proteins (Tait and Green, 2010). However, the cross talk between extrinsic and intrinsic signaling regulators cFLIP and Bcl-2 in context of mitochondrion associated apoptosis is not well explored. To achieve this aim, the mitochondrial dynamics of cell death was examined upon siRNA targeted knockdown of endogenous cFLIP$_L$ (cFLIP$_L^{KD}$) in HEK 293T and MCF-7 cells. The results suggest that, siRNA of cFLIP$_L$ effectively knockdown the endogenous expression of cFLIP$_L$ and induces cell death in HKE 293T and MCF-7 cells, however minimal effect were noticed on the viability of non-cancerous NIH 3T3 cells (Figure 27a-d).

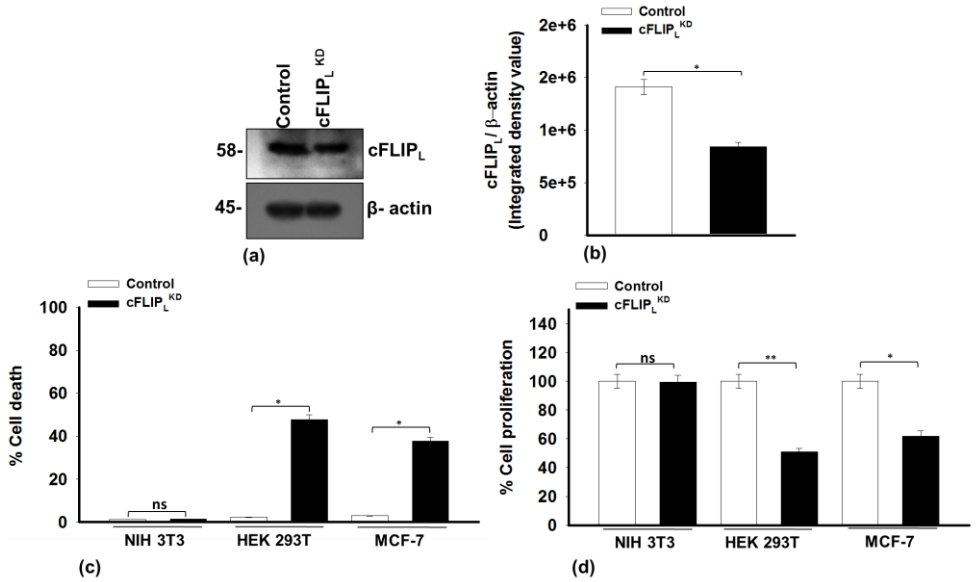

Figure 27. Selective knockdown of cFLIP$_L$ augments cell death. The HEK 293T, MCF-7 and NIH 3T3 cells were transfected with siRNA targeted against cFLIP$_L$, control represents non-targeting siRNA transfected cells, post 48 h of incubation (a) Western blot of cFLIP$_L$ in HEK 293T cells (b) Densitometry analysis for Fig 25 a; IDV- Integrated density value. (c) Percent cell viability and (d) Percent cell proliferation. Error bars represent mean±SEM from three independent experiments. The P value indicates *P≤0.05, **P≤0.01, control vs. experimental cells (n ≥ 3, where n is the number of independent experiments). ns-non-significant.

3.2.4 Knockdown of cFLIP$_L$ alters mitochondrial integrity

Further to analyze the mitochondrial dynamics, the pEGFP-Bcl2 and pmCherry-Bid constructs were co-transfected in HEK 293T and MCF-7 cells, post 24 h of incubation the cells were transfected with siRNA of cFLIP$_L$ and incubated for an additional 48 h. The fluorescent microscopy analysis shows that, cFLIP$_L^{KD}$ alters Bcl-2 integrity accompanied with fragmentation of Bid in HEK 293T and MCF-7 cells as compared to control cells (Figure 28a). Next, the mitochondrial integrity and diffusion of cytochrome c upon cFLIP$_L^{KD}$ in HEK 293T and MCF-7 cells were examined. Interestingly, cFLIP$_L^{KD}$ reduces the number of healthy mitochondria with concurrent cytosolic diffusion of cytochrome c as compared to the control cells (Figure 28b). In addition, the protein expression of mitochondrial associated Bcl-2 and cytochrome c were examined by Western blotting. It was noticed that cFLIP$_L^{KD}$ down regulates the protein expression of mitochondrion associated Bcl-2 and cytochrome c as compared to the control cells of HEK 293T and MCF-7 cells (Figure 28c & d). Furthermore, to corroborate these findings, the mitochondrial membrane potential (MMP) was examined in cFLIP$_L^{KD}$ cells. A remarkable alteration of MMP was noticed in HEK 293T and MCF-7 cells upon knockdown of the cFLIP$_L$, whereas no significant changes were observed in non-cancerous NIH 3T3 cells (Figure 28e). Thus, these results indicate that knockdown of endogenous cFLIP$_L$ challenges the expression of Bcl-2 accompanied with the loss of mitochondrial integrity.

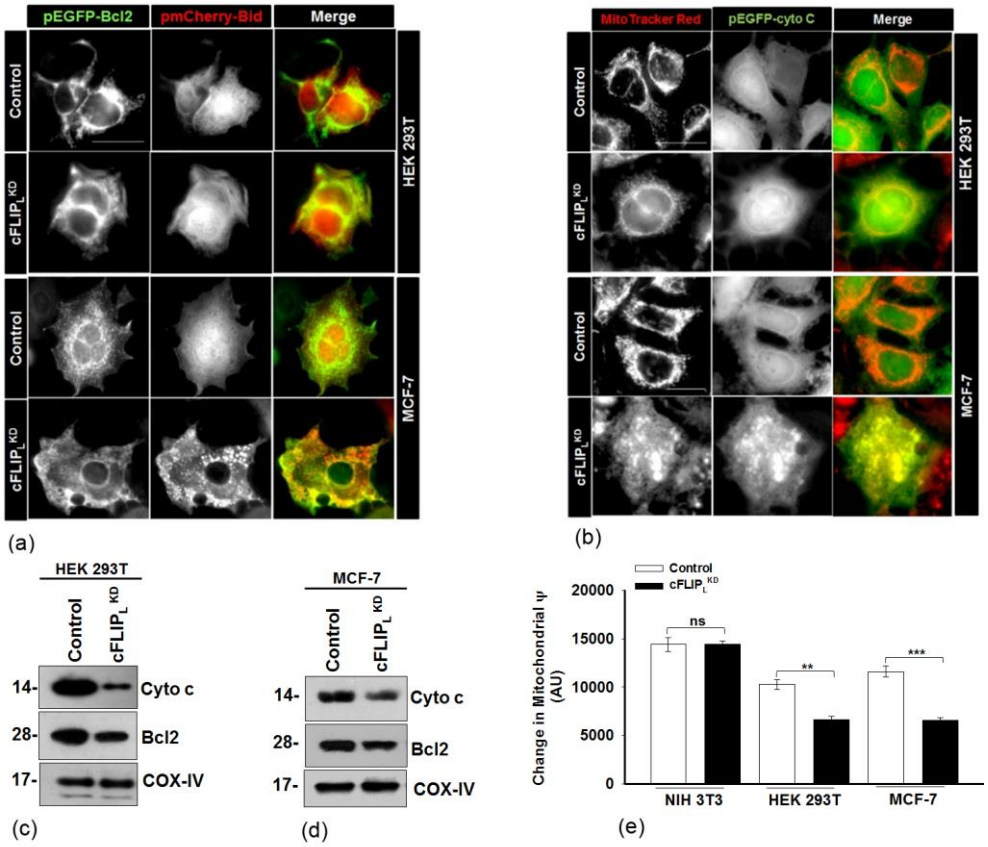

Figure 28. Transient silencing of cFLIP$_L$ challenges mitochondrial integrity. (a) The co-localization and integrity of Bcl-2 and Bid was observed under fluorescent microscope; control represents non-targeting siRNA transfected cells. (b) The HEK 293T and MCF-7 cells were transfected with GFP-cytochrome c and incubated for 24 h followed by knockdown of cFLIP$_L$ for an additional 48 h, further cells were stained with Mitotracker red dye and observed under fluorescent microscope, more than 100 cells from three random fields were observed, scale bar- 10 µm. (c-d) Expression of mitochondrial cytochrome c, Bcl-2 and Cox –IV, (e) Changes in mitochondrial membrane potential. Error bars represent mean±SEM from three independent experiments. The P value indicates **P≤0.01, ***P≤0.001, control vs. experimental cells (n ≥ 3, where n is the number of independent experiments).

3.2.5 TNF-α stimulation unable to protect cell death during knockdown of cFLIP$_L$

Indeed, TNF-α is a potent stimulator of cFLIP$_L$ to support cancer cell proliferation (Micheau and Tschopp, 2003). As mentioned above, knockdown of cFLIP$_L$ (cFLIP$_L^{KD}$) augments cell death, independent of death receptor stimulation. Next, the TNF-α primed HEK 293T cells were selectively knocked down of cFLIP$_L$ (cFLIP$_L^{KD}$) and the outcomes were compared with alone TNF-α treated and cFLIP$_L^{KD}$ cells. The results show that, TNF-α pre-stimulation failed to protect the viability and colony forming abilities of cells subjected to cFLIP$_L^{KD}$ as compared to control and alone TNF-α treated cells (Figure 29a & b). Moreover, a gradual increase in the propidium iodide stained cells were observed in cFLIP$_L^{KD}$ and TNF-α primed cFLIP$_L^{KD}$ cells (Figure 29c). A further study was carried out to investigate the mode of cell death in cFLIP$_L$ knockdown cells. The results suggest that,

selective knockdown of $cFLIP_L$ attributes to apoptosis signaling of cell death with the significant increase in Annexin-V FITC positive cells by Tali cytometer and FACS analysis (Figure 30a & b). Furthermore, the GFP-cytochrome c transfected cells were subjected to knockdown of $cFLIP_L$ followed by mitochondrial staining. The result shows that, $cFLIP_L^{KD}$ dissipates mitochondrial integrity with concurrent alteration of cytochrome c (Figure 30c). Further, the analysis of apoptosis regulatory proteins was carried out. It was observed, pre-stimulation of TNF-α was not able to protect the expression of Bcl-2 upon knockdown of $cFLIP_L$, moreover cytosolic accumulation of cytochrome c accompanied by activation of procaspase-3, procaspase-7 and cleavage of PARP were observed (Figure 30d). In addition, a significant increase in the activities of caspase-8 and caspase-3 were monitored in $cFLIP_L$ knockdown cells as compared to TNF-α exposed celles. (Figure 30e & f). Altogether, these results confirm that altering the expression of $cFLIP_L$ transduces apoptotic cell death independent of TNF-α stimulation (Ranjan and Pathak, Sci. Rep., 2016).

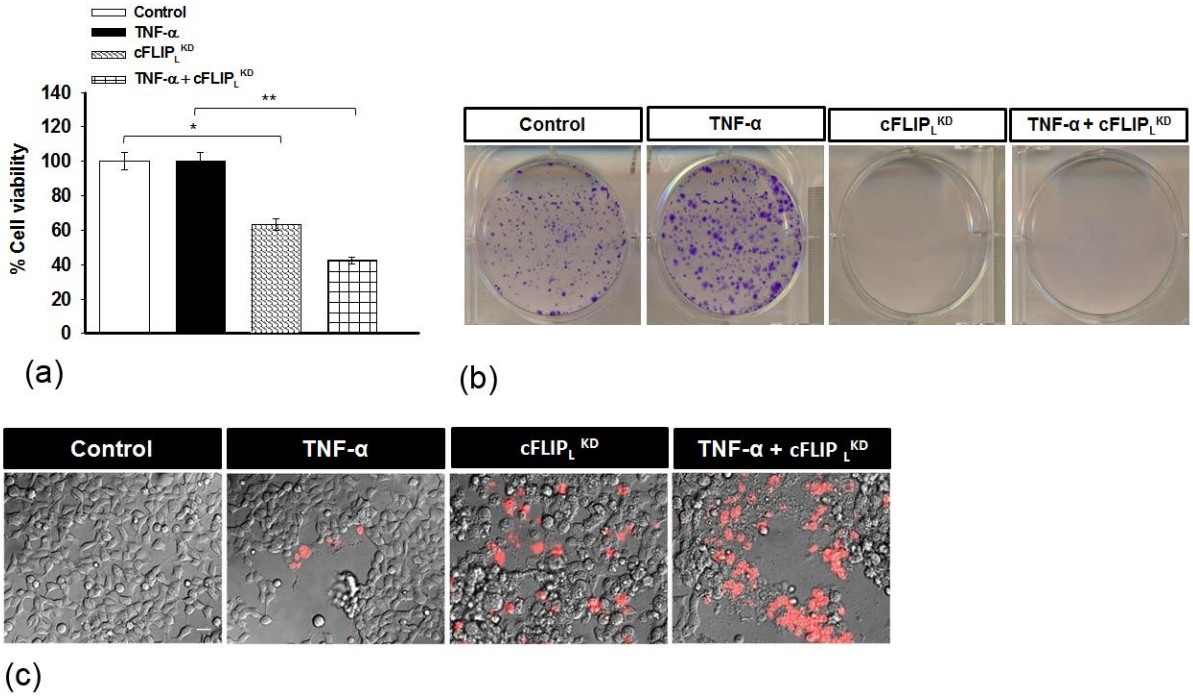

Figure 29. Knockdown of $cFLIP_L$ augments cell death, independent of TNF-α stimulation. The HEK 293T cells were subjected to TNF-α (10 ng/ml) treatment for 12 h (lane 2), transfected with siRNA directed against $cFLIP_L$ ($cFLIP_L^{KD}$; lane 3) for 48 h and TNF-α (10 ng/ml) primed (12 h) cells transfected with siRNA against $cFLIP_L$ (TNF-α + $cFLIP_L^{KD}$; *lane 4*) for an additional 48 h, control represents non-targeting siRNA transfected cells (lane 1), (a) percent cell viability, (b) colony formation assay and (c) Propidium iodide staining. More than 150 cells from three random fields were examined, scale bar- 2 µm. Error bars represent mean ±SD, the P values represents *P ≤0.05, **P ≤0.01 (student t-test, n ≥ 3, where n is the number of independent experiments).

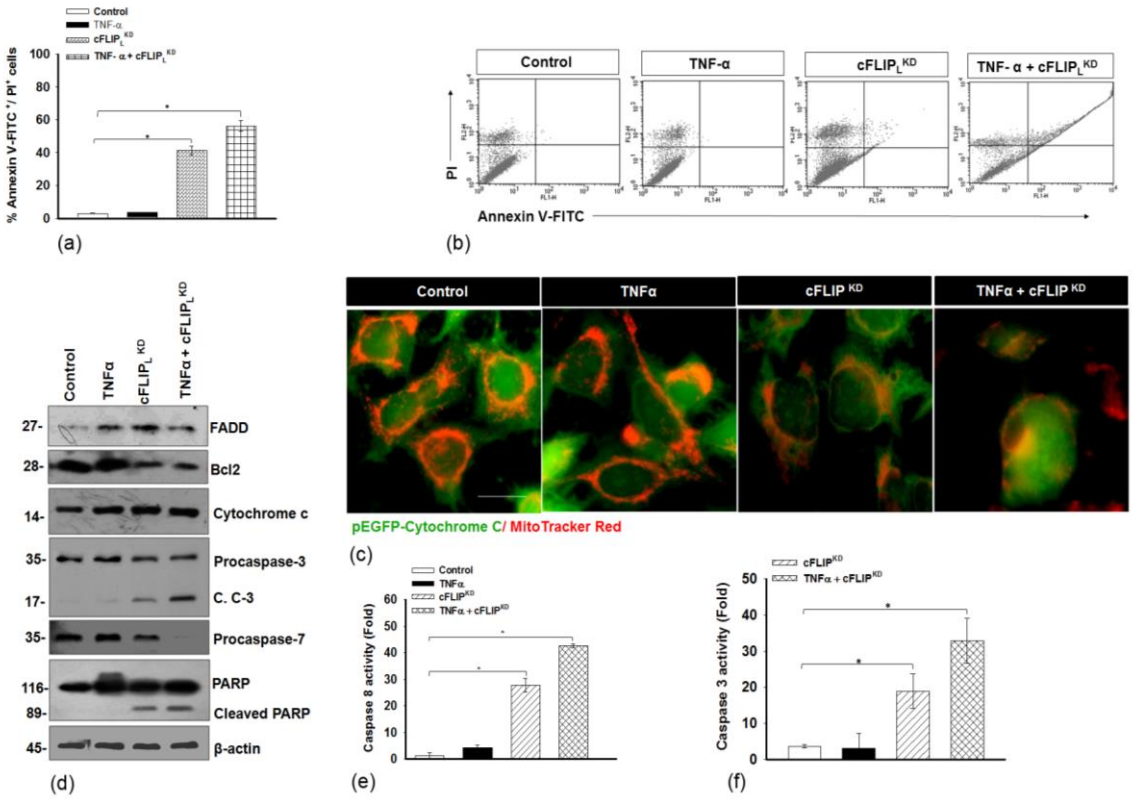

Figure 30. Knockdown of cFLIP$_L$ induces apoptosis, independent of TNF-α stimulation. The HEK 293T cells were treated as mentioned in figure legend 29, and (a) percent Apoptotic death by Tali™ cytometer, (b) FACS analysis, (c) The GFP-cytochrome c was transfected to HEK 293T cells and post 24 h the cells were treated as mentioned in figure legend 29, post incubation cells were stained with Mitotracker red, More than 150 cells from three random fields were examined, scale bar- 5 µm. (d) representative Western blot of mentioned proteins, (e) Caspae-8 activity and (f) Caspase-3 activity assay, C. C-3- (cleaved caspase-3). Error bars represent mean ±SD, the P values represents *P ≤0.05 (student t-test, n ≥ 3, where n is the number of independent experiments).

PART III

3.3 FADD REGULATES NF-KB ACTIVATION AND PROMOTES UBIQUITINATION OF CFLIP$_L$ TO INDUCE APOPTOSIS

3.3.1 FADD induces apoptosis independent of TNF-α stimulation

The stimulation of TNF-α is known to trigger an intracellular cascade of signaling that plays an important role in determining the fate of cell death or survival (Wajant et al., 2003). Now it was important to determine the sub-lethal concentration and incubation time for TNF-α stimulation that have minimum effect on the cell viability. The HEK 293T cells were subjected to 5, 10 and 15 ng/ml of TNF-α and incubated for 6-24 h. It was noticed that the 2 & 3% of cell death was found in 10 and 15 ng/ml of TNF-α treatment respectively post 24 h of incubation (Figure 31a & b). Therefore, the further study was carried out with 10 ng/ml of TNF-α. Furthermore, cell viability, cell proliferation and colony formation assay were carried out in vector transfected and 48 h of FADD expressed HEK 293T, HCT 116 and MCF-7 cells followed by TNF-α (10 ng/ml) exposure for 6–24 h. No major changes in the cell viability, proliferation and colony formation upon TNF-α treatment to non-transfected cells were noticed. However, FADD expressed cells treated with TNF-α abolishes the cell viability, cell proliferation and colony forming abilities (Figure 32a-d). Further, mode of cell death was confirmed by propidium iodide (PI) staining, flow cytometry and Tali cytometer. It was noticed that TNF-α treatment to FADD expressed HEK 293T cells showing a gradual increase of PI positive cells and percent of apoptotic cell death as compared to the vector transfected and untreated cells (Figure 33a–c). More importantly, FADD expressed cells exposed to TNF-α showed activation of initiator procaspase-8, executioner procaspase-3, procaspase-7 with cleavage of PARP as well as elevated activities of caspase-8 and caspase-3 activity (Figure 37d-f) (Ranjan and Pathak, Sci. Rep., 2016).

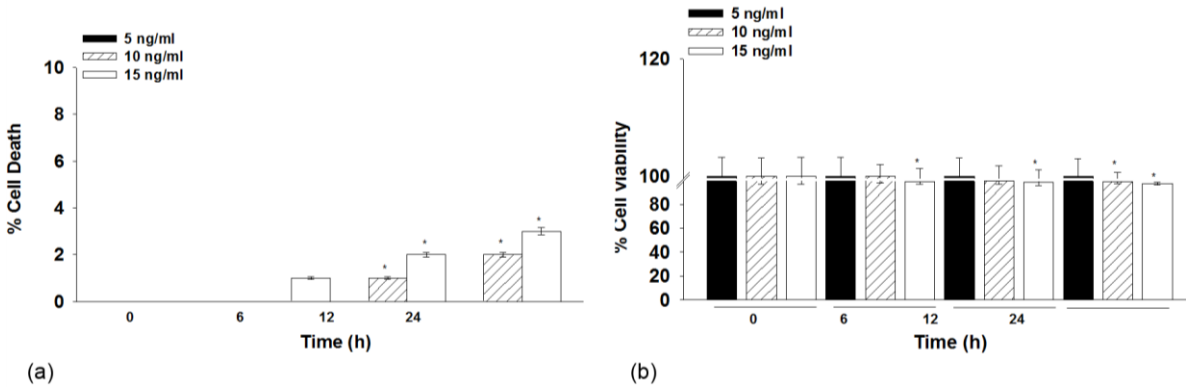

Figure 31. TNF-α stimulation to HKE 293T cells. TNF-α (5, 10 & 15 ng/ml) was subjected to HEK 293T cells for 6-24 h, Control represents without TNF-α treated cells (shown as 0 h time point) and post incubation (a) Percent cell death and (b) percent cell viability. Error bars represent mean ±SD, The P value indicates *P ≤0.05, (student t-test, n ≥ 3, where n is the number of independent experiments).

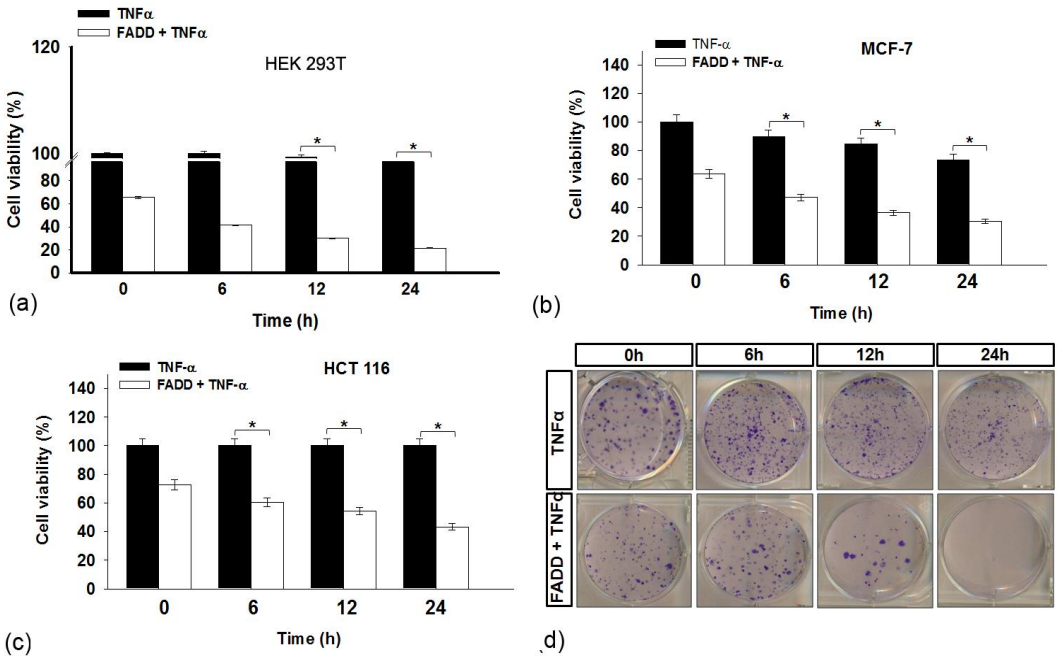

Figure 32. FADD augments cell death in TNF-α stimulated cells. TNF-α (10 ng/ml) was subjected to vector transfected and 48 h of pcDNA3.1-FADD transfected HEK 293T, MCF-7 and HCT 116 cells. Control represents without TNF-α treated (black bar) and 48 h pcDNA3.1-FADD transfcted cells (white bar) (shown as 0 h time point). (a-c) Percent cell viability and (d) colony formation assay. Error bars represent mean ±SD, The P value indicates *P ≤0.05, (student t-test, n ≥ 3, where n is the number of independent experiments).

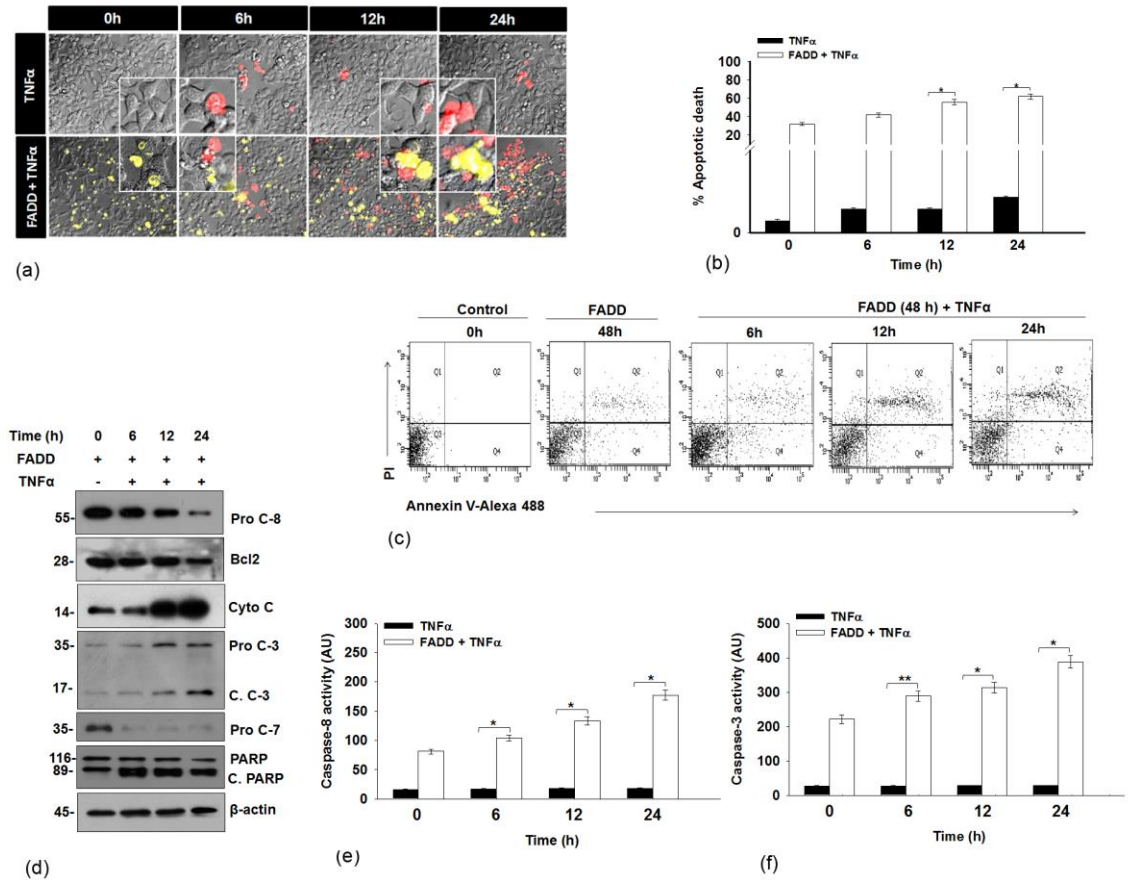

Figure 33. FADD augments downstream apoptosis signaling in TNF-α stimulated cells. HEK 293T cells were treated as mentioned in figure legend 32. (a) Propidium iodide (PI) staining (pEYFP-FADD construct was used in this experiment) (b) Percent apoptotic death by Tali™ cytometer, (c) Flow cytometric analysis (d) Western blotting of mentioned proteins, (e) caspase-8 activity, (f) caspase-3 activity. More than 150 cells from three random field were selected, scale bar- 2 µm. Error bars represent mean±SD, *P ≤0.05, **P ≤0.01 n ≥ 3, where n is number of independent experiment.

3.3.2 FADD inhibits NF-κB activation with subsequent ablation of $cFLIP_L$

Indeed, TNF-α induced activation of NF-κB signaling renders apoptosis by up regulating the anti-apoptotic genes such as *cIAPs, XIAPs* and *cFLIP* etc. (Karin and Lin, 2002). Moreover, the cFLIP is a known modulator of NF-κB activation and extrinsic signaling of apoptosis (Golks et al., 2006; Micheau et al., 2001). The above mentioned results showed that induced expression of FADD regulated the expression of $cFLIP_L$ and restricts its binding at the DISC. Now, it was important to examine the involvement of FADD in regulation of anti-apoptotic signaling of NF-κB in TNF-α stimulated cells. To achieve this aim, the pcDNA3.1-FADD was transfected into HEK 293T, HCT 116 and MCF-7 cells and incubated for 48 h followed by stimulation with TNF-α and the results were compared with vector transfected cells stimulated with TNF-α. The results show that induced expression of FADD in HEK 293T cells downregulates the cytosolic expression of NF-κB subunit p65 and $cFLIP_L$ as the time progresses from 48 h onwards (Figure 34a). Next, HEK 293T cells were exposed to TNF-α for 6-24 h and the activation of NF-κB and expression of $cFLIP_L$ were examined. As expected, expression of NF-κB subunit p65 canonically up regulated in response to TNF-α; in contrast, a moderate change was observed in the level of $cFLIP_L$ (Figure 34b). Surprisingly, exposure of TNF-α to 48 h of FADD expressed HEK 293T, MCF-7 and HCT 116 cells were not able to canonically protect the expression of p65 and $cFLIP_L$ (Figure 34c-e). Similarly the NF-κB luciferase reporter assay in HEK 293T, MCF-7 and HCT 116 cells showed that FADD abolishes NF-κB activation, independent of TNF-α stimulation (Figure 34f-h). Altogether, these results indicate that $cFLIP_L$ acts as an essential component for strengthening NF-κB signalling, but FADD has the enormous potential to abrogate NF-κB activation and $cFLIP_L$ expression, independent of TNF-α stimulation (Ranjan and Pathak, Sci. Rep., 2016).

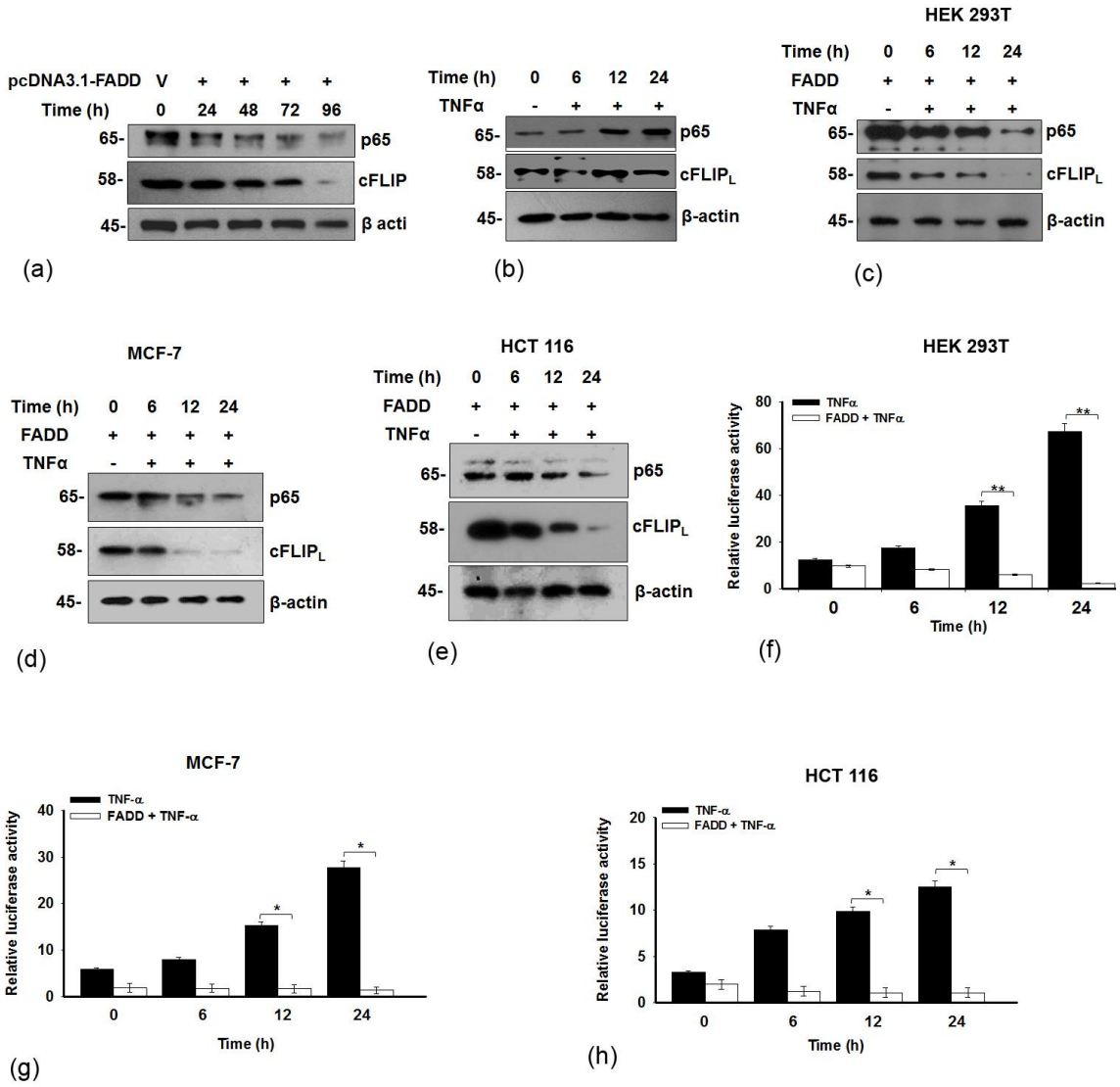

Figure 34. Induced expression of FADD inhibits NF-κB activation, independent of TNF-α stimulation. (a) HEK 293T cells were transfected with pcDNA3.1-FADD and expressed for 24-96 h, control represents vector (V) transfected cells. Expression of p65 and cFLIP$_L$. (b) HEK 293T cells exposed to TNF-α (10 ng/ml) for 6-24 h, control represents TNF-α untreated cells (shown as 0 h time point), Expression of p65 and cFLIP$_L$. The 48 h of pcDNA-FADD transfected (c) HEK 293T, (d) MCF-7, (e) HCT 116 cell; subjected to TNF-α (10 ng/ml) treatment for an additional 6-24 h. Control represents cells without TNF-α treatment (black bar) and 48 h pcDNA-FADD transfected HEK 293T cells (white bar) (shown as 0 h time point). Expression of p65 and cFLIP$_L$, cells were treated as mentioned in c-e and NF-κB Luciferase reporter assay in (f) HEK 293T, (g) MCF-7 and (h) HCT 116. Error bars represent mean±SEM from three independent experiments. The P value indicates *P≤0.05, **P≤0.001, control vs. experimental cells (n ≥ 3, where n is the number of independent experiments).

3.3.3 FADD ubiquitinates IKKβ to stabilize IκBα expression

In response to TNF-α, the NF-κB subunit p65 translocates from cytosol to nucleus and induces the transcription of anti-apoptotic proteins cIAPs, XIAPs and $cFLIP_L$ (Dempsey et al., 2003). In contrast, the cytosolic protein IκBα sequesters p65 within cytoplasm and restricts their nuclear translocation in various cancer cells (Ea et al., 2006). Interestingly, the kinase IKKβ degrade IκBα during NF-κB activation to release p65 followed by its nuclear translocation (Marques-Fernandez et al., 2013; Ea et al., 2006; Wang et al., 2008). The results shown above, highlights the potential of FADD mediated ablation of p65 expression in different origin of transformed and cancer cells. Next, it was important to investigate whether FADD has a potential to modulate IKKβ expression. The results show that exposure of TNF-α to HEK 293T has no major effect on the integrity of IKKβ; however, induced expression of FADD ubiquitinate and degrade IKKβ (Figure 35). Thus, these findings demonstrate that FADD ubiquitinates IKKβ to stabilize IκBα that restricts nuclear translocation and expression of p65 for NF-kB activation (Ranjan and Pathak, Sci. Rep., 2016).

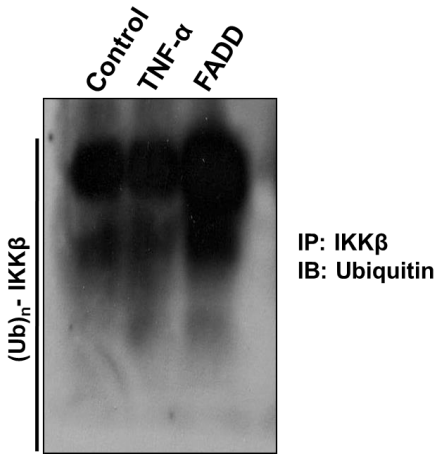

Figure 35. FADD ubiquitinate IKKβ. HEK 293T cells exposed to TNF-α (10 ng/ml) for 12 h (lane 2), transfected with pcDNA3.1-FADD for 48 h (lane 3), and control represents vector transfected cells untreated with TNF-α. Post incubation, the total cell lysate were subjected to Co-immunoprecipitation assay with anti-IKKβ antibody followed by Western blot with anti-ubiquitin antibody. IP-immunoprecipitation; IB-Immunoblotting.

3.3.4 Knockdown of cFLIP$_L$ mitigates NF-κB activation

Earlier reports suggest that, TNF-α mediated activation of transcription factor NF-κB translocate the p65 subunit to the nucleus and orchestrate the activation of anti-apoptotic protein cFLIP and Bcl-2 (Karin and Lin, 2002; Kreuz et al., 2001; Micheau and Tschopp, 2003). Interestingly, the elevated expression of cFLIP may activate NF-κB signaling to promote cell survival and malignancy (Golks et al., 2006). However, the direct evidence on cFLIP$_L$ mediate regulation of NF-κB signaling and downstream consequences of cell death and survival remains elusive. To achieve this aim, the expression of cFLIP$_L$ was transiently silenced by siRNA followed by evaluation of NF-κB activity. The results show that, selective knockdown of cFLIP$_L$ (cFLIP$_L^{KD}$) alters GFP-p65 nuclear translocation, p65 expression and NF-κB luciferase activity as compared to TNF-α (NF-κB inducer) stimulated cells; moreover the priming of TNF-α fails to protect the expression and activity of NF-κB in cFLIP$_L$ knockdown cells (Figure 36a-c) (Ranjan and Pathak, Sci. Rep., 2016).

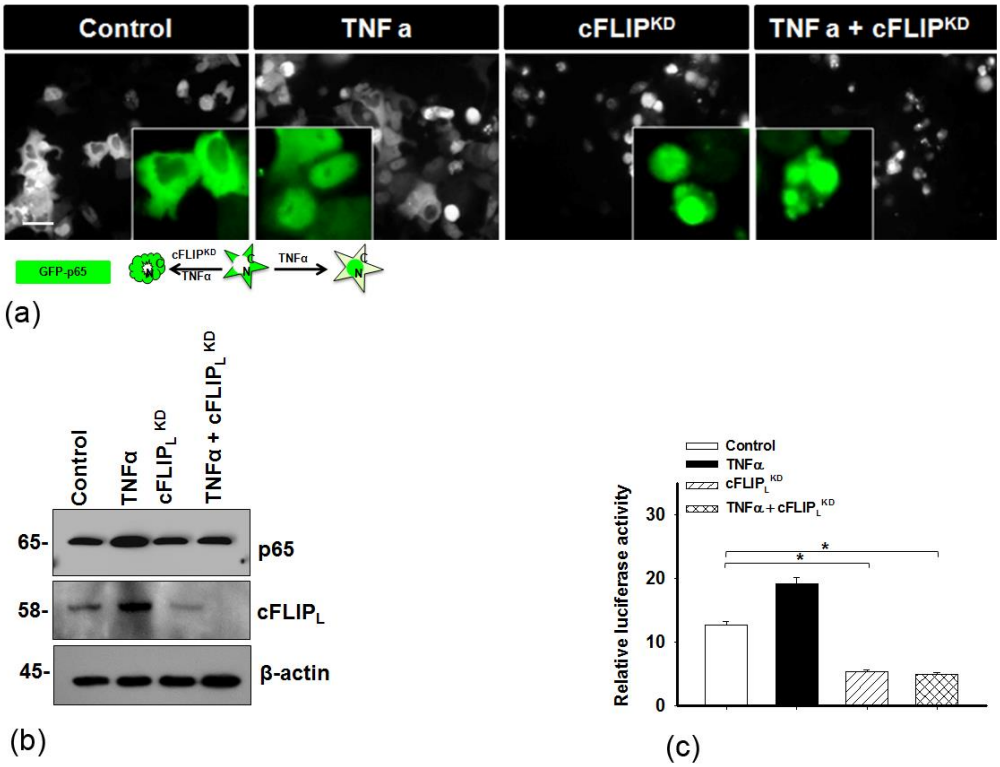

Figure 36. Knockdown of cFLIP$_L$ mitigates NF-κB activation. The HEK 293T cells were subjected to TNF-α (10 ng/ml) treatment for 12 h (lane 2), transfected with siRNA directed against cFLIP$_L$ (cFLIP$_L^{KD}$; lane 3) for 48 h and TNF-α (10 ng/ml) primed (12 h) cells transfected with siRNA against cFLIP$_L$ (TNF-α + cFLIP$_L^{KD}$; *lane 4*) for an additional 48 h to monitor, (a) GFP-p65 translocation assay, (b) representative Western blot images of 965 and cFLIP$_L$ and (c) NF-κB luciferase activity. Error bars represent mean ±SD, the P values represents *P ≤0.05 (student t-test, n ≥ 3, where n is the number of independent experiments).

3.3.5 Mutations in the DED domains of FADD and cFLIP$_L$ modulates NF-κB signaling

Next, the domain specific mutants of FADD and cFLIP$_L$ (Figure 37a) were expressed in HEK 293T cells to monitor NF-κB activity and cFLIP$_L$ expression. The results show that, expression of FADD-DD (FADD without DED) and FADD-SLT2 (inactive DED (Tungteakkhun et al., 2008)) provokes NF-κB activity, which is comparable to the p65 and wt cFLIP$_L$ expressed cells. This suggests that DD of FADD interact with a DD of death receptor to block downstream cell death signaling to support pro-survival NF-κB signaling (Figure 37b). Notably, mutant FLIP (DM-FLIP (Thurau et al., 2006)) did not show major changes in NF-κB activity, p65 and cFLIP$_L$ expression as compared to wt cFLIP$_L$ and p65 expressed cells (Figure 37c-d). Moreover, the mutants showed no remarkable alteration on cell viability as compared to the cells expressing death inducer IκBα (Figure 37d). Altogether, these results suggest that integrity of individual domains of FADD and cFLIP$_L$ were essentially required to regulate NF-κB activation and cellular response (Ranjan and Pathak, Sci. Rep., 2016).

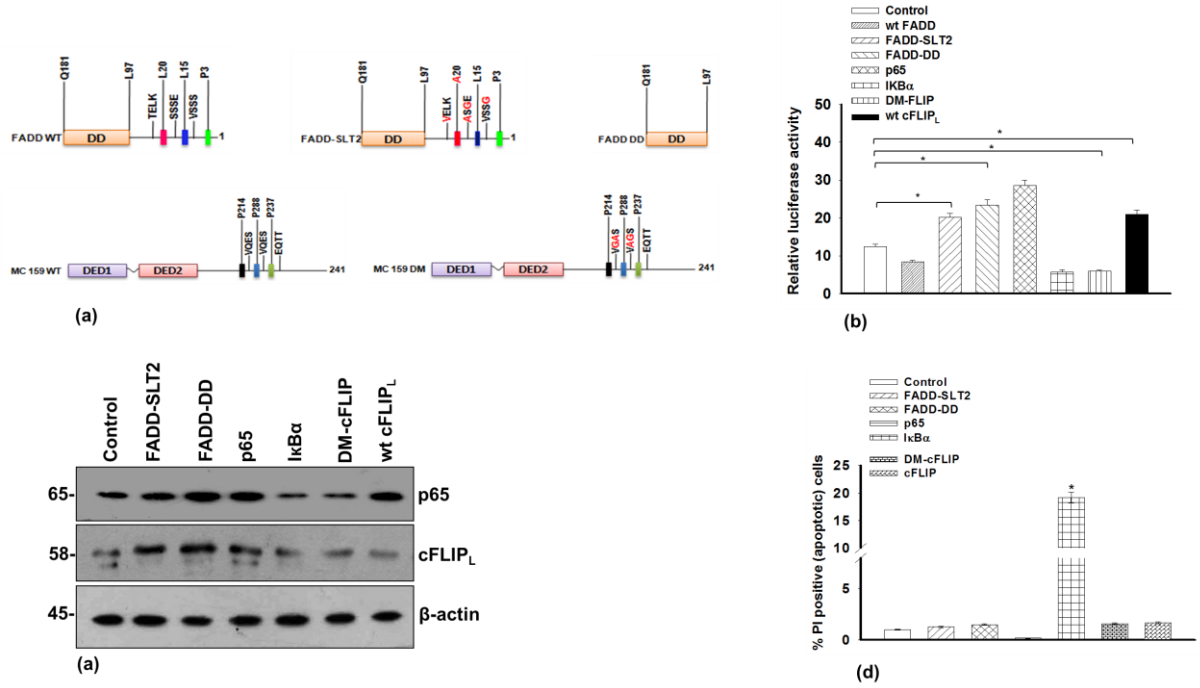

Figure 37. Mutation of specific amino acids in the FADD and cFLIP$_L$ modulates NF-κB activity. (a) Schematic diagram of pcDNA3.1-FADD wild type (WT), mutated FADD (FADD-SLT2; S14G, S16A, S18G, L20A and T21V), death domain (DD) of the FADD (FADD without DED), pLXSN-cFLIP$_L$ WT, pCR3-MC 159 WT and mutated MC159 (FLIP-DM; an analogous of cFLIP$_L$ unable to activate NF-κB signaling), all mutating sites are marked in red. HEK 293T cells were transfected with mentioned plasmids (wt FADD, FADD-SLT2, FADD-DD, wt pEGFP-p65, pECFP-IKBα, FLIP-DM and wt cFLIP$_L$). After 48 h, cells were harvested to monitor the (b) NF-κB luciferase reporter activity and (c) The expression of p65 and cFLIP$_L$ and (d) % PI positive cells, control represents vector transfected cells. Error bars represent mean ±SD, The P value indicates *P ≤0.05, (student t-test, n ≥ 3, where n is the number of independent experiments).

3.3.6 FADD interacts with RIP1 by inhibiting the expression of cIAP2

Although, stimulation of TNF-α rapidly initiates formation of complex I for NF-κB activation and cell survival; however, in the absence of NF-κB activation TNF-α signaling also triggers downstream extrinsic apoptosis *via* formation of complex II (Micheau and Tschopp, 2003). Indeed, the formation of pro-apoptotic complex II between FADD, RIP1 and procaspase-8 remains under the vigilance of anti-apoptotic proteins cIAPs and cFLIP (Feoktistova et al., 2011; Micheau and Tschopp, 2003; Tenev et al., 2011). Therefore, next, it was important to investigate the involvement of FADD in the regulation of cIAPs (Figure 38a). The results show that transient expression of FADD remarkably reduces the expression of cIAP2 in HEK 293T cells (Figure 38b & c). Next, the co-immunoprecipitation analysis of FADD and RIP1 showed that mitigating the expression of cIAP2 propels interaction of RIP1 with FADD (Figure 38d). Altogether, induced expression of FADD suppresses the anti-apoptotic expression of cIAP2 to favour RIP1 dependent complex II formation (Ranjan and Pathak, Sci. Rep., 2016).

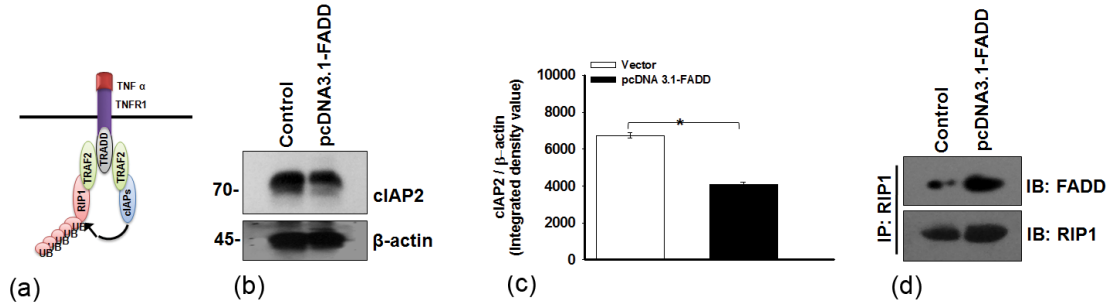

Figure 38. FADD abrogates cIAP2 expression and interacts with RIP1 and procaspases-8. (a) Illustration represents cIAPs mediated regulation of RIP1 at complex I. (b) HEK 293T cells were transfected with pcDNA3.1-FADD for 48 h and then cells were harvested and subjected to Western blot analysis to examine the expression of cIAP2 and (c) Densitometry (IDV- Integrated density value) of cIAP2 immunoblot, (d) Co-immunoprecipitation analysis of FADD and RIP1 in 48 h of FADD transfected HEK 293T cells. Control represents vector (pcDNA3.1) transfected cells. Error bars represent mean ±SD, The P value indicates *P ≤0.05, (student t-test, n ≥ 3, where n is the number of independent experiments).

3.3.7 FADD stabilizes the integrity of RIP1

Previously, it has been shown that, cIAPs mediated ubiquitination of RIP1 tightly regulate the formation of RIP1 mediated pro-apoptotic complex II (Ofengeim and Yuan, 2013). In this context, the results shown above indicate that FADD represses cIAP2 expression and favors RIP1 binding to FADD. Next, it was important to investigate the in-depth mechanism of FADD association with RIP1. To achieve this aim, the ubiquitination of RIP1 in TNF-α and FADD expressed cells stimulated with TNF-α were examined. As anticipated, TNF-α stimulation instigates degradation of RIP1 as observed by smearing and laddering pattern with the progression of time from 6 h onwards (Figure 39a). In contrast, induced

expression of FADD downregulates the mRNA levels of cIAP2 and reduces the degradation of RIP1, which indicates that FADD protects RIP1 even in the presence of TNF-α with subsequent activation of procaspase-8 (Figure 39b & c). In addition, transient expression of FADD in HEK 293T cells showing upregulated mRNA expression of RIP1, independent of TNF-α stimulation (Figure 39d) (Ranjan and Pathak, Sci. Rep., 2016).

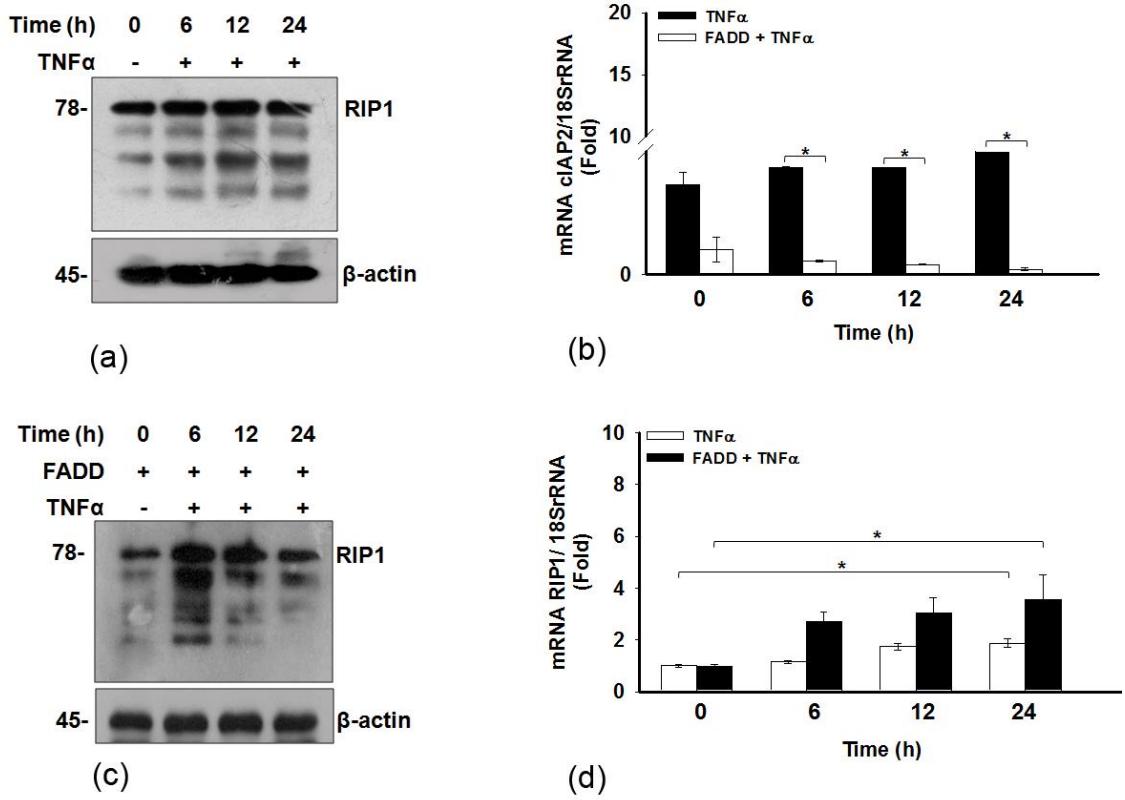

Figure 39. FADD protects RIP1 integrity. HEK 293T and pcDNA-FADD expressed HEK 293T cells were treated with TNF-α for 6-24 h, control represents untreated (white bar) and 48 h of FADD expresses cells (black bar), post incubations (a) Western blot of RIP1 in TNF-α treated cells, (b) mRNA expression of cIAP2, (c) Western blot of RIP1 in 48 h of FADD expressed cells treated with TNF-α and (d) mRNA expression of RIP1. Error bars represent mean ±SD, The P value indicates *P ≤0.05, (student t-test, n ≥ 3, where n is the number of independent experiments).

3.3.8 *In silico* binding interaction of FADD and RIP1

Furthermore, the in-depth analysis of FADD driven stability to RIP1 and their binding interaction was analyzed by *in silco* approach. The molecular models of DD of FADD (FADD-DD) (red) and RIP1-DD (green) were constructed and molecular docking was performed by GRAMMX software (Tovchigrechko and Vakser, 2006). *In silico* analysis of protein-protein interaction (PPI) suggests that involvement of a large number of hydrogen bonding along with other intermolecular interactions (such as electrostatic and vanderwaals) and larger contact interface provides a strong confirmation stability and

specificity towards molecular recognition of FADD-DD by RIP1-DD and *vice –versa* (Figure 40a & b) (Ranjan and Pathak, Sci. Rep., 2016).

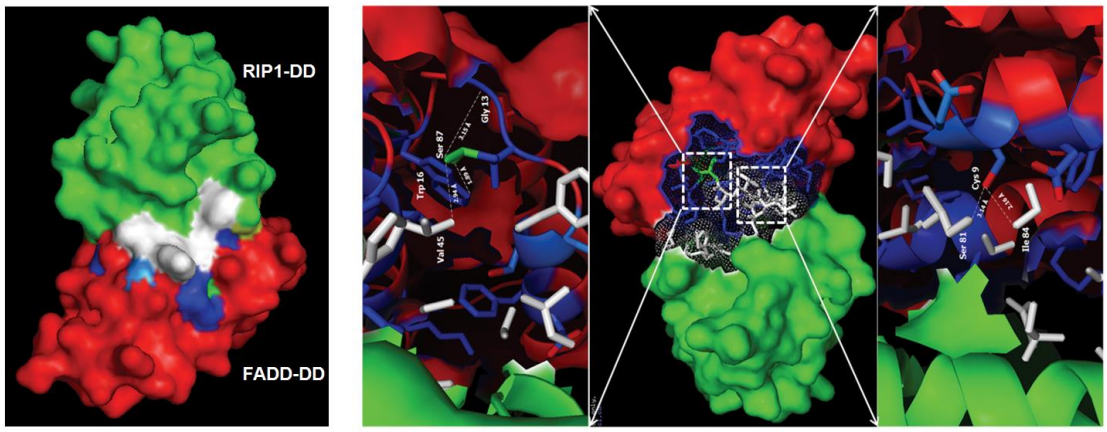

Figure 40. *In silico* molecular docking between death domains (DD) of FADD and RIP1. (a) The possible interaction of FADD-RIP1 shown by the molecular docking model, (b) FADD-RIP1 interaction represents that Trp16 and Val45 were located on α2 and α4 helix of FADD-DD respectively and interacts with Ser 87 located on the α5 helices of RIP 1 DD; Cys9 located on α1 helix of FADD-DD interacts with Ser81 and Ile84 located on α5 helices of RIP 1-DD, H-bond in angstrom (Å) denoted with lines.

3.3.9 FADD and cFLIP$_L$ synergistically regulates NF-κB signaling and RIP1 interaction with procaspase-8

Next, it was important to investigate the effect of co-alteration in the expression of FADD and cFLIP$_L$ on NF-κB activation. The HEK 293T cells were co-expressed with FADD and siRNA against cFLIP$_L$ and the expression of p65, cFLIP$_L$ and NF-κB Luciferase reporter activity was monitored. The results suggest that silencing of cFLIP$_L$ negatively act on the expression of p65 and NF-κB activity (cFLIP$_L^{KD}$; lane 3), and the effect was more radical upon cFLIP$_L$ knockdown in FADD expressed HEK 293T cells (FADD + cFLIP$_L^{KD}$; lane 4) (Figure 41a-c). Moreover, the co-immunoprecipitation assay suggest that altering the expression of cFLIP$_L$ facilitates interaction of FADD and procaspases-8 with RIP1 to form pro-apoptotic complex II (Figure 41d). Altogether, these results indicate that FADD and cFLIP$_L$ are essential to regulate NF-κB signaling and RIP1 associated complex II formation to commence apoptotic cell death (Ranjan and Pathak, Sci. Rep., 2016).

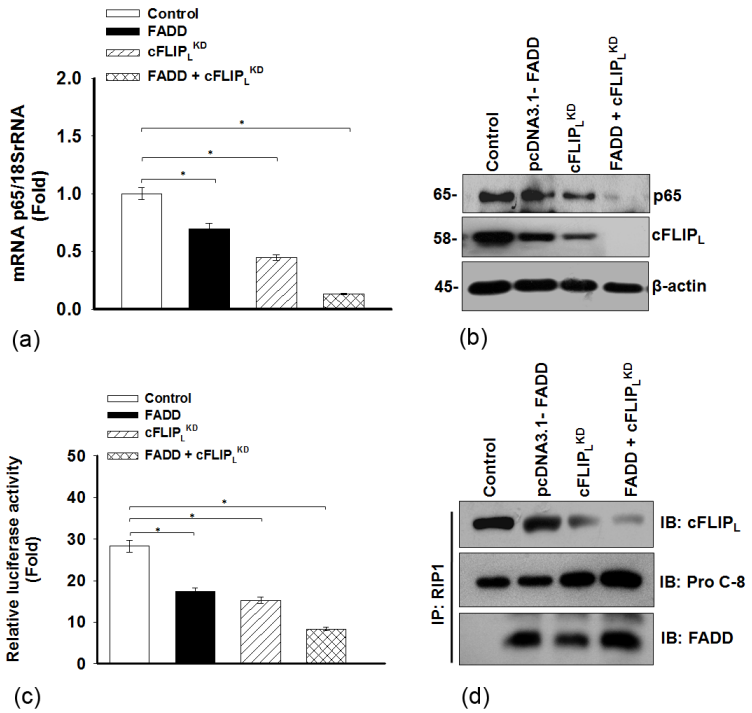

Figure 41. FADD and cFLIP$_L$ synergistically regulates NF-κB signaling. HEK 293T cells transfected with pEYFP-FADD (lane 2), siRNA directed against cFLIP$_L$ (cFLIP$_L^{KD}$; lane 3) and pEYFP-FADD with cFLIP$_L^{KD}$ (FADD + cFLIP$_L^{KD}$; lane 4), control represents vector and nontargeting siRNA transfected cells (lane1) for 48 h, post incubation; (a) RT-qPCR of p65, (b) expression of p65 and cFLIP$_L$, (c) NF-κB luciferase reporter assay and (d) Co-immunoprecipitation assay RIP1 with mentioned protein followed by Western blotting. *P ≤0.05, (student t-test, n ≥ 3) where n is the number of independent experiments. IP-Immunoprecipitation; IB-immunoblotting.

3.3.10 Knockdown of cFLIP$_L$ facilitates RIP1 to form complex with FADD

The anti-apoptotic protein cFLIP$_L$ regulates the formation of RIP1 and FADD associated complex II in order to suppress apoptoic commencement (Tenev et al., 2011). As shown above, knockdown of cFLIP$_L$ regulates NF-κB activation and augments apoptotic cell death, independent of death receptor stimulation. Next, it was important to investigate the involvement of cFLIP$_L$ in the regulation of RIP1 dependent proapoptotic complex II formation. The HEK 293T cells were stimulated with TNF-α to stabilize complex I and further knockdown the expression of cFLIP$_L$. It was noticed that transient silencing of cFLIP$_L$ favors RIP1-FADD interaction *(lane 3).* Interestingly, priming of TNF-α with simultaneous knockdown of cFLIP$_L$ *(lane 4)* profoundly drive FADD-RIP1-procaspase-8 associated complex II formation (Figure 42a). Thus, above results suggest that relieving the expression of cFLIP$_L$ facilitates RIP1 to interact with FADD and procaspase-8 (Ranjan and Pathak, Sci. Rep., 2016).

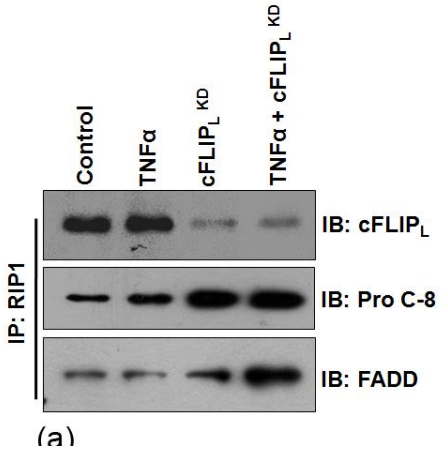

Figure 42. Knockdown of cFLIP$_L$ facilitates RIP1-FADD complex formation. The HEK 293T cells were subjected to TNF-α (10 ng/ml) treatment for 12 h (lane 2), transfected with siRNA directed against cFLIP$_L$ (cFLIP$_L^{KD}$; lane 3) for 48 h and TNF-α (10 ng/ml) primed (12 h) cells transfected with siRNA against cFLIP$_L$ (TNF-α + cFLIP$_L^{KD}$; *lane 4*) for an additional 48 h to monitor, (a) The total cell lysate was subjected to co-immunoprecipitation assay for the analysis of RIP1 interaction with FADD and procaspases-8. IP-immunoprecipitation; IB-Immunoblotting.

3.3.11 FADD augments apoptosis rather than necrosis

An earlier report states the involvement of TNF-α in necrotic cell death (Festjens et al., 2007). Hence, the involvement of necropoptotic cell death was also analyzed in FADD expressed cells stimulated with TNF-α. The HEK 293T cells were pre-incubated with Necrostatin-1 (an inhibitor of necroptosis) to rule out the possibilities of endogenous necroptosis. Necrostatin-1 treated cells were transfected with pcDNA3.1-FADD followed by the stimulation with TNF-α. There was no any remarkable release of LDH (a marker of necrosis) found in FADD expressed cells stimulated with TNF-α form 6-24 h as cpmoared to TNF-α and Necrostatin-1 treatrd cells (Figure 43a). Moreover, the cleavage pattern of PARP was observed in FADD transfected cells exposed with TNF-α and Necrostatin-1. These results clearly indicate that mode of cell death with the aid of FADD was apoptosis rather than necrotic (Figure 43b) (Ranjan and Pathak, Sci. Rep., 2016).

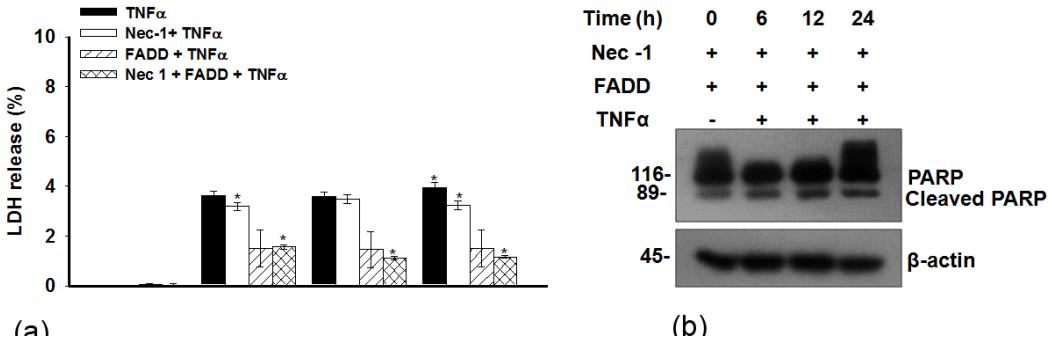

Figure 43. FADD augments apoptotic death rather than necropotosis in TNF-α stimulated cells. HEK 293T cells were pretreated with Necrostatin-1 (20μM) for 18 h and further stimulated with TNF-α (10 ng/ml) in HEK 293T and 48 h of pcDNA-FADD expressed HEK 293T cells to monitor (a) Percent LDH release and, (b) Cells were lyzed and the activation of PARP was monitored by Western blot analysis. Control represents untreated and FADD expressed cells for 48 h (shown as 0 min time). Error bars represent mean±SD, *P ≤0.05, n ≥ 3, where n is number of independent experiment.

3.3.12 FADD promotes ROS accumulation and JNK1 mediated ubiqutination of cFLIP$_L$

Some previous studies have shown that, the suppression of NF-κB and cFLIP accumulate cellular ROS and activates JNK1 dependent cell death (Lin, 2003; Nakano, 2004; Shen and Liu, 2006). Moreover, activation of JNK1 has been shown to regulate the turnover of cFLIP$_L$ by activating ubiquitin ligase ITCH (Chang et al., 2006). Therefore, it was important to investigate the underlying mechanism of FADD mediated regulation of cFLIP$_L$ in HEK 293T cells. The results show that induced expression of FADD accumulates intracellular ROS with the simultaneous activation of JNK1 and E3 ubiquitin ligase ITCH (Figure 44a & b). Moreover, FADD induces time dependent ubiqutination of cFLIP$_L$ and strongly interacts with RIP1 (Figure 44c). Altogether, these findings can be co-related with above shown results of successive loss of cFLIP$_L$ at DISC in FADD expressed cells (Ranjan and Pathak, Sci. Rep., 2016).

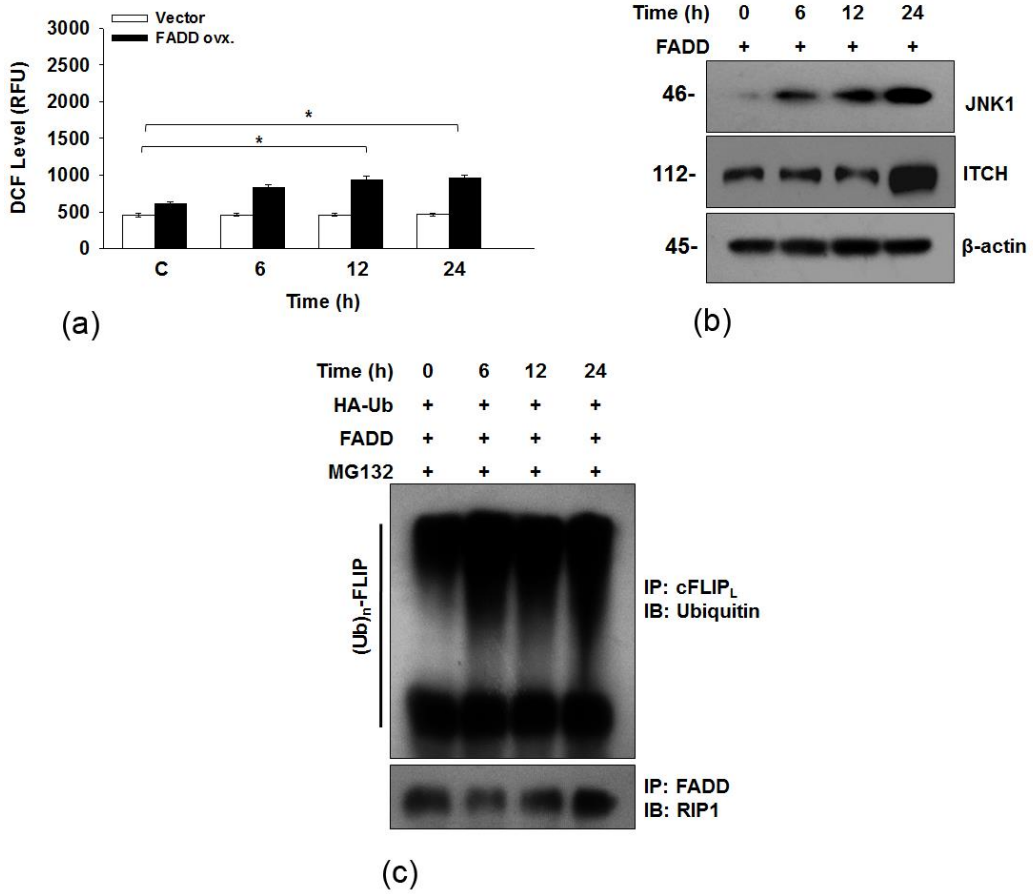

Figure 44. FADD triggers JNK1 mediate ubiquitination of cFLIP$_L$. (a) HEK 293T cells were transfected with pcDNA3.1-FADD for 48 h and furher incubated for a additional 6-24 h, control represents 48 h of FADD (shown as 0 h time point) expressed cells, to examine the cellular ROS, (b) Expression of JNK1 and ITCH and (c) The ubiquitination of cFLIP$_L$ in MG132 (10 μM for 3 h) pre-treated cells subjected to co-immunoprecipitation analysis. From the same cell lysate the co-imunoprecipitation of FADD with RIP1 was carried out. Error bars represent mean ±SD, The P value indicates *P ≤0.05, (student t-test, n ≥ 3, where n is the number of independent experiments).

3.3.13 Expression of FADD and cFLIP$_L$ balances redox signaling

Earlier it was noticed that selective knockdown of cFLIP$_L$ (cFLIP$_L^{KD}$) accumulates cellular ROS and activates JNK1 to induce apoptosis signaling (Corda et al., 2001; Fiers et al., 1999; Shoji et al., 1995). As shown above induced expression of FADD provokes ROS accumulation and JNK1 dependent ubiquitination of cFLIP$_L$, next the study was directed to investigate the oxidative status and JNK1 expression upon simultaneous modulation of FADD and cFLIP$_L$ in HEK 293T cells. Interestingly, it was noticed that FADD overexpression together with cFLIP$_L^{KD}$ profoundly generates ROS and JNK1 activation in comparisons to individual incubations of FADD and siRNA of cFLIP$_L$ (Figure 45a & b). However, abolishing the generation of ROS by NAC pretreatment (ROS scavenger) restores the levels of ROS and expression of JNK1 (Figure 45c & d).

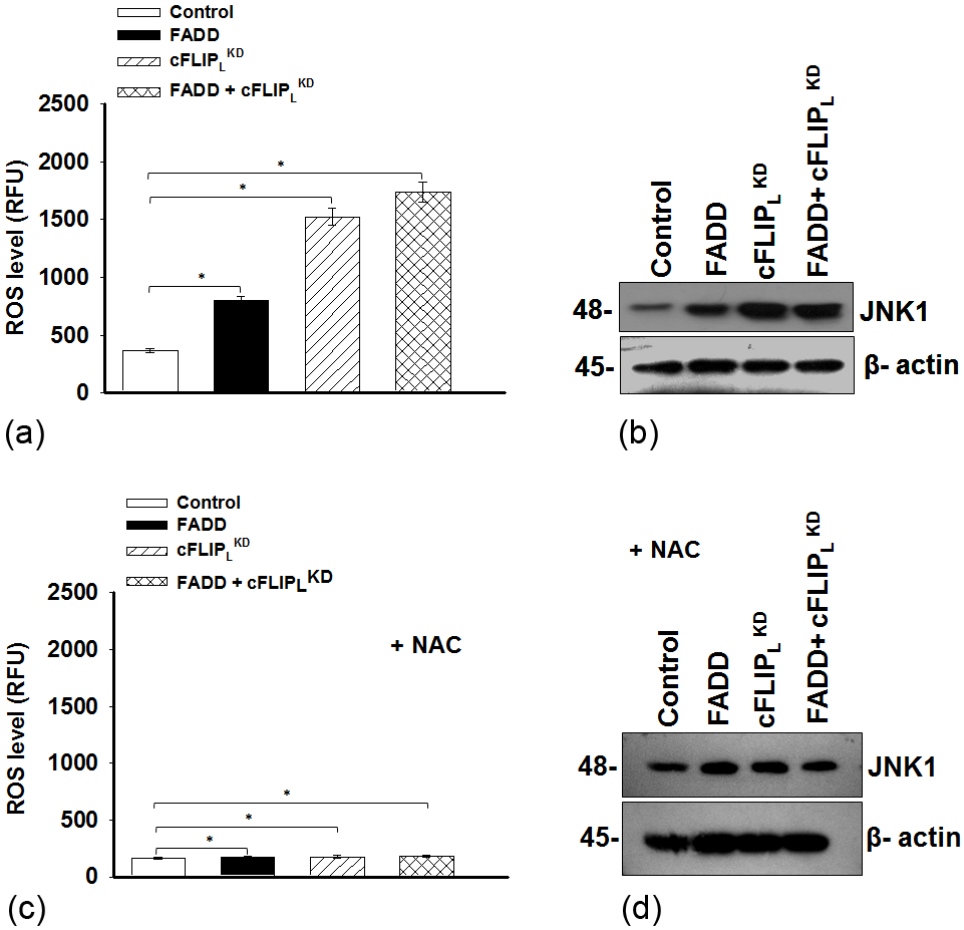

Figure 45. FADD and cFLIP$_L$ regulates oxidative stress and JNK1 expression. (a) HEK 293T cells were transfected with pcDNA3.1-FADD (lane 2), siRNA of cFLIP$_L$ (lane 3) and FADD + cFLIP$_L$ (lane 4) all incubation were for 48 h, control represents vector and non-targeting siRNA transfected cells, post incubation (a) measurement of intracellular ROS, (b) Expression of JNK1 and ITCH. The 48h pcDNA3.1-FADD transfected HEK 293T cells pre-treated with N-acetyl cysteine (NAC) (25μM for 3h) followed by treatment of TNF-α (10ng/ml) for mentioned time points and level of (c) cellular ROS and (d) Expression of JNK1 and ITCH. Error bars represent mean ±SD, The P value indicates *P ≤0.05, (student t-test, n ≥ 3, where n is the number of independent experiments).

3.3.14 FADD ubiquitinates cFLIP$_L$, independent of TNF-α stimulation

Furthermore, the potential of FADD in regulation of cFLIP$_L$ ubiquitination was confirmed in TNF-α treated HEK 293T and FADD expressed HEK 293T cells. The results show, that exposure of TNF-α alone to HEK 293T suppresses intracellular ROS and had a negligible effect on the expression of JNK1 and ubiquitin ligase ITCH (Figure 46a & b). Surprisingly, in FADD expressed cells the exposure of TNF-α elevated intracellular level of ROS with subsequent activation of JNK1 and ITCH mediated ubiquitination of cFLIP$_L$ (Figure 46c & d) (Ranjan & Pathak, Sci. Rep., 2016).

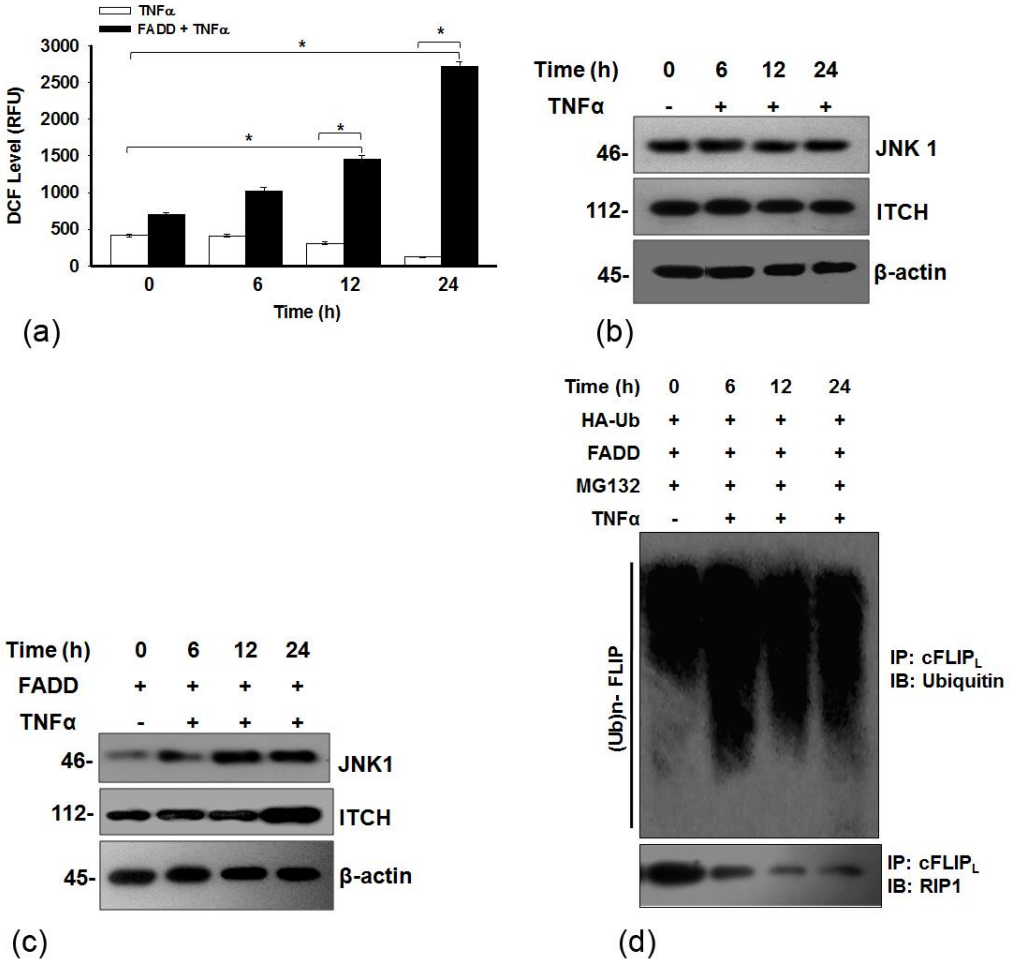

Figure 46. FADD triggers JNK1 mediate ubiquitination of cFLIP$_L$ in the presence of TNF-α. HEK 293T cells and 48 h of FADD expressed HEK 293T cells were treated with TNF-α (10 ng/ml) for mentioned time points, control represents vector transfected and untreated to TNF-α to monitor (a) cellular ROS, (b-c) Expression of JNK1 and ITCH and (d) The 48 h pcDNA3.1-FADD transfected HEK 293T cells pre-treated with MG132 (10 μM for 3 h) followed by treatment of TNF-α and subjected to Co-IP assay for monitoring the ubiquitination of cFLIP$_L$ and expression of RIP1. Error bars represent mean ±SD, The P value indicates *P ≤0.05, (student t-test, n ≥ 3, where n is the number of independent experiments).

3.3.15 Knockdown of cFLIP$_L$ triggers ROS dependent JNK1 activation

As the results shown above suggest that knockdown ofcFLIP$_L$ dismantle the integrity of NF-κB; next it was important to investigate the levels of ROS and JNK1 in cFLIPL$_L$ knockdown cells. The results show that, knockdown of cFLIP$_L$ in HEK 293T and TNF-α pre-stimulated HEK 293T cells triggers the accumulation of intracecellular ROS followed by JNK1 and ITCH activation (Figure 47a & b). In contrast, pre-treatment with NAC (potent ROS scavenger) followed by knockdown of cFLIP$_L$ has no effect on ROS alteration and JNK1 and ITCH expression (Figure 47c & d). Altogether, these results indicate that expression of cFLIP$_L$ is essential to balance the levels of ROS and JNK1 for cell survival (Ranjan & Pathak, Sci. Rep., 2016).

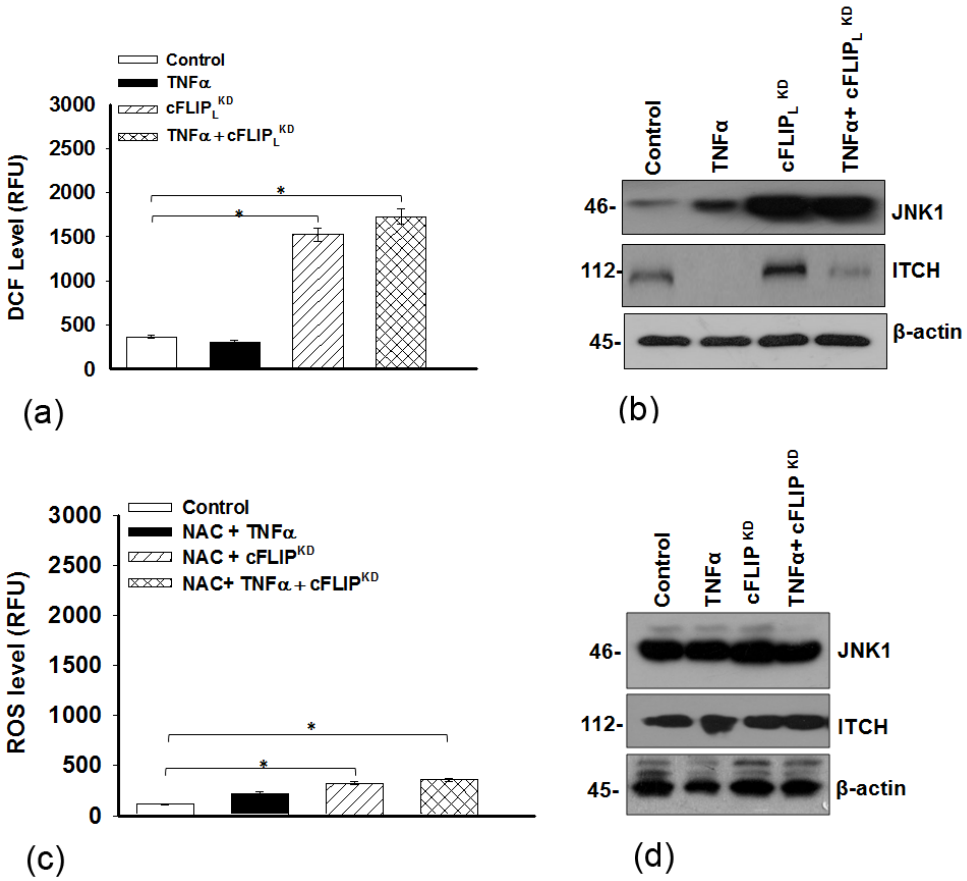

Figure 47. Knockdown of cFLIP$_L$ triggers ROS generation and JNK1 activation. The HEK 293T cells were subjected to TNF-α (10 ng/ml) treatment for 12 h (lane 2), transfected with siRNA directed against cFLIP$_L$ (cFLIP$_L^{KD}$; lane 3) for 48 h and TNF-α (10 ng/ml) primed (12 h) cells transfected with siRNA against cFLIP$_L$ (TNF-α + cFLIP$_L^{KD}$; lane 4) for an additional 48 h to monitor, (a) ROS measurement, (b) representative Western blot of JNK1 and ITCH. HEK 293T cells pre-treated with N-acetyl cysteine (NAC) (25μM for 3h) followed by treatment as mentioned in figure legend 47a, (c) ROS measurement, (d) representative Western blot of JNK1 and ITCH.. Error bars represent mean ±SD, the P values represents *P ≤0.05, (student t-test, n ≥ 3, where n is the number of independent experiments).

PART IV

3.4 FADD AND CFLIP$_L$ REGULATES AUTOPHAGY SIGNALING

3.4.1 FADD and cFLIP$_L$ regulates autophagic cell death

The interplay between autophagy and apoptosis is dependent on the extent of cellular stress. For instance, the homeostatic imbalance promptly triggers autophagy in cells, but prolonged stress may leads to cell death (Marino, 2014). Earlier reports states that, FADD in association with autophagic protein Atg5 commences cell death, whereas the nature of this induction remains uncertain (Thorburn et al., 2005; Bell et al., 2008; Pyo et al., 2005). In contrast, the cFLIP has been reported as a potent regulator of autophagy during viral and drug induced cellular stress (Li et al., 2009). However, the extent of FADD and cFLIP in the interplay between autophagy and apoptosis remains to be resolved clearly. To elucidate the role of FADD and cFLIP$_L$ in the selectivity over autophagy or apoptosis, the autophagic turnover followed by apoptosis commencement in FADD expressed and cFLIP$_L^{KD}$ were examined in HEK 293T cells. The result shows that, induced expression of FADD reduces the basal number of puncta and autophagic conversion of LC3-I to LC3-II. In contrast the cFLIP$_L^{KD}$ cells accumulate puncta formation and turnover of LC-3. Interestingly, upon simultaneous overexpression of FADD and cFLIP$_L^{KD}$ leads to formation of fused autophagosome and initiation cell death (Figure 48a-d). Thus, these results indicate that FADD expressed or cFLIP$_L$ knockdown cells induces autophagic stress at the initial level and later on subjected to apoptotic demise.

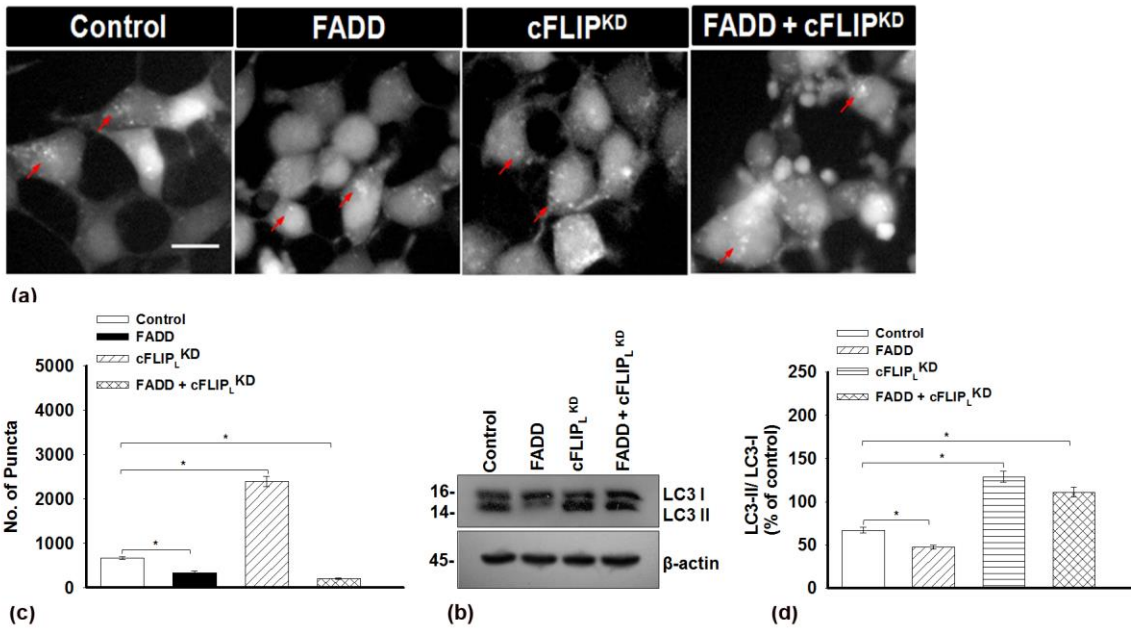

Figure 48. FADD and cFLIP$_L$ regulates autophagy signaling. The GFP-LC3 stable cells of HEK 293T cells were transfected with pcDNA-FADD (lane 2), siRNA targeted against cFLIP$_L$ (lane 3) and FADD + siRNA of cFLIP$_L$ (lane 4), vector transfected cells were taken as control (lane 1), post incubations (a) the induction of autophagic puncta was monitored under fluorescent microscope, more than 150 cells from three random fields were observed, scale bar- 5μm, (b) count of autophagic puncta per cell with the aid of Image J software, (c) representative Western blot images of LC-3 protein, (d) LC3-II/LC3-I turnover by densitometry. Error bars represent mean ±SD, the P values represents *P ≤0.05, (student t-test, n ≥ 3, where n is the number of independent experiments).

3.4.2 cFLIP$_L$ inhibits oxidative stress induced accumulation of HMGB1

An earlier report showed that the autophagy inducer Rapamycin triggers oxidative stress in cells and enforces translocation of nuclear bound HMGB1 to the cytosol to disrupt the interaction between Bcl-2 and Beclin-1 during the setting of autophagy (Tang et al., 2010a). Herein, the study was aimed to investigate the role of cFLIP$_L$ in maintaining the autophagic equilibrium during oxidative stress. First, the pLSXN-cFLIP$_L$ plamid was transfected into GFP-LC3 stable HEK 293T cells followed by exposure with rapamycin (100 nM) for an additional 3 h, and the outcomes were compared with vector transfected HEK 293T cells treated with rapamycin. It was noticed that treatment of rapamycin effectively induces the accumulation of autophagic puncta in HEK 293T cells, but unable to mount a similar stress in cFLIP$_L$ transfected cells (Figure 49a & b). Next, the autophagic turnover of LC3-I to LC3-II in both rapamycin treated and cFLIP$_L$ expressed cells treated with rapamycin by Western blotting. The results show that rapamycin treated cells induces turnover of LC3-I to LC3-II, however, cFLIP$_L$ overexpressed cells restrict rapamycin induced conversion of LC3-I to LC3-II. (Figure 49c & d**).** Subsequently, it was found that rapamycin treatment on HEK 293T cells generates intense autophagic vacuoles, however, cFLIP$_L$ transfected cells treated with rapamycin failed to retain its pro-autophagic activity (Figure 49e). In addition, the cytotoxic stress and apoptotic cell death during exposure of rapamycin in HEK 293T cells were also monitored. It was found that, ectopic expression of cFLIP$_L$ mitigates the cytotoxicity executed by rapamycin through retaining the viability of cells (Figure 50a & b). Moreover, the ectopic expression of cFLIP$_L$ mitigates rapamycin induced apoptotic stress, as confirmed by monitoring the mitochondrial membrane potential (MMP), Western blot analysis of PARP and FACS analysis (Figure 50c & d). Further, it was noticed that ectopic expression of cFLIP$_L$ surmounts rapamycin induced oxidative burden with subsequent inhibition of HMGB1 cytosolic accumulation, as compared to the vector transfected cells treated with rapamycin (Figure 51a-c). Next, the role of cFLIP$_L$ on maintaining the interaction of Bcl-2 with Beclin-1 upon rapamycin induced autophagic stress was examined. The results show that overexpression of cFLIP$_L$ precludes HMGB1 and retains a strong binding interaction of Bcl-2 with Beclin-1, independent of rapamycin treatment to resist autophagy induction

(Figure 51d). Thus, these results suggest that cFLIP$_L$ has an enormous potential to protect the cells against oxidative stress-induced autophagy. (Ranjan & Pathak, J. Cell. Biochem, 2016).

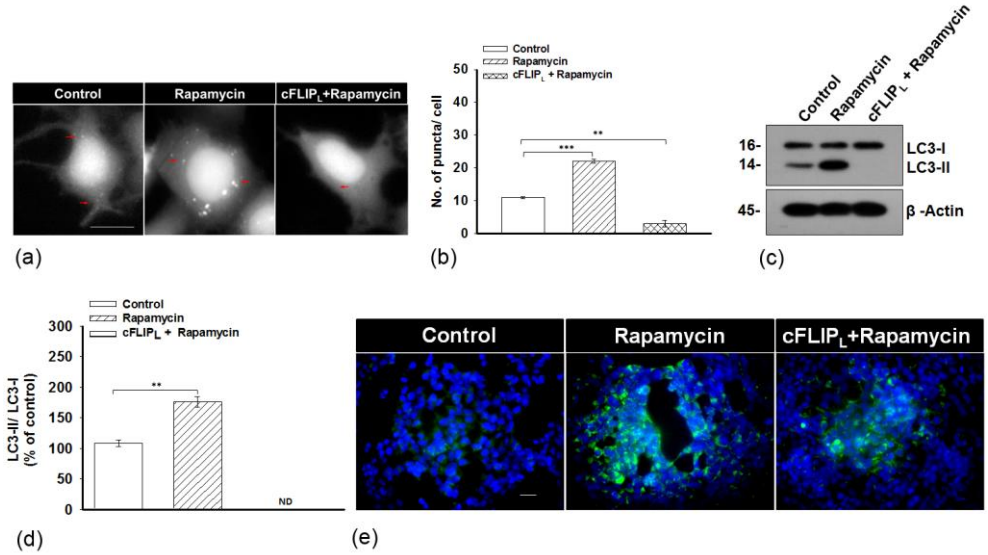

Figure 50. Ectopic expression of cFLIP$_L$ suppresses rapamycin induced autophagy. The GFP-LC3 stable cells of HEK 293T cells (lane 2) and pLSXN-cFLIP$_L$ expressed HEK 293T (48 h) cells (lane 3) were treated with rapamycin (100 nM) for 3 h, vector transfected cells untreated to rapamycin (lane 1) was taken as control, post incubations (a) the induction of autophagic puncta was monitored under fluorescent microscope, more than 150 cells from three random fields were observed, scale bar- 5 µm, (b) count of autophagic puncta per cell with the aid of Image J software, (c) representative Western blot images of LC-3 protein, (d) LC3-II/LC3-I turnover by densitometry and (e) Detection of autophagic vacuoles with Cyto ID Autophagy detection kit; scale bar- 2µm. Error bars represent mean ±SD, the P values represents **P ≤0.001, ***P ≤0.01 (student t-test, n ≥ 3, where n is the number of independent experiments).

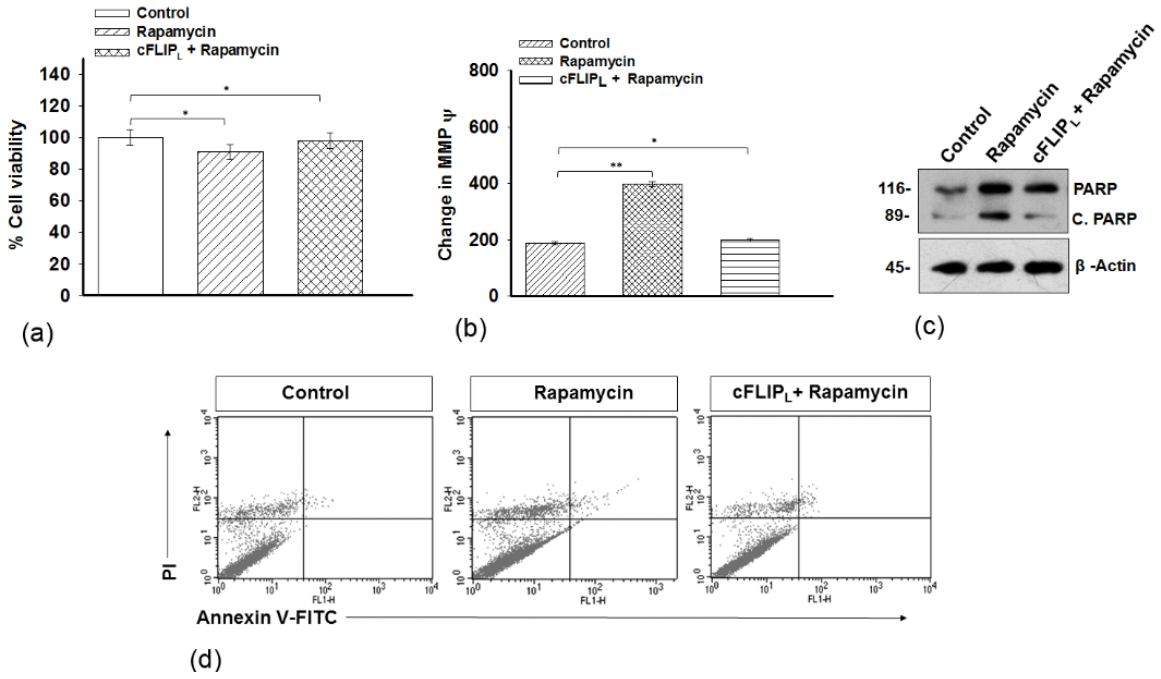

Figure 49. Induced expression of cFLIP$_L$ suppresses rapamycin induced cell death. The GFP-LC3 stable cells of HEK 293T cells were treated as mentioned in Fig. legend 49, post incubations (a) percent cell viability, (b) mitochondrial membrane potential (MMP) by JC-1 assay (c) Western blot images of PARP and (d) FACS analysis. Error bars represent mean ±SD, the P values represents *P ≤0.005, **P ≤0.01, (student t-test, n ≥ 3, where n is the number of independent experiments).

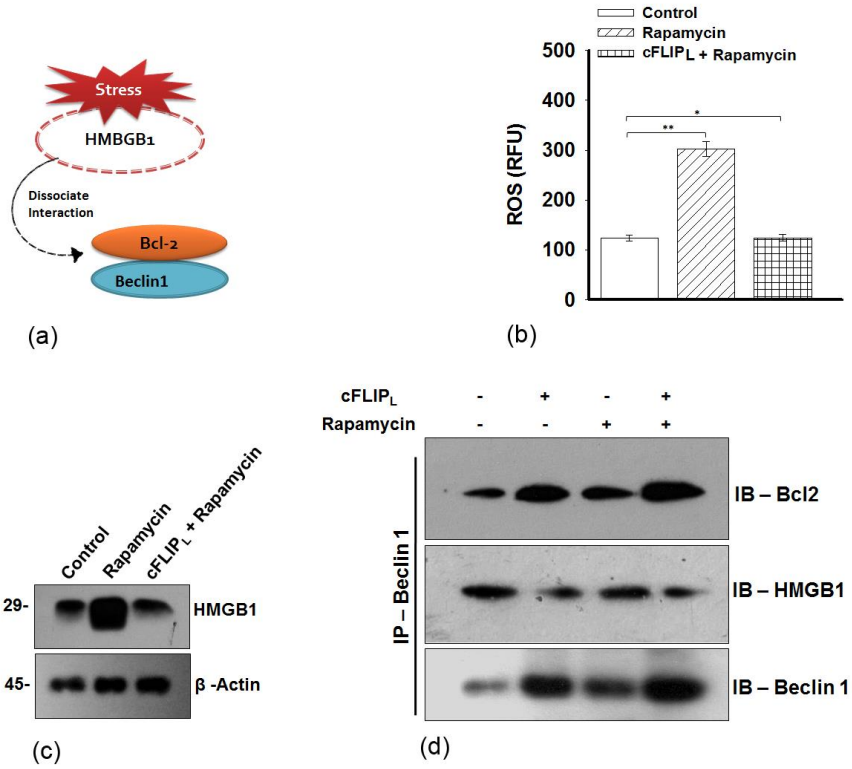

Figure 51. Expression of cFLIP$_L$ balances Bcl-2 interaction with Beclin-1. (a) Model representing stress induced disassociation of Bcl-2-Beclin1 interaction. The HEK 293T cells The GFP-LC3 stable cells of HEK 293T cells were treated as mentioned in Fig. legend 49, post incubations (b) level of intracellular ROS, (c) Western blot of HMGB1 and (d) the co-immunoprecipitation assay of Bcl-2, HMGB1 with Beclin-1. Error bars represent mean ±SD, the P values represents *P ≤0.005, **P ≤0.01, (student t-test, n ≥ 3, where n is the number of independent experiments).

3.4.3 Expression of cFLIP$_L$ balances autophagic stress

Apoptosis and autophagy are two distinct mechanisms of cell death and survival, which often occur in the same cell, but autophagy manifests for pro-survival well before apoptosis. However, blockade of apoptosis intensifies the process of autophagy concomitantly (Marino et al., 2014). Next, it was important to examine the cellular response of autophagy and apoptosis upon challenging the expression of cFLIP$_L$. The endogenous expression of cFLIP$_L$ (cFLIP$_L^{KD}$) was selectively knocked down by siRNA in GFP-LC3 stable HEK 293T cells and further cFLIP$_L$ was re-expressed in the cFLIP$_L^{KD}$ cells for an additional 48 h (Figure 52a-c). The results were compared with cFLIP$_L^{KD}$ in the presence of 3-MA (a potent autophagy suppressor). First, the cell viability and apoptotic signaling were monitored in cFLIP$_L^{KD}$ and cFLIP$_L$ re-expressed in the cFLIP$_L^{KD}$ cells. The results show that cFLIP$_L^{KD}$ challenges the viability of cells with concomitant loss of mitochondrial membrane potential (MMP), however re-expression of cFLIP$_L$ in the cFLIP$_L^{KD}$ cells regains the integrity of the cells as confirmed by monitoring the expression

of PARP and apoptotic death by FACS analysis (Figure 53a-d). Furthermore, it was found that, the $cFLIP_L^{KD}$ triggers a rapid accumulation of the autophagic puncta (middle panel) as compared to control (non-targeting siRNA transfected cells) (left panel); however the re-introduction of $cFLIP_L$ to $cFLIP_L^{KD}$ cells apparently mitigates autophagic stress and diminishes puncta formation (right panel) (Figure 54a & b). Further, the LC3 turnover was examined in $cFLIP_L^{KD}$ and re-expressed $cFLIP_L$ in $cFLIP_L^{KD}$ cells by Western blot analysis. The $cFLIP_L^{KD}$ shows a more autophagic turnover of LC3-I into LC3-II, but surprisingly re-expression of $cFLIP_L$ to knockdown cells the conversion ratio of LC3-II/LC3-1 were comparable to control and 3-MA treated cells (Figure 54c-f). In addition, it was noticed that $cFLIP_L^{KD}$ triggers the formation of autophagic vacuoles, but upon re-expressing $cFLIP_L$ to the $cFLIP_L^{KD}$ cells reduces the formation of autophagic vacuoles (Figure 54g). Thus, these results suggest that re-expression of $cFLIP_L$ in the $cFLIP_L^{KD}$ cells resist autophagosome fusion with lysosome to protect the HEK 293T cells from autophagic cell death. Altogether, results suggest that endogenous expression of $cFLIP_L$ protects cellular stress, as challenging the expression induces autophagic stress before commencement of apoptotic cell death (Ranjan & Pathak, J. Cell. Biochem, 2016).

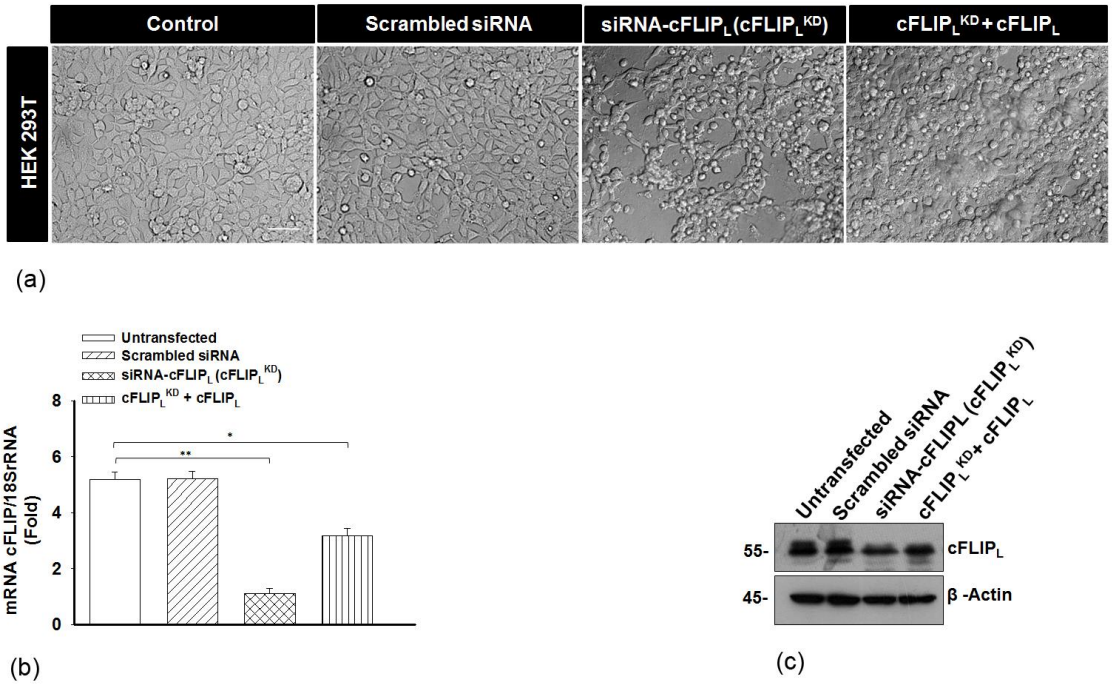

Figure 52. Knockdown of $cFLIP_L$ ($cFLIP_L^{KD}$) and re-expression of $cFLIP_L$ in $cFLIP_L^{KD}$ cells. The HEK 293T cells were transfected with siRNA directed against $cFLIP_L$ ($cFLIP_L^{KD}$, lane 3) (48 h) and re-introduction of pLXSN-$cFLIP_L$ in $cFLIP_L^{KD}$ HEK 293T cells ($cFLIP_L^{KD}$ + $cFLIP_L$, lane 4) for an additional 48 h, control represents non transfected cells (lane 1) and no-trageting siRNA transfected cells (lane 2), post incubation (a) Morphology of cells were analysed under microscope with DIC mode, more than 150 cells from three random fields were analysed, scale bar- 2µm. (b) mRNA expression of $cFLIP_L$, (c) Western blot analysis of $cFLIP_L$. Error bars represent mean ±SD, the P values represents *P ≤0.05, **P ≤0.01 (student t-test, n ≥ 3, where n is the number of independent experiments).

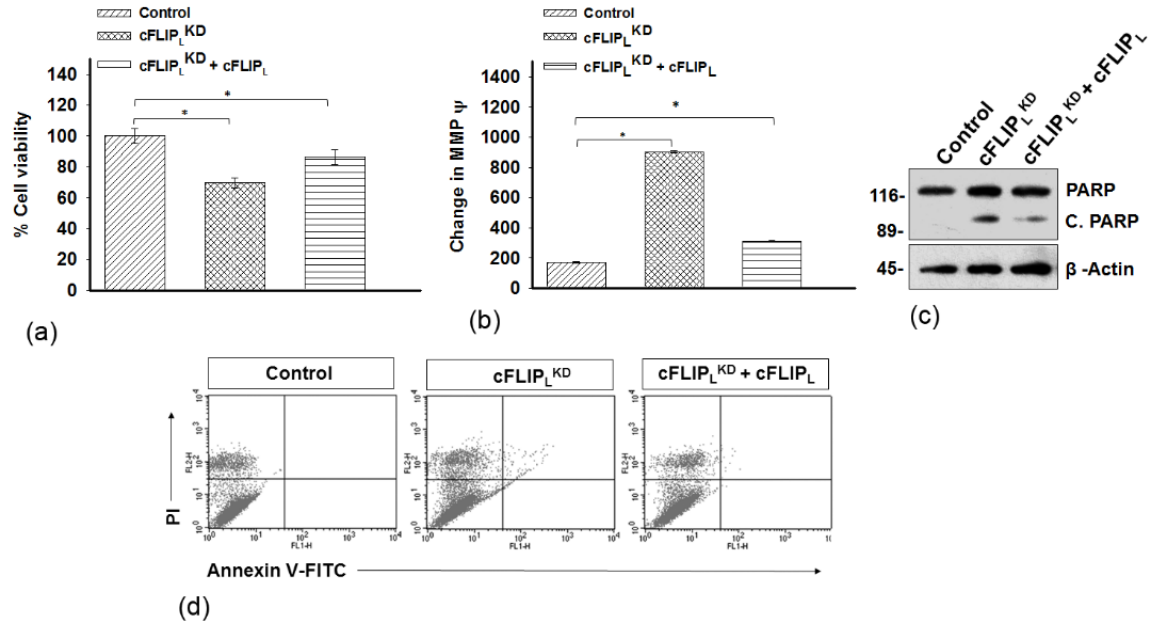

Figure 53. cFLIP$_L$ maintains cell viability. The HEK 293T cells were treated as mentioned in figure legend 52, control represents non-targeting siRNA transfected cells, post incubation, (a) percent cell viability, (b) JC-1 assay, (c) Western blotting of PARP and (d) FACS analysis, Error bars represent mean ±SD, the P values represents *P ≤0.05 (student t-test, n ≥ 3, where n is the number of independent experiments).

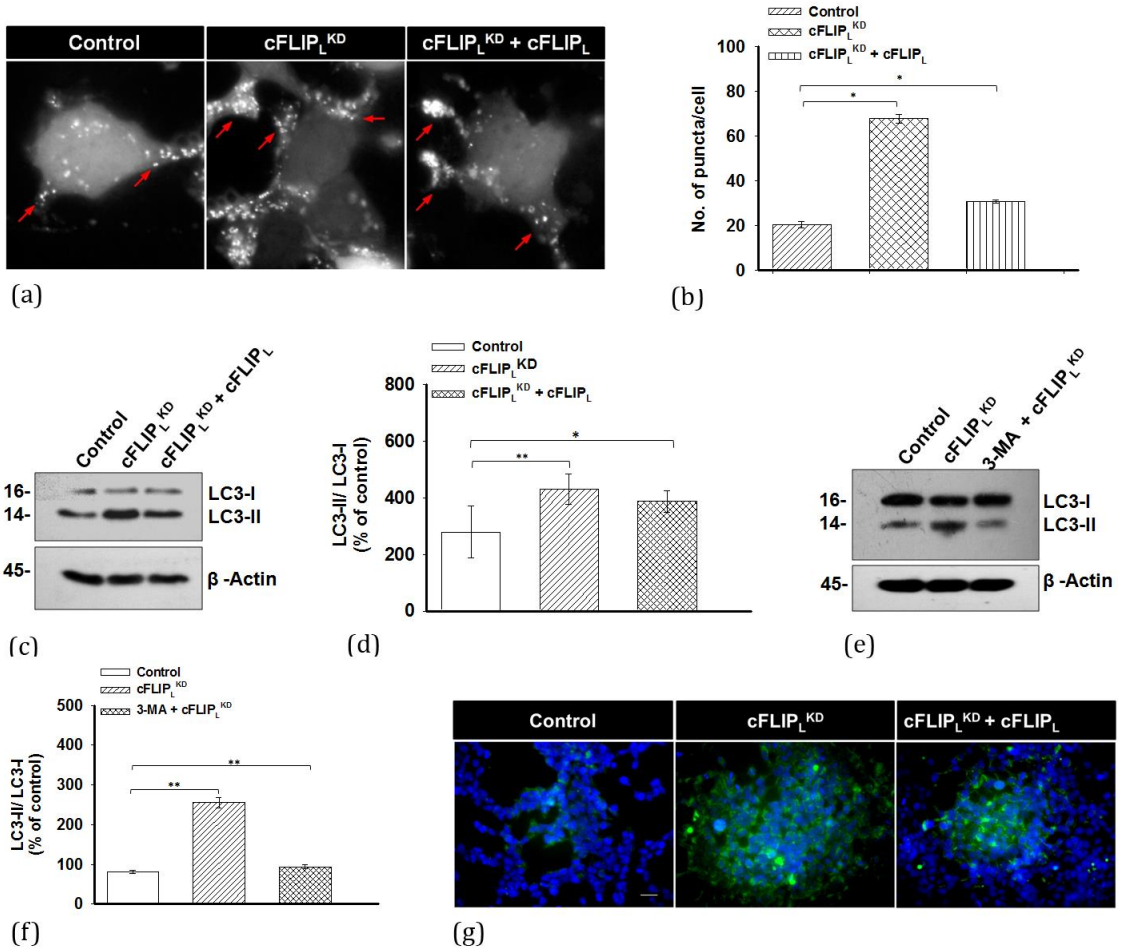

Figure 54. Depletion of cFLIP$_L$ imbalances autophagic equilibrium. The GFP-LC3 stable cells of HEK 293T cells were treated as mentioned in figure legend 52, control represents non-targeting siRNA transfected cells, post incubation, (a) the induction of autophagic puncta was monitored under fluorescent microscope, scale bar- 10 μm (b) count of autophagic puncta per cell with the aid of Image J software, more than 150 cells from three random fields were analysed, (c) Western blot images of LC-3 protein, (d) densitometry of LC3-Ii/LC3-I. HEK 293T cells were pre-incubated with 3-MA (3-Methyl Adenine) (10 mM for 1 h) and subjected to cFLIP$_L^{KD}$, (e) Western blot images of LC-3 protein, (f) densitometry of LC3-Ii/LC3-I and (g) Detection of autophagic vacuoles with Cyto ID Autophagy detection kit; scale bar- 2μm, Error bars represent mean ±SD, the P values represents *P ≤0.05, **P ≤0.01 (student t-test, n ≥ 3, where n is the number of independent experiments).

3.4.4 Knockdown of cFLIP$_L$ generates oxidative stress and autophagy by Beclin-1 and HMGB1 interaction

The anti-apoptotic proteins cFLIP$_L$ and Bcl-2 both suppresses apoptosis and autophagy associated cell death (Pattingre et al., 2005; Budd et al., 2006). Although, Bcl-2 interacts with Beclin-1 and represses autophagy, however JNK1 mediated phosphorylation of Bcl-2 may dissociate its interaction with Beclin-1 (Wei et al., 2008). Indeed, during stress conditions HMGB1 translocates to cytosol and interacts with Beclin1 to sustain autophagy (Tang et al., 2010a). Here, the effect of cFLIP$_L$ knockdown (cFLIP$_L^{KD}$) on cellular oxidative levels and the expression of JNK1, HMGB1 and Bcl-2 was examined. It was found that cFLIP$_L^{KD}$ accumulates intracellular ROS and upregulates JNK1 and HMGB1 levels, but the expression of Bcl-2 was suppressed in HEK 293T, MCF-7, HeLa and HCT 116 cells. However, re-expression of cFLIP$_L$ in cFLIP$_L^{KD}$ cells restores the basal levels of ROS and expression of JNK1, Bcl-2, and HMGB1 (Figure 55a–f). Next, the interaction of Bcl-2 and HMGB1 with Beclin-1 during cFLIP$_L^{KD}$ was examined. The co-immunoprecipitation analysis suggests that suppression of the cFLIP$_L$ allows HMGB1 and Beclin-1 interaction to repel Bcl- 2; however, upon re-expression of cFLIP$_L$ in cFLIP$_L^{KD}$ cells the HMGB1 was unable to maintain the similar interaction with Beclin-1 in HEK 293T cells (Figure 56a &b). Further, this outcome was confirmed with the H_2O_2 (an inducer of ROS). The results show that treatment of H_2O_2 (100 nM for 3 h) up regulates the intracellular ROS, however, cFLIP$_L$ over expressed cells subjected with H_2O_2 was failed to accumulation of ROS and it was comparable to the control and N-acetyl cysteine (NAC- ROS scavenger) treated cells (Figure 56c). Next, it was noticed that during oxidative stress HMGB1 and Bcl-2 strongly interacts with Beclin-1. However, in the presence of NAC moderate restriction was observed in the binding between HMGB1 and Beclin-1 (Figure 56d). Thus, following results suggest that cFLIP$_L^{KD}$ imparts oxidative stress and turn on JNK1 expression to phosphorylate Bcl-2 followed by its dissociation from Beclin-1, however retaining the expression of cFLIP$_L$ favors the canonical Bcl-2-Beclin-1 interaction to suppress autophagic stress (Ranjan & Pathak, J. Cell. Biochem, 2016).

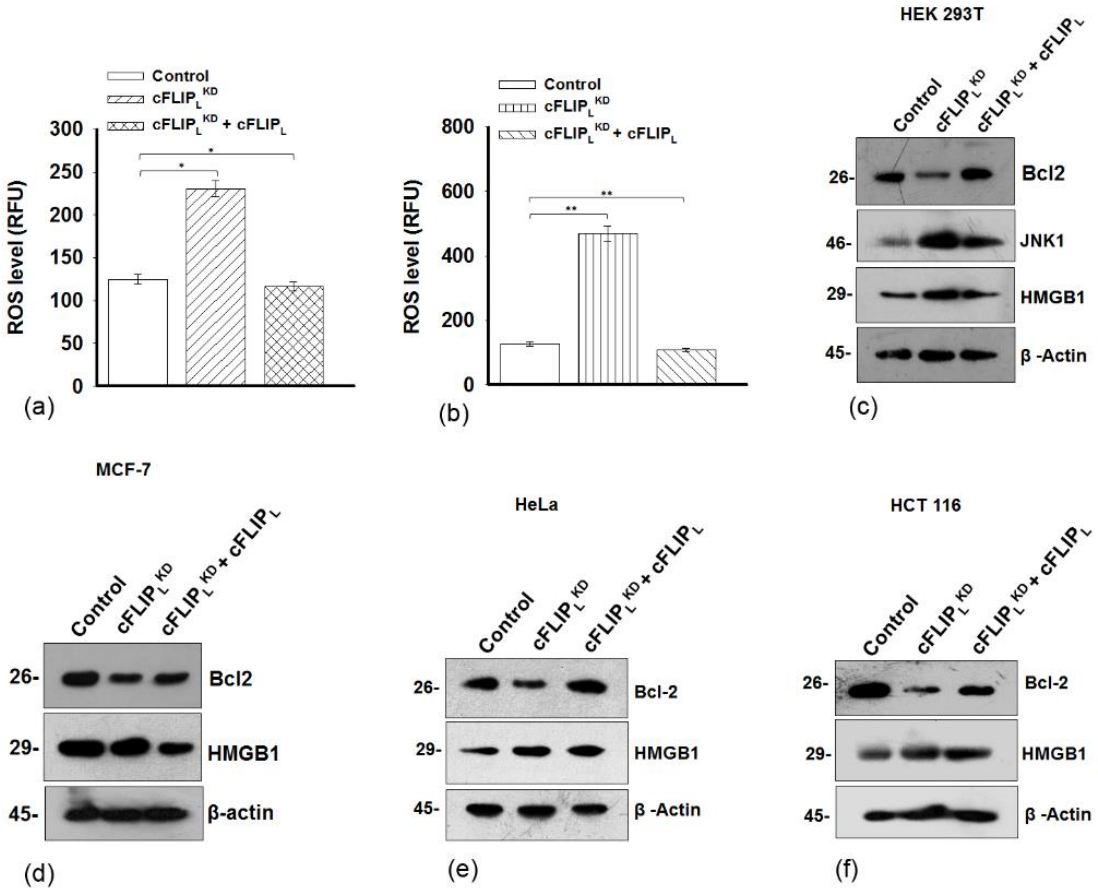

Figure 55. cFLIP$_L$ stabilizes the interaction of Beclin-1 with Bcl-2. The HEK 293T, HeLa and HCT 116 cells were transfected with siRNA directed against cFLIP$_L$ (cFLIP$_L^{KD}$, lane 2) (48 h) and re-introduction of pLXSN-cFLIP$_L$ in cFLIP$_L^{KD}$ HEK 293T cells (cFLIP$_L^{KD}$ + cFLIP$_L$, lane 3) for an additional 48 h, control represents no-trageting siRNA transfected cells (lane 1), post incubation (a) level of ROS in HEK 293T cells and (b) level of ROS in MCF-7 cells. Western blot images of Bcl-2, JNK1, HMGB1 and β-actin in, (c) HEK 293T cells, (d) MCF-7 cells, (e) HeLa cells and (f) HCT 116 cells. Error bars represent mean ±SD, the P values represents *P ≤0.05, **P ≤0.01 (student t-test, n ≥ 3, where n is the number of independent experiments).

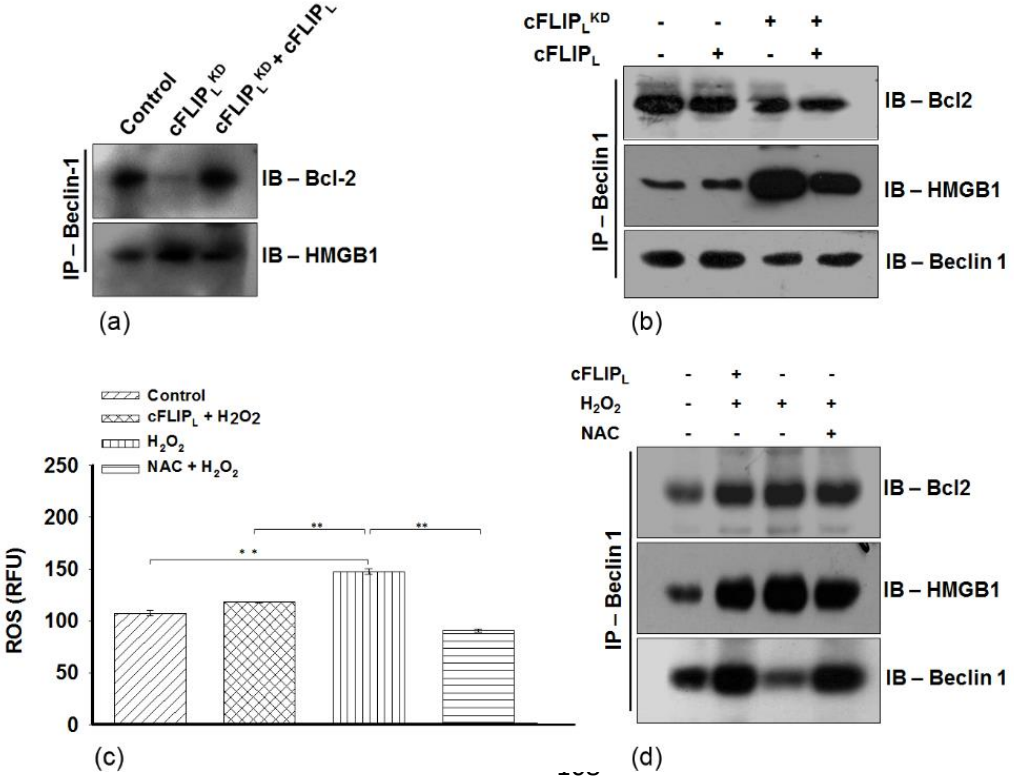

Figure 56. cFLIP$_L$ mitigates oxidative stress and restore interaction of Beclin-1 with Bcl-2. The HEK 293T cells were treated as mentioned in figure legend 52, (a-b) the co-immunoprecipitation assay of Bcl-2, HMGB1 with Beclin-1. The pLXSN-cFLIP$_L$ overexpressed (48 h) HEK 293T cells were subjected to H_2O_2 (100 nM for 3 h) in the absence (-) or presence (+) of NAC (100 mM pre-incubation for 3 h), (c) ROS measurement and (d) co-immunoprecipitation analysis to investigate the binding interaction of Bcl-2, HMGB1 with Beclin-1, vector transfected and untreated cells were taken as control. Error bars represent mean ±SD, the P values represents *P ≤0.05, **P ≤0.01 (student t-test, n ≥ 3, where n is the number of independent experiments).

3.4.5 cFLIP$_L$ protects p53 dependent ubiquitination of Beclin-1

The tumor suppressor protein p53 is instrumental to regulate apoptosis and autophagy (Crighton et al., 2006; Feng et al., 2005; Maiuri et al., 2010). The p53 negatively regulates the HMGB1/Beclin1 complex to determine the fate of apoptosis and autophagy (Livesey et al., 2012). It was previously demonstrated that HMGB1 induces the expression of tumor suppressor protein p53 to either phosphorylate Bcl-2 or to turn over the expression of Beclin-1 during autophagy stress (Livesey et al., 2012; Lorin et al., 2010). The results shown above demonstrate that HMGB1 accumulates in the cytosol and interacts with Beclin-1 during stress condition to sustain autophagy. Further, it was important to investigate the interaction of p53 with Beclin-1 during stress condition augmented by cFLIP$_L^{KD}$ (Figure 57a). The result shows that, transient silencing of cFLIP$_L$ enforces p53 to interact with Beclin-1. However, upon re-expression of cFLIP$_L$ in cFLIP$_L^{KD}$ cells the binding of p53 with Beclin-1 was comparable to the control (Figure 57b). Thus, cFLIP$_L$ potentially regulated apoptosis and autophagy by modulating p53 and Bcl-2 expression. Further, the ubiquitination of Beclin-1 were examined to confirm autophagy associated cell death induced by knockdown of cFLIP$_L$. More interestingly, knockdown of cFLIP$_L$ ubiquitinates Beclin1, however the re-expression of cFLIP$_L$ in cFLIP$_L^{KD}$ cells represses the ubiquitination of Beclin-1 that was comparable to the control (Figure 57c). Altogether, these results suggest that endogenous expression of cFLIP$_L$ is essential to maintain the integrity of Beclin-1 to suppress autophagic stress and provide stability for Beclin1-Bcl-2 interaction (Ranjan & Pathak, J. Cell. Biochem, 2016).

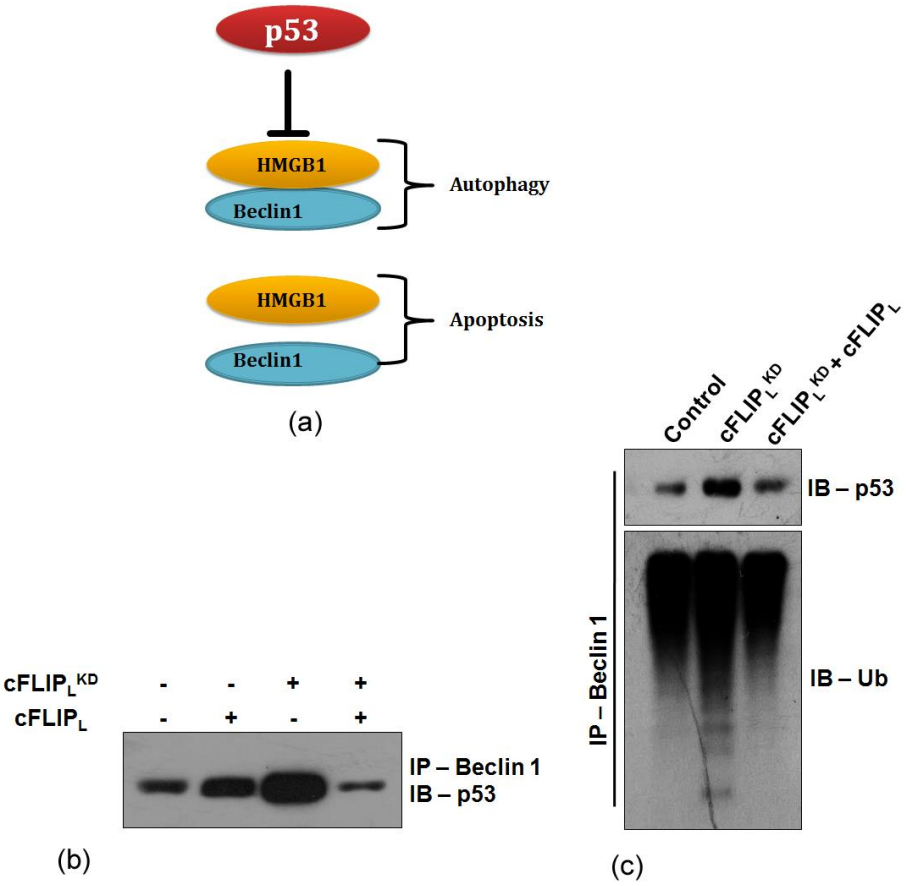

Figure 57. Knockdown of cFLIP$_L$ induces p53 dependent ubiquitination of Beclin-1. (a) Model represents p53 mediated regulation of HMGB1 and Beclin1 interaction. HEK 293T cells were treated as mentioned above in figure legend 52. Post incubation cells were subjected to co-immunoprecipitation analysis to investigate the binding interaction of (b) p53 with Beclin-1 and (c) ubiquitination of Beclin-1, vector and non-targeting siRNA transfected cells were taken as a control.

3.4.6 Stimulation of TNF-α during knockdown of cFLIP$_L$ unable to sustain autophagy

TNF-α stimulation sustains the expression of cFLIP$_L$ to restrict cell death in a variety of cancer cells (Karin and Lin, 2002; Micheau and Tschopp, 2003). However, TNF-α has also been reported in the regulation of autophagy (Djavaheri-Mergny et al., 2006; Laplante and Sabatini, 2012). Here, it was interesting to investigate the effect of TNF-α on autophagy in context of modulation of cFLIP$_L$ expression. To achieve this aim, the GFP-LC3 stable HEK 293T cells were preincubated with TNF-α followed by siRNA targeted depletion of endogenous cFLIP$_L$. It was found that, transient silencing of cFLIP$_L$ aggressively mount autophagic stress within the cells as compared to untreated and TNF-a treated cells, however the pre-exposure of TNF-α was showing minimal effect to repress autophagic stress in cFLIP$_L$ knockdown cells (Figure 58a & b). The protein turnover of LC3 was confirmed by Western blotting and found that, siRNA mediated suppression of cFLIP$_L$ expression has higher conversion of LC3-I to LC3-II as compared to control and TNF-α

treated cells. Moreover $cFLIP_L^{KD}$ cells pre-exposed to TNF-α has moderate changes in LC3-I to LC3-II conversion as compared to the $cFLIP_L$ knockdown cells (Figure 58c & d). Furthermore, it was noticed that $cFLIP_L$ knockdown cells generate more autophagic vacuoles under stress conditions as compared to TNF-α treated cells, and surprisingly TNF-α pre-stimulated cells subjected to $cFLIP_L$ knockdown, the number of autophagic vacuoles were comparable to the $cFLIP_L$ knockdown cells (Figure 58e). The following outcomes prompted to examine the expression of proautophagic HMGB1 and tumor suppressor p53 in similar condition. The result shows, cytosolic accumulation of HMGB1 and p53 in $cFLIP_L$ knockdown cells as compared to control and TNF-α treated cells, however, pre-stimulation of TNF-α subjected to knockdown of $cFLIP_L$ showing negligible effect in HMGB1 and p53 expression (Figure 59). Altogether, these results demonstrated that exposure of TNF-α failed to protect the cells against $cFLIP_L^{KD}$ induced autophagic stress accompanied by accumulation of HMGB1 and p53 in HEK 293T cells (Ranjan & Pathak, J. Cell. Biochem, 2016).

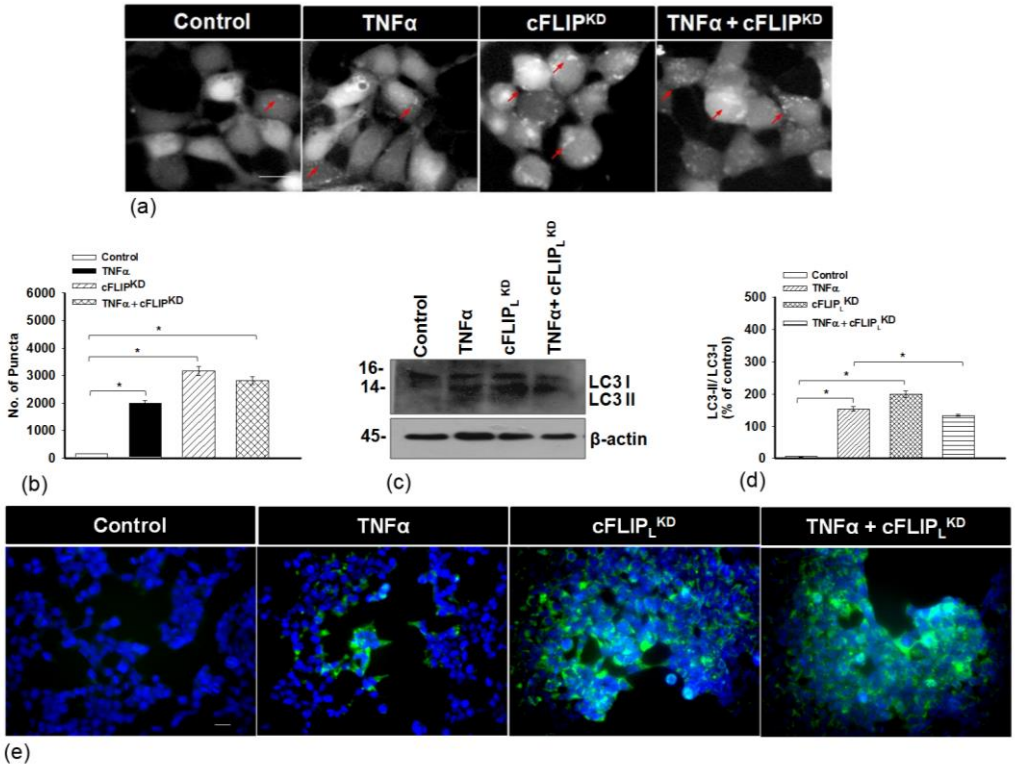

Figure 58. Knockdown of $cFLIP_L$ mitigates TNF-α response for cell survival. The GFP-LC3 stable HEK 293T cells were subjected to TNF-α (10 ng/ml) treatment for 12 h (lane 2), transfected with siRNA directed against $cFLIP_L$ ($cFLIP_L^{KD}$; lane 3) for 48 h and TNF-α (10 ng/ml) primed (12 h) cells transfected with siRNA against $cFLIP_L$ (TNF-α + $cFLIP_L^{KD}$; *lane 4*) for an additional 48 h to monitor, (a-d) as mentioned above in (Fig. 58a-d) and (e) Detection of autophagic vacuoles with Cyto ID Autophagy detection kit, scale bar- 2μm Untreated and nontargeting siRNA transfected cells were taken as control. Error bars represent mean ±SD, the P values represents *P ≤0.05 (student t-test, n ≥ 3, where n is the number of independent experiments).

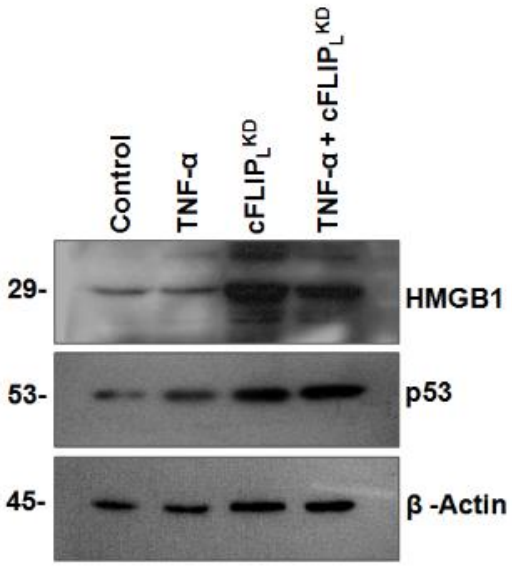

Figure 59. Knockdown of cFLIP$_L$ induces p53 dependent ubiquitination of Beclin-1. HEK 293T cells were treated as mentioned above in figure legend 58. Post incubation cells were subjected to Western blot analysis of HMGB1 and p53, vector and non-targeting siRNA transfected cells were taken as a control.

PART V

3.5 FADD REGULATES INFLAMMASOME MEDIATED ACTIVATION OF IL-1β

3.5.1 FADD regulates the expression of Pro-IL1β

Up regulation of pro-inflammatory cytokine and activation of NF-kB provide tumor microenvronment. Lipopolysaccharide (LPS) is a well known inducer of NF-κB and transcription of proinflammatory cytokines. (Ma et al., 2004; Kawai and Akira, 2007). Activation of NF-kB is mainly depends upon interaction with DD containing protein MyD88 and IL-1 receptor-associated kinase 1 (IRAK1) (Bannerman et al., 2002; Zhande et al., 2007). In contrast, the DD of FADD interact with DD of MyD88 and hinders TLR4 mediated activation of NF-κB (Aliprantis et al., 2000; Bannerman et al., 2002). As mentioned above, FADD effectively regulated the activation of NF-κB in HCT 116 cells. Therefore, it was important to examine the ability of FADD in the regulation of LPS mediated NF-κB activation and Proinflammatory cytokine. To achieve this aim, the HCT 116 cells were transfected with FADD and stimulated with LPS. The results show that LPS provokes the activation of NF-κB and expression of proIL-1β (Figure 60a & b). However, FADD expressed cells exposed to LPS attenuates the expression of p65 and the level of IL-1β (Figure 60a, c & d). Altogether, these results suggest that FADD suppresses the activation of NF-κBand pro-inflammatory cytokine IL-1β in response to LPS.

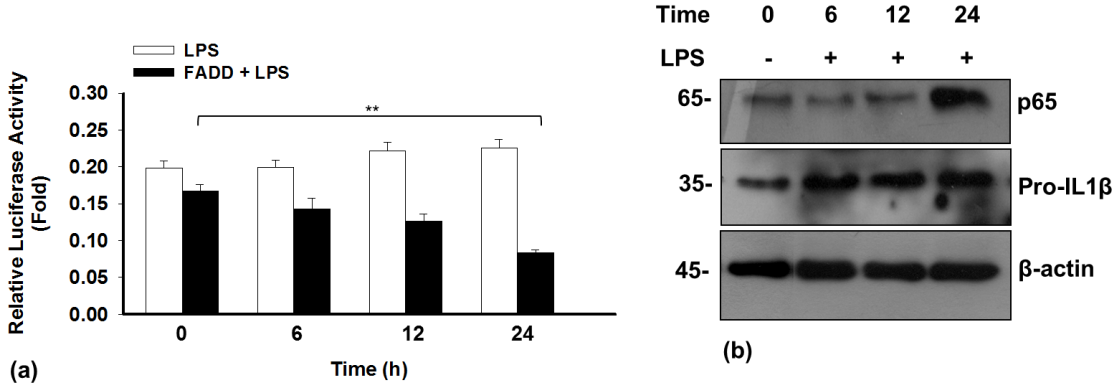

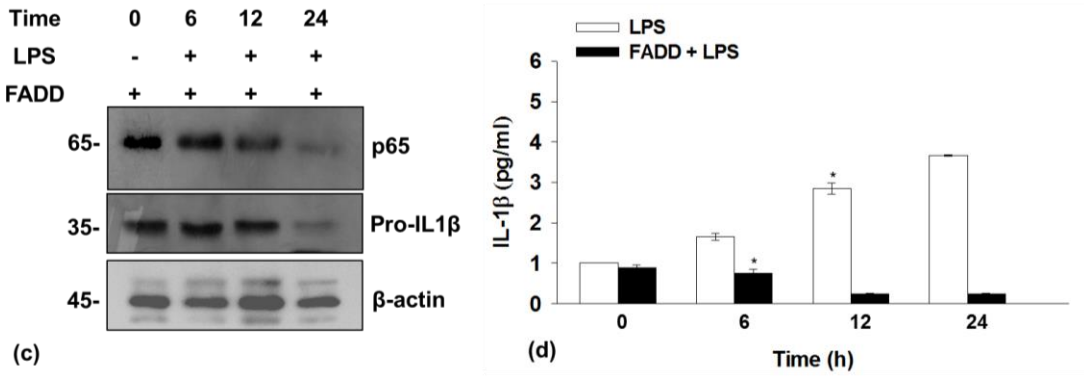

Figure 60. FADD regulates proIL-1β. HCT 116 cells were transfeted with pEYFP-FADD (48 h) and further teated with LPS (20 ng/ml) for an additional 6-24 h, control (shown as 0 h time point) represents cells unteated to LPS (white bar) and FADD expressed cell untreated to LPS, post incubation (a) The NF-κB relative luciferase activity, (b) Western blot of p65 and proIL-1β in LPS treated cells, (c) Western blot of p65 and proIL-1β in FADD expressed cells treated with LPS and (d) ELISA assay to measure IL-1β released in culture media. Error bars represent mean ±SD, the P values represents *P ≤0.05, **P ≤0.01 (student t-test, n ≥ 3, where n is the number of independent experiments).

3.5.2 Over expression of FADD inhibits inflammasome mediated maturation of IL-1β

Previous reports highlight that chemotherapy-induced dying tumor cells release some bio-molecules such as ATP, uric acid and hyaluronan to trigger NLRP3 inflammasome mediated activation of pro-inflammatory cytokine IL-1β (Zhou et al., 2010). Mechanistically, LPS triggers TLR4 mediated NF-kB activation and synthesis of proIL-1β with the aid of inflammasome for final maturation of IL-1β (Latz et al., 2013). In fact, an inflammasome complex consists with Nlrp3, Asc1 and Procaspase-1 that facilitates the activation of procaspase-1, which is mainly responsible for the processing of proIL-1β (Abderrazak et al., 2015). Although, recent reports suggest that, FADD induces the non-canonical maturation of IL-1β (Bossaller et al., 2012; Moriwaki et al., 2015). Whether FADD is involved in NLRP3 inflammasome signaling to activate the IL-1β has not been clearly understood. Therefore, it was prompted to investigate the involvement of FADD during the canonical response of LPS and ATP mediated activation of caspase-1 and maturation of IL-1β. To achieve this aim, the FADD expressed HCT 116 cells were co-stimulated with LPS and ATP and the results were compared with LPS and ATP co-stimulated cells. The results show that, co-stimulation of LPS and ATP resulted activation of inflammasome component, including caspases-1, NLRP-3 and IL-1β was noticed (Figure 61a & b). However, FADD expressed cells exposed to LPS and ATP shuttle down inflammasome activation (Figure 61c & d). Moreover, the ELISA assay suggests that over expression of FADD suppresses the LPS and ATP mediated processing and maturation of

IL-1β. Altogether, these results indicate that FADD has enormous potential to suppress the inflammasome mediated activation of IL-1β.

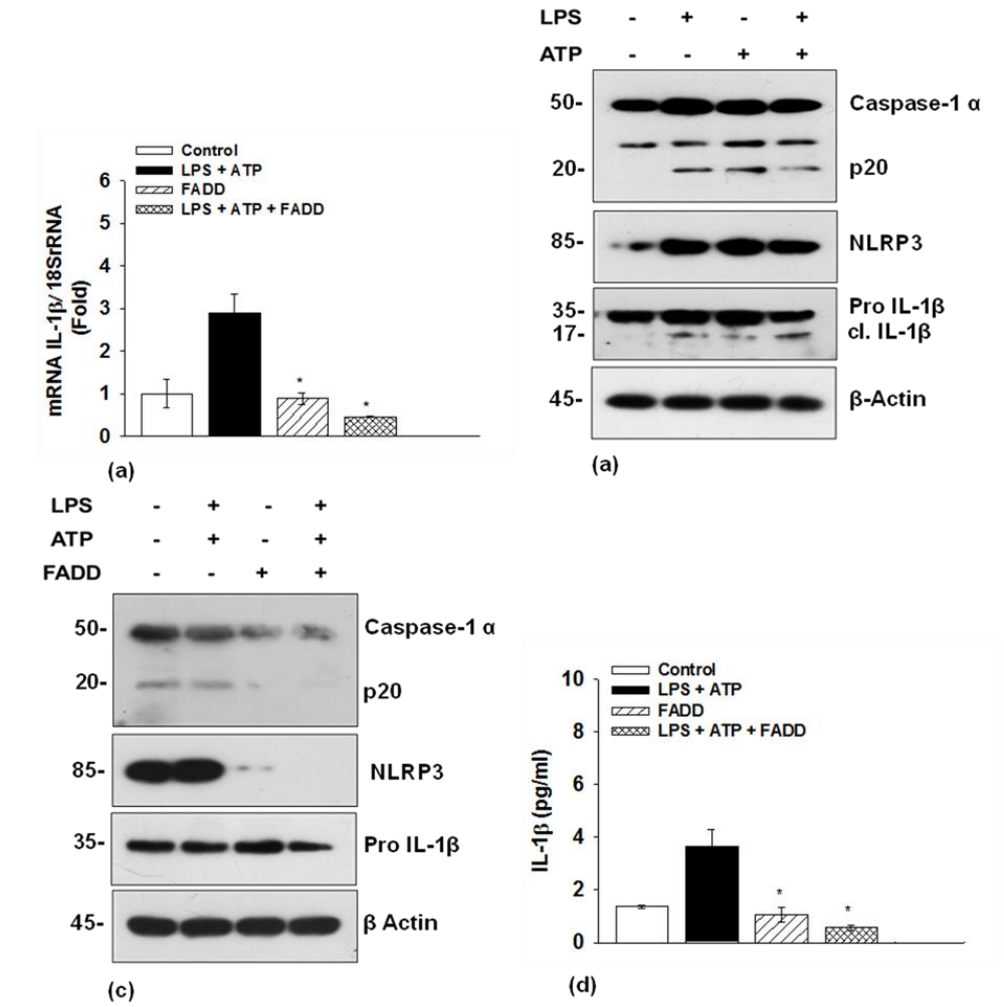

Figure 61. FADD supresses Inflamasome activation. HCT 116 cells were teated with LPS (20 ng/ml 16 h), ATP (200 µM, 18 h) and FADD expressed cells (48 h) treated with LPS + ATP, post incubation (a) Westren blot analysis of caspase-1, Nlrp3 and pro IL-1β, (b) RT-qPCR analysis of pro IL-1β, (c) The Westren blot analysis of mentioned proteins and (d) ELISA assay to measure IL-1β released in culture media. Error bars represent mean ±SD, the P values represents *P ≤0.05 (student t-test, n ≥ 3, where n is the number of independent experiments).

PART VI

3.6 PEPTIDE MEDIATED DELIVERY OF FADD IN CANCER CELLS

The study was designed for cloning, purification and intracellular delivery of hFADD in cancer and transformed cells with the aid of cell permeable peptides (CP).

3.6.1 Quantitative and qualitative analysis of total RNA and cDNA

The total RNA was extracted from HCT 116 cells followed by cDNA synthesis for the amplification othe human *FADD* gene. The quantitative and qualitative analysis of total RNA and cDNA were confirmed by spectrophotometric analysis and agarose gel electrophoresis. The quantitative estimations of RNA and cDNA were carried out at A $_{260/280}$ nm shown in Table 2. The qualitative analysis of total RNA was confirmed by 1.2% agarose gel electrophoresis (Figure 62a, lane 2). Further, cDNA was subjected to gradient PCR (Tm ranging from 60-70^{0}C) by using human FADD specific primers and the amplicons were resolved on 1.2 % agarose gel electrophoresis. The gradient PCR analysis suggests that the melting temperature (Tm) of 70 ^{0}C, was appropriate to obtain human *FADD* (627 bp) cDNA amplicons (Figure 62b).

Oligos	A $_{260\ nm}$	A $_{280\ nm}$	Ratio A $_{260/280\ nm}$	Concn. (ng/ µl)
RNA	0.023±0.05	0.013±0.05	1.77	260
cDNA	0.051±.0.05	0.030±0.05	1.70	1275

Table 2. Quantitative estimation of RNA and cDNA. The total RNA was isolated from exponentially growing HCT 116 cells and subjected to cDNA synthesis. The purified RNA and cDNA were quantified by UV-spectrophotometer at 260 and 280 nm followed by determination of concentration. An elution buffer was taken as a blank control (blank). All the values represents were from 3 independent experiments.

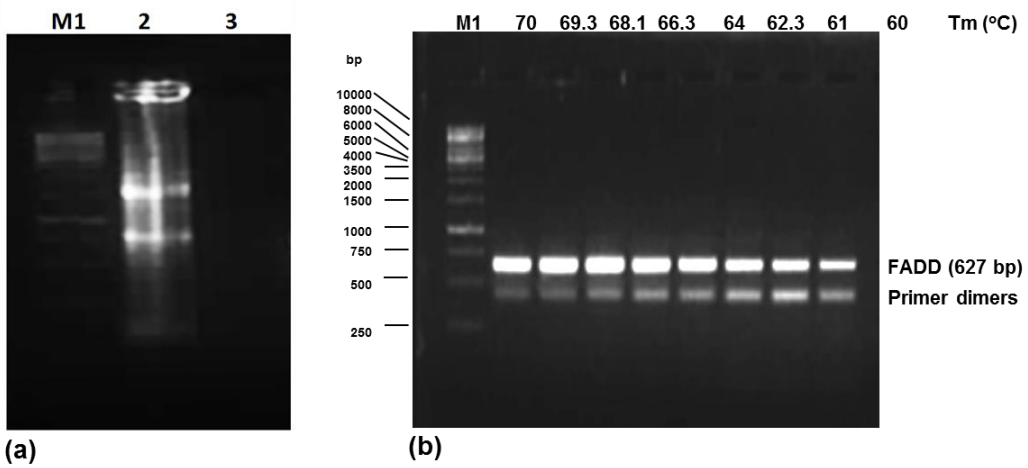

Figure 62. Isolation of total RNA and cDNA synthesis. (a) The total RNA (lane 2) was isolated from HCT 116 followed by cDNA synthesis (lane 3) and analysed on 1.2% agarose gel electrophoresis, (b) Gradient PCR (Tm- 60-70^{0}C) of Human *FADD* and cDNA amplicons were resolved on 1.2 % agarose gel electrophoresis. M1- O'GeneRuler 1 kb DNA Ladder. Human FADD NCBI reference sequence: NP_003815.1; GeneBank no: CR456738.1. bp-base pair.

3.6.2 Cloning of human FADD (hFADD)

Next, the purified cDNA amplicons of human *FADD* and the bacterial expression vector pET28a (+) were subjected to double digestion with restriction enzymes (REs) *EcoR1* and *BamH1* for 16 h at 37^{0}C (Figure 63a & b). The digested products of insert (cDNA of FADD) and vector pET 28 (+) were purified followed by concentration determination using UV-spectrophotometer at A $_{260/280\ nm}$ and the yield was calculated as shown in Table 3. Further, the digested products were processed by ligation by using T4 DNA ligase and the recombinant clone of pET 28 (+)-FADD (pET-FADD) was confirmed by PCR amplification and REs double digestion. The 627 bp amplification of *FADD* was obtained that was corresponding to the molecular weight marker (Fig 63c). In addition, the restriction digestion analysis of recombinant PET–FADD clone shows a sharp fall of 627 bp FADD insert corresponding to the molecular weight marker (Figure 63d).

Oligos	$A_{260\ nm}$	$A_{280\ nm}$	Ratio $A_{260/280\ nm}$	Concn. (ng/ µl)
FADD insert	0.005±0.05	0.003±0.05	1.66	125
pET 28a (+)	0.010±0.05	0.006±.0.05	1.66	250
pET-FADD	0.020±0.05	0.013±0.05	1.53	500

Table 3. Quantification of RE digested insert and vector. The cDNA amplicons of FADD and pET 28(a) expression vector were double digested by RE *EcoR1* and *BamH1* followed by purification and quantitative estimation. Integrity of the insert and vector were confirmed by UV-spectrophotometer before proceeded for the ligation.

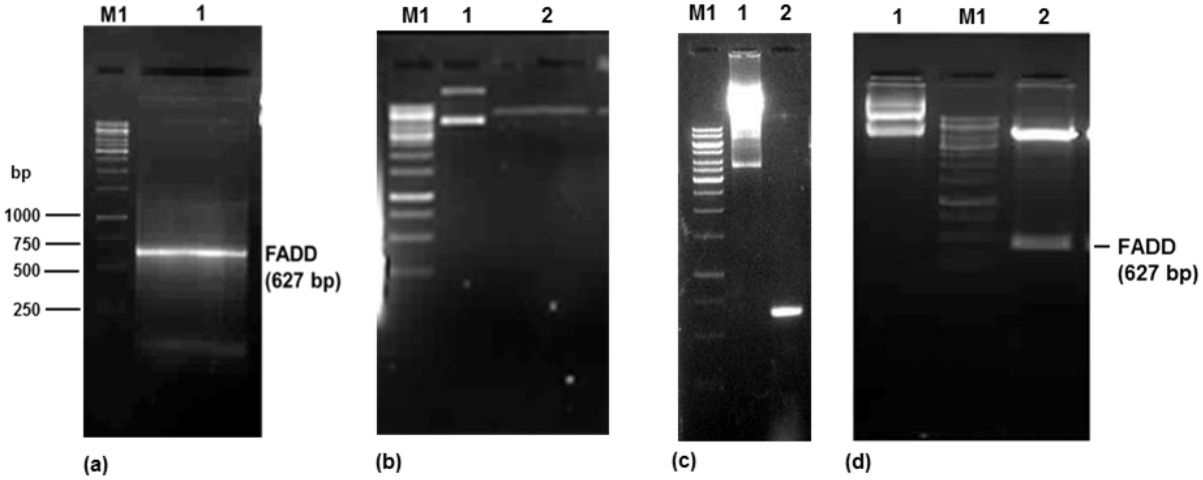

Figure 63. Cloning of human FADD. (a) Preparation of insert- cDNA amplicons of humn *FADD* was double with with *Eco*R1 and *Bam*H1 (lane 1), (b) vector preparation- pET 28 a (+) (lane 1) was double digested with *Eco*R1 and *Bam*H1 (lane 2), (c) The recombinant clone of pET 28a (+)-FADD (lane 1) were confirmed by PCR amplification at Tm- 70^{0}C and the 627 bp product of human *FADD* (lane 2) and (d) the double digested clones of pET-FADD (lane 1) and the expected product of human FADD (627 bp) (lane 2). All the agarose gel were of 1.2%. M1- O'GeneRuler 1 kb DNA Ladder as mentioned in figure 62.

3.6.3 Expression of human FADD (hFADD)

The confirmed recombinant of clone pET-FADD was further transformed into competent cells of *E. coli* BL21 (*DE3*)-pLysS for the expression of protein. The transformed colonies of *E. coli* BL21 was grown in fresh LB medium for 1-3 h followed by induction with 1mM IPTG for an additional 4 h at 25^{0}C as shown in Table 4. After separation of proteins on SDS-PAGE, a sharp band of His-hFADD of MW of ~31kDa was obtained in IPTG induced culture as compared to un-induced cultur (Figure 64a). In addition, the expression of hFADD was confirmed by Western blot analysis using GAPDH as a loading control (Figure 62b). Finally, the *E. coli* BL21 (*DE3*) -pLysS cells containing recombinant clones of pET-FADD were preceded for the large scale protein purification.

Constructs	Pre-incubation time (h)	A $_{600\ nm}$	IPTG (mM)	Incubation time (h)
pET 28a (+)	3	0.269±0.05	1	4
pET-FADD	1	0.058±0.05	1	4
pET-FADD	2	0.158±0.05	1	4
pET-FADD	3	0.279±0.05	1	4

Table 4. IPTG induction profile. Overnight grown culture of *E.coli* BL21 (*DE3*)-pLysS containing recombinant clones of pET-FADD was freshly inoculated in 10 ml of LB medium and incubated from 1-3 h followed by induction with the 1mM IPTG for 4 h at 25^{0}C. Post incubation, the optical density of culture was recorded at A 600 nm by taking LB medium as a reference blank.

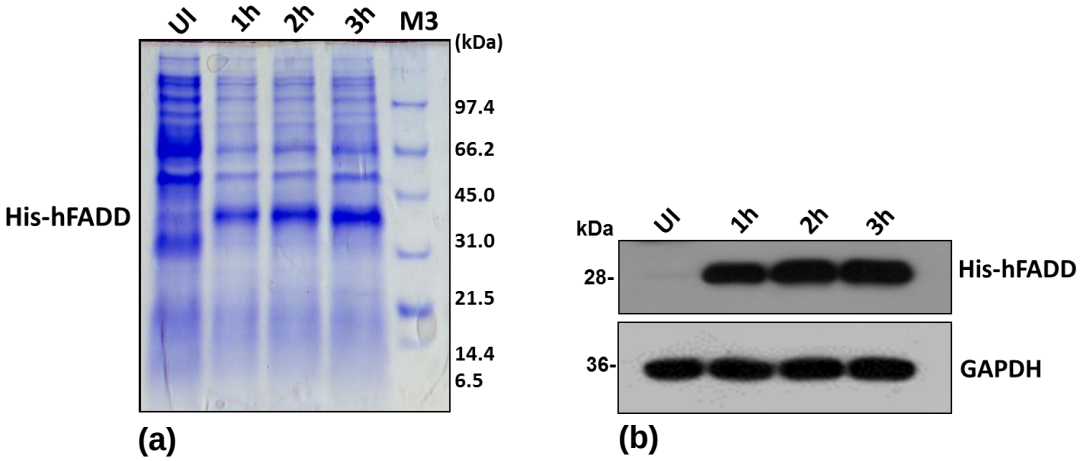

Figure 64. Expression of pET-FADD in *E. coli* BL21 (*DE3*)-pLys cells. The BL21 (*DE3*)-pLyS cells containing the recombinant clones of pET-FADD induced with 1mM IPTG as mentioned in table 4, Post incubation, the 1 ml culture was spun down and the pellet was re-suspended in 1X loading buffe followed by lysis at 100^{0}C, and the samples were analysed by (a) SDS-PAGE analysis and (b) Western blot analysis of His-hFADD. uninduced (UI) cells were taken as reference control, M3- Unstained SDS-PAGE Standards protein ladder.

3.6.4 Refolding and purification of human FADD (hFADD)

The pET-FADD was expressed with a fused 6His-tag and purified by Ni^{2+} NTA affinity column chromatography. It was noticed that expressed His-hFADD protein (T) was highly insoluble and the majority of His-hFADD protein was found in the bacterial pellet (P) as compared to the supernatant (S). Next, the insoluble fraction of His-hFADD was denatured and properly refolded *in vitro* by the use of 6M Gn-HCl (pH 8.0.). The refolded His-hFADD was passed through the Ni^{+2}-NTA affinity column and the eluted fractions were analyzed by SDS-PAGE (E1 & E2). The SDS-PAGE analysis shows an expected molecular weight of around ~31 kDa purified homogenous band of His-hFADD protein (Figure 65). Furthermore, the yield of purified His-hFADD protein was quantified and found 6.34 mg/ml as shown in Table 5.

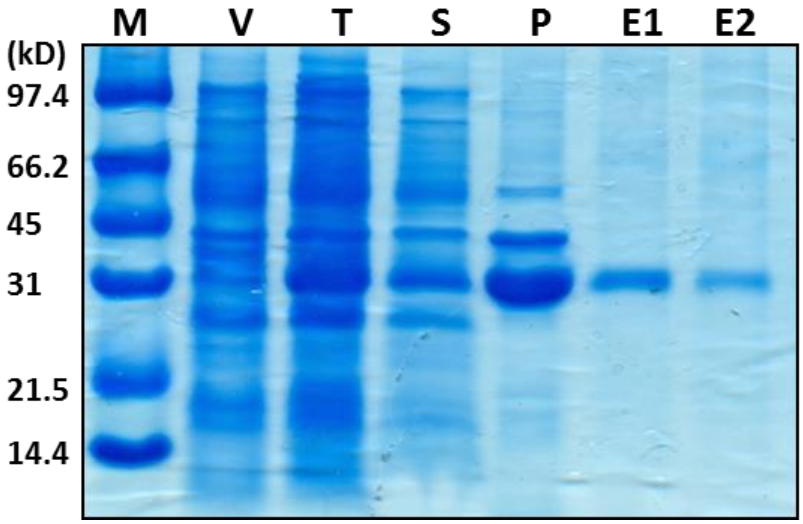

Figure 65. Purification of His tagged human FADD (hFADD). A 200 ml fresh culture of BL21-pET-FADD was induced with 1mM IPTG-induced and incubated for 4h at 25^0C. Post incubation, 1 ml induced culture were lyzed by sonication and centrifuged to separate the pellet and supernatant. The bacterial pellet was re-suspended in Gn-HCl buffer for re-folding followed by pass through Ni^{+2}-NTA affinity column. All the fractions were analysed by SDS-PAGE. M- Mol. wt. marker, V- IPTG induced vector (Total lysate), T - IPTG induced pET-FADD (Total lysate), S- IPTG induced Supernatant, P- IPTG induced Pellet , E- Eluent

	Total lysate	Supernatant	Pellet	Purified FADD
Protein (mg/ml)	60	25	15	6.34
% yield of FADD	10.58 ±0.05	-	42.26 ±0.05	-

Table 5. Purification yield of human FADD (hFADD) protein. The His-hFADD protein was estimated in total cell lysate, supernatant and pellet fractions by BCA protein estimation kit. The percent (%) of His-hFADD was calculated by dividing the concentration of purified FADD to total protein from lysate and pellet fraction respectively. All the experiments were carried out in triplicate.

3.6.5 Characterization and *in vitro* protein-protein interaction of purified FADD

Next, the preliminary characterizations of purified FADD were carried out by the analysis of the intrinsic fluorescence spectrum and *in vitro* protein-protein interaction assays. The different eluted fractions of refolded His-hFADD protein were quantified at two different wavelengths ($A_{205/280\ nm}$) to determine the concentration of purified FADD protein. The UV-spectrophotometric analysis shows that fraction no. 1 has high yield as compared to other fractions as shown in Table 6. Indeed, the presence of aromatic residues *viz.* tryptophan (Trp) and tyrosine (Tyr) within a protein has a characteristic to produce fluorescence spectrum. The purified fractions no.1 was subjected to lamba scanning, the results suggest that the maximum emission of FADD was recorded at 340 nm, suggests that Trp and Tyr residues were mainly located in nonpolar environment. It also suggests that the presence of His tag did not interfere with the refolding of denatured FADD protein (Fig 66a). Next, the biological integrity of refolded purified His-FADD was characterized by protein-protein interaction study. The purified FADD was incubated with total cell lysate of HCT 116 cells to interact with the cFLIP protein under optimum condition. The bound complex of FADD-cFLIP was eluted with anti-cFLIP antibody and confirmed by Western blotting. The result shows that purified hFADD successfully interacts with cFLIP as confirmed by presence of approx ~60 kDa molecular band corresponding to cFLIP protein (Figure 66b).

Fraction no.	A_{205nm}	A_{280nm}	Concn. (mM)
1	0.148	0.013	0.3542
2	0.112	0.010	0.2725
3	0.072	0.006	0.1635
4	0.011	0.002	0.0545

Table 6. Quantification of purified hFADD. Different purified fractions of hFADD eluted from Ni^{2+} Nickel column were quantified by UV-spectrophotometer at wavelengths of A_{205nm} and A_{280nm} taking elution buffer as a reference blank with corresponding determination of concentration by protein estimation by BCA protein estimation kit.

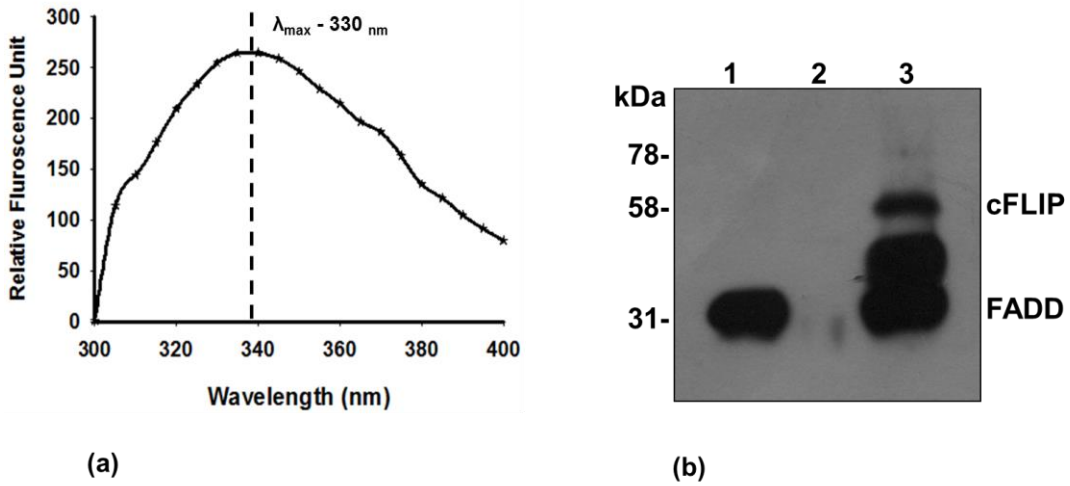

Figure 66. Characterization of purified FADD. (a) Intrinsic fluorescence spectrum of hFADD. Purified hFADD was excited at $A_{280\ nm}$ and emission spectrum were recorded from $A_{300\text{-}400}$ nm. The elution buffer was taken as reference blank. (b) *In vitro* FADD – cFLIP interaction assay. The complex of FADD-cFLIP$_L$ was eluted by using anti-His antibody. Purified FADD (lane 1), total cell lysate from HCT 116 (lane 2), unbound hFADD and eluted cFLIP (lane 3). The eluted cFLIP was detected at MW- 60 kDa.

3.6.6 MALDI-TOF analysis of purified FADD

The molecular masss of the purified hFADD was also determined by matrix-assisted laser desorption ionization time-of-flight (MALDI-TOF) on an Autoflex (Bruker Daltonics, Billerica, USA). The spectrum was acquired in a linear mode and resulting mass spectra were submitted to automatic baseline subtraction. Sinapinic acid was used as the matrix. The major peaks from the spectrum were analysed seperately. It was noticed that a major peak at *m/z* 732 was corresponding to human FADD.

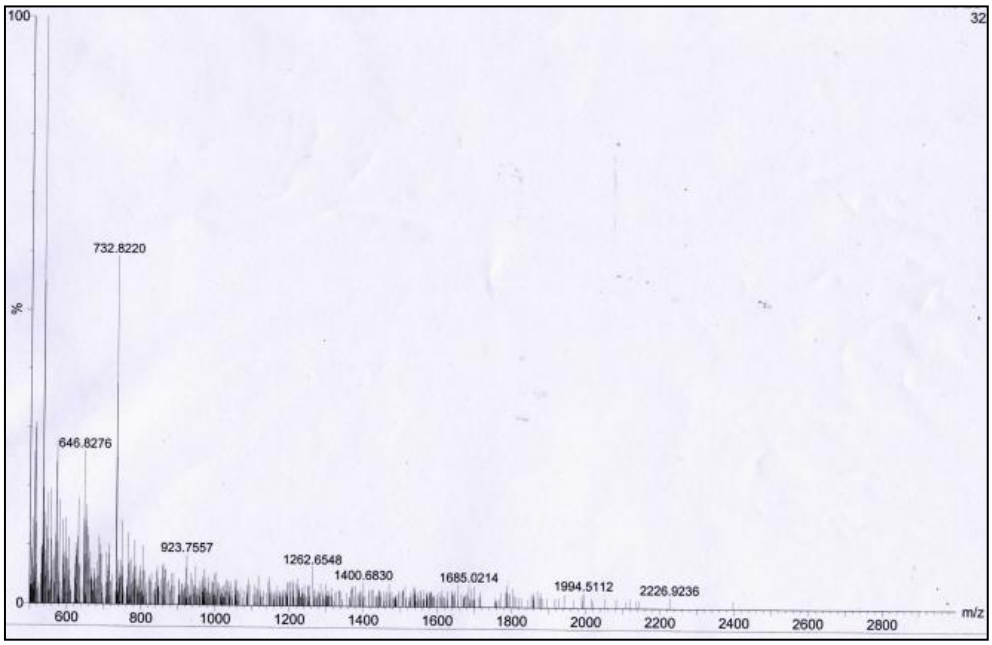

Figure 67. Mass determination of purified FADD by MALDI-TOF mass spectrometry. The purified fraction of hFADD was resolved on 12% SDS-PAGE and the obtained band was excised from the gel aseptically. The gel was further proceeded for Mass spectrometry. The peak of Mass spectra showed match of its spectra with the FADD proteins of human origin. The resulting mass spectra were submitted to automatic baseline subtraction.

3.6.7 Characterization of cell permeable peptides (CP) conjugated hFADD

The purified hFADD was chemically cross-linked with permeable peptides and characterized by quantification by UV-spectrometry and fluorescence spectra analyses. The UV-spectrum suggests that conjugate of hFADD with CP peptide (CP-FADD) showing a maximum absorbance at 280 nm as compared to the individual hFADD protein and CP peptide as shown in Table 7. Furthermore, the fluorescence spectrum of the CP-FADD conjugate shows a reduced shift of 5 nm relative fluorescence unit as compared to an individual fluorescence spectrum of FADD protein and CP peptide (Figure 68). The results obtained from UV-spectral analyses show that, purified FADD was successfully conjugated with CP peptide.

Fraction no.	A_{205nm}	A_{280nm}	Concn. (mM)
Purified hFADD	2.513	0.012	0.3270
CP peptide	0.042	0.002	0.7812
CP-FADD	2.411	0.026	0.6623

Table 7. Quantitative analysis of CP-FADD. The chemically conjugated hFADD with cell permeable peptide (CP-FADD) was quantified at wavelengths of $A_{205\ nm}$ and $A_{280\ nm}$, taking elution buffer as reference blank. At the wavelength of 280 nm the maximum observation was noticed. The concentration of all samples were calculated.

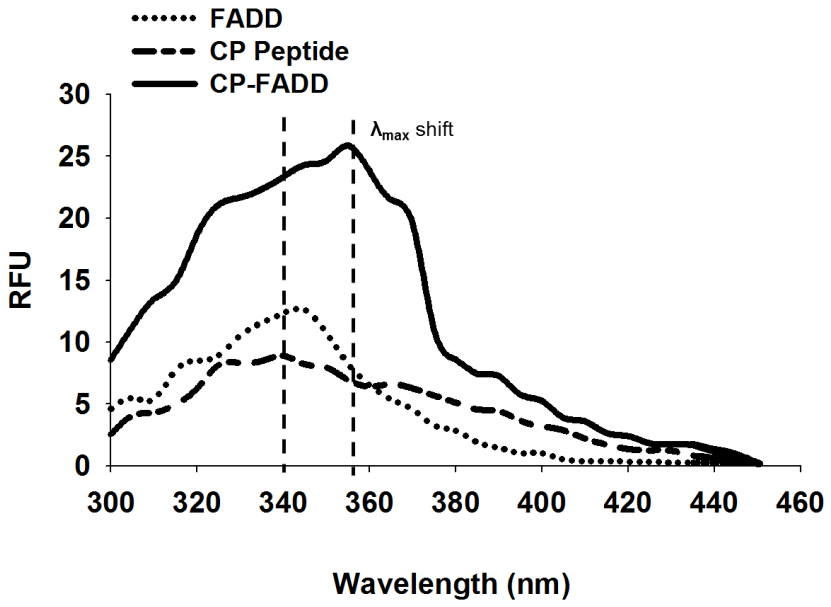

Figure 68. Intrinsic fluorescence spectrum. Purified His-hFADD, CP peptide and conjugated CP-FADD were excited at 280nm and emission spectrum were recorded at 300-450nm. The 50 mM Tris-EDTA (pH- 7.5) buffer was used as a reference blank, all the experiment were performed three time independently.

3.6.8 FT-IR analysis of CP-FADD

The degree of chemical conjugation of CP peptide with purified FADD was analyzed by FT-IR spectroscopy. The FT-IR spectrum shows the characteristic spectrum of acidic amide in the range of 1630-1695 cm-1 was more intense in the conjugated product of CP-FADD and less in FADD protein, which indicates that extra amount of acidic amide present in the mixture consumed in the reaction and facilitate the interaction of CP peptide with FADD protein. The sharp peak of aromatic amine was noticed from the range of 1250-1300 cm-1, which was drastically reduced in the conjugate product of CP-FADD (Figure 69). In conclusion, purified FADD protein was successfully conjugated with CP peptide.

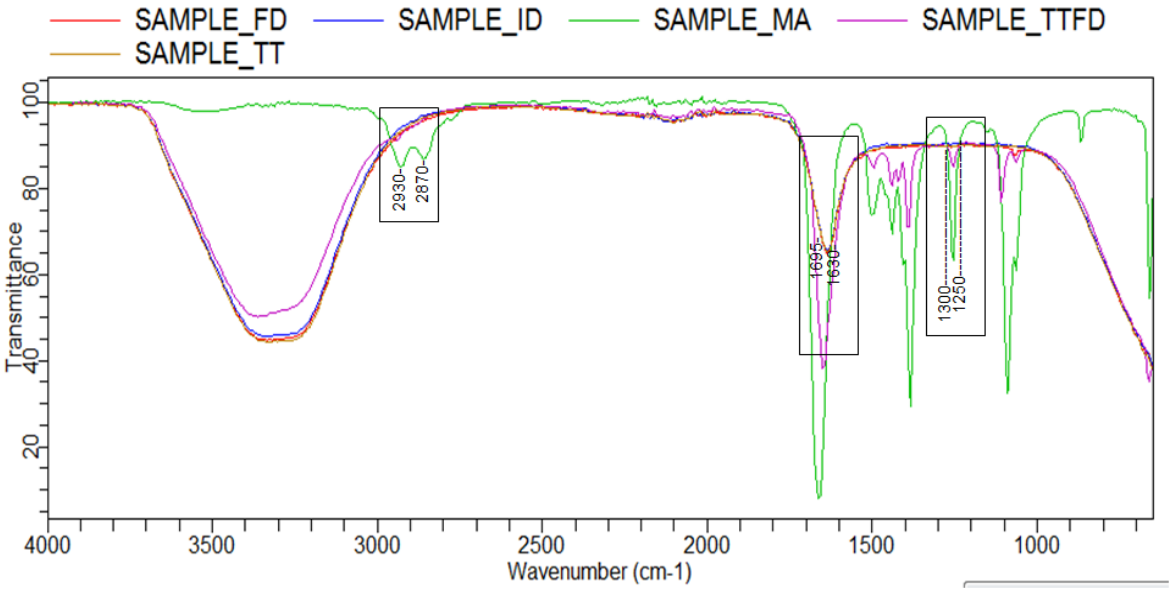

Figure 69. FT-IR analysis of CP-FADD. Upon preliminary charecterization of CP-FADD conjugate the degree of conjugation was determined by FT-IR spectroscopy. The x-axis indicates frequency and the y-axis represents transmission of radiations. Abbreaviations- FD-purified FADD protein, TTFD-CP-FADD conjugte.

3.6.9 Intracellular delivery and cellular localization of CP-FADD

The conjugate of CP-FADD were further screened for the determination of biological activity in different cell lines. To examine the intracellular uptake, HCT 116, HEK 293T, MCF-7 and HeLa cells were treated with 5 μM of CP-FADD for 3-12 h followed by co-immunopreciptaion assay using anti-His antibody. The result shows that, CP-FADD accumulates intracellularly from 3-12 h (Figure 70a). Next, intracellular delivery of CP-FADD was confirmed by immunostaining. The immunofluoroscence analysis shows that CP-FADD efficiently delivered inside the HEK 293T cell within 3 h of incubation (Figure

70b). Thus, obtained results suggest that CP-FADD conjugate efficiently internalized and stable within cells.

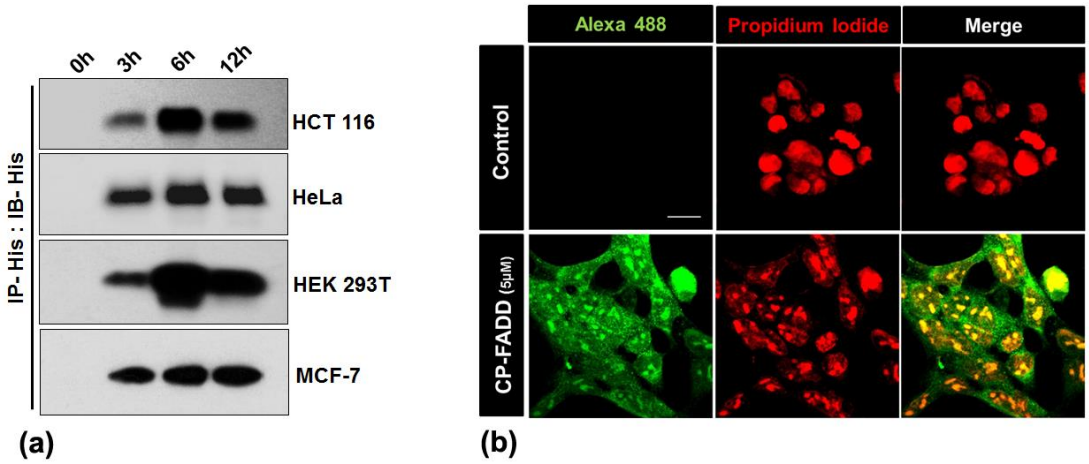

Figure 70. Cellular localization of CP-FADD inside the cells. (a) HCT 116, HeLa, HEK 293T and MCF-7 cells were treated with 5 μM of CP-FADD for given time points, post incubation the total cell lysate was subjected to co-immunoprecipitation assay using anti-His antibody, (b) The HEK 293T cells were incubated CP-FADD (5 μM, 3 h), followed by immunofluorescence with anti-His antibody, the cells were counterstained with PI (20 ng/ml for 5 min) and analyzed under confocal microscope. 100 cells from three random fields were examined, scale bar - 5 μm.

3.6.10 Apoptotic potential of CP-FADD on cancer cells

Furthermore, the anti-proliferative and apoptotic activity of the CP-FADD were examined in HCT116 and HEK 293T cells. The cell death analysis by MTT assay reveal that cells were treated with CP-FADD inhibits cell viability (Figure 71a). Next, the commencement of apoptotic death was confirmed by Tali image based cytometer. The results show that, CP-FADD significantly induces the commencement of apoptotic cell death and approximately 45 % of apoptotic death in HCT 116 cells at 12 h. (Figure 71b). Furthermore, apoptotic cell death was validated by examining the expression of cell death regulatory proteins. The Western blot analysis shows that CP-FADD efficiently triggers the processing and activation of activation of caspase-8, caspase-9 and PARP along with increased activity of caspase-8 to 3 fold (Figure 71c & d). Taken together, the results highlight that CP-FADD conjugate triggers apoptotic cell death in HCT 116 cells.

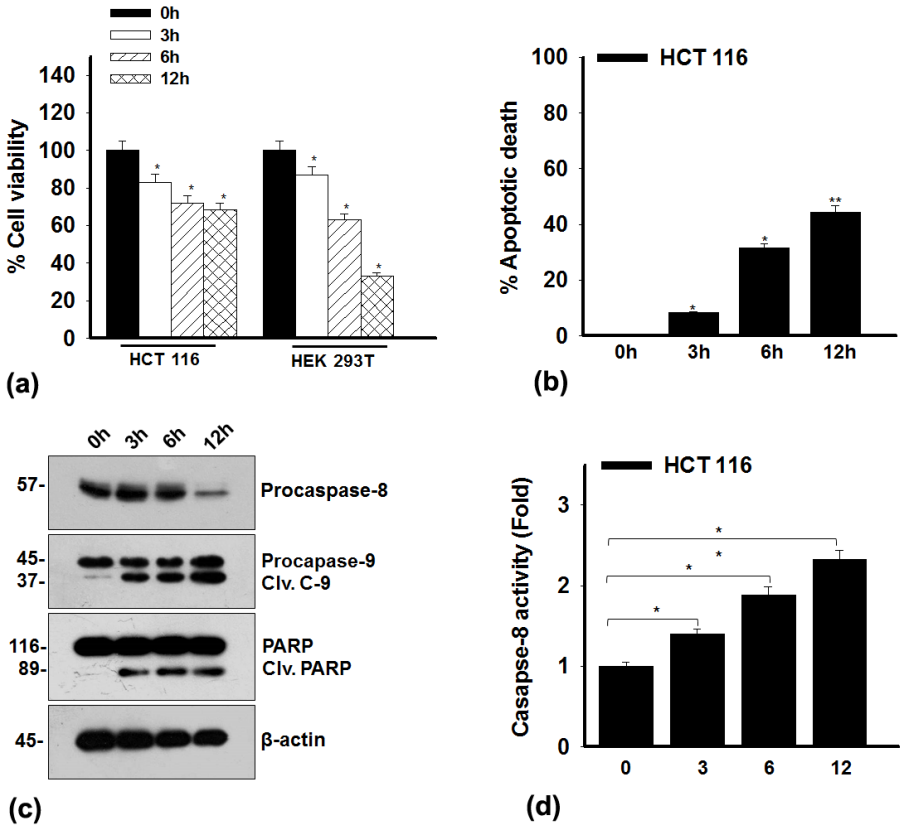

Figure 71. Apoptotic potential of CP-FADD. (a) Treatment of CP-FADD to HCT 116 and HEK 293T cells and measurement of percent cell viability. CP-FADD treatment to HCT 116, control represents reaction buffer treated cells (indicated as 0 h time point) and (b) percent apoptotic death by Tali cytometer, (c) Western blot of apoptosis regulatory proteins and (d) caspase-8 activity. Error bars represent mean±SD; The P value indicates *P ≤0.05, **P ≤0.01, control vs. experimental cells (n ≥ 3, where n is the number of independent experiments)

3.6.11 CP-FADD affects activation of NF-κB and inflammatory cytokines

Several reports advocate that, NF-κB is a key regulator for various sets of genes responsible for inflammatory response and cell proliferation (Karin and Lin, 2002). Now, it was important to investigate the effect of CP-FADD on NF-κB activity and associated inflammatory response. The HCT 116 cells were subjected to CP-FADD to examine the NF-κB activation. The results show that CP-FADD negatively acts on the NF-κB activation as compared to the control cells (Figure 72a & b). Next, HCT 116 cells were subjected CP-FADD for the given time points and the expression of proinflammatory cytokine IL-1β was monitored. The RT-qPCR analyses suggest that treatment of CP-FADD to HCT 116 cells downregulates the endogenous expression of pro-IL-1β with the incubation time (Fig 72c & d). In addition, the Western blot and ELISA assay indicate that CP-FADD regulates the expression of IL-1β as compared to the control and LPS (inducer of IL-1β) stimulated cells

(Figure 72e & f). These results indicate that CP-FADD efficiently suppresses the NF-κB activation and associated pro-inflammatory cytokine IL-1β.

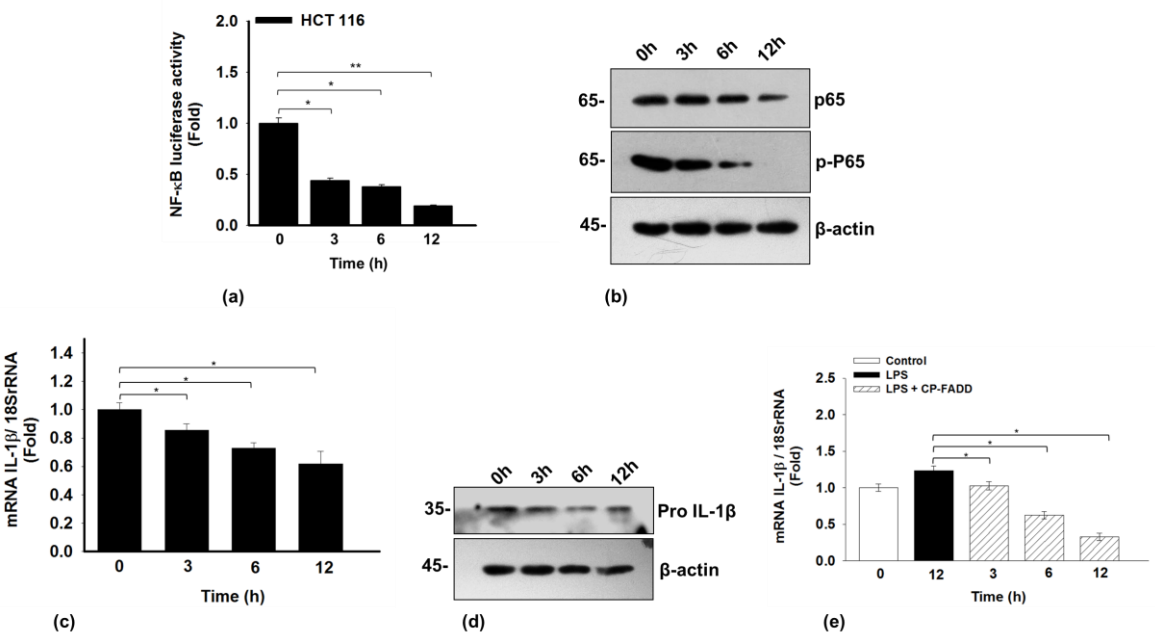

Figure 72. Anti-inflammatory potential of CP-FADD. HCT 116 cells were treated with LPS and CP-FADD (a) NF-κB Luciferase repoeter assay, (b) Western blot of p65 and phosphor p65. HCT 116 cells were treated with CP-FADD and the expression of pro-IL-1β, was monitored by (c) RT-qPCR, (d) Western blot analysis and (e) ELISA analysis, untreated cells (shown as 0 h time point) were taken as control and HCT 116 cells were stimulated with LPS (20 ng/ml for 12 h for optimal pro-IL-1β induction) in ELISA . Error bars represent mean±SD; The P value indicates *P ≤0.05, **P ≤0.01, control vs. experimental cells (n ≥ 3, where n is the number of independent experiments).

3.6.12 Comparative analysis of cell death induced by CP-FADD and known apoptosis inducer molecules

The result shown above signifies that CP-FADD can activates the cascade of apoptosis signaling. Now, it was important to validate the potential of CP-FADD as compare to know chemical inducers of the apoptosis. To achieve this aim, the death ligands CD95L, TNF-α along with pro-apoptotic molecules such as Etoposide, HA14-1 and cycloheximide were incubated with HCT 116 cells for 3-12 h. First, the viability of the cells was monitored by MTT assay. The results showed that the cell viability in the presence of death ligand TNF-α and pro-apoptotic molecules HA14-1 and cycloheximide was observed 65%, 70% and 60% respectively at 12 h and interestingly 55% of cell viability was observed in CP-FADD treated cells at 12 h of treatment (Figure 73a-c). Finally, this outcome was validated by Western blot analysis of major apoptotic proteins procaspase-7 and PARP at different time points. The result shows a significant processing and activation of PARP and procaspase-7 at 3 h in the CP-FADD treated cells as similar to the treatment of apoptosis

inducers. Moreover, at 6 & 12 h the activation of caspases-7 and PAPR were comparable in all molecules that were equivalent to CP-FADD treated cells (Figure 73d-f). Altogether, these findings suggest that CP-FADD significantly induces pro-apoptotic response similar to known apoptotic inducers.

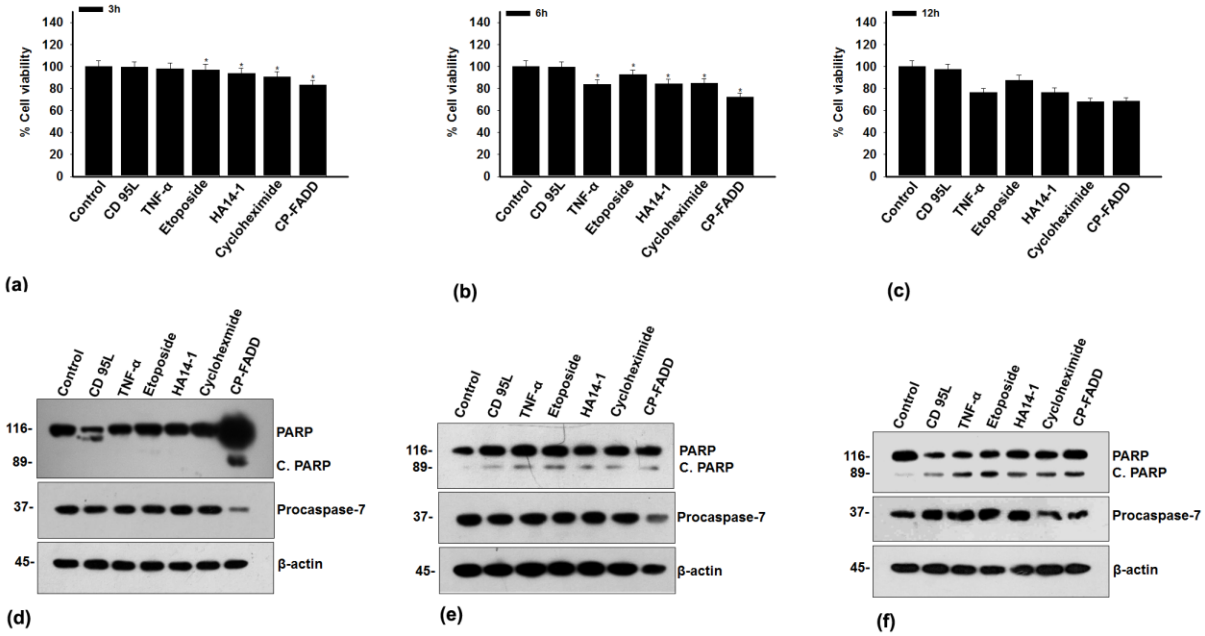

Figure 73. Comparative analysis of CP-FADD with conventional apoptotic inducers. HCT 116 cells were treated with mentioned molecules and (a-c) percent cell viability, (d-f) Western blot of PARP and cspase-7. Error bars represent mean±SD; The P value indicates *P ≤0.05, control vs. drugs tteated cells (n ≥ 3, where n is the number of independent experiments).